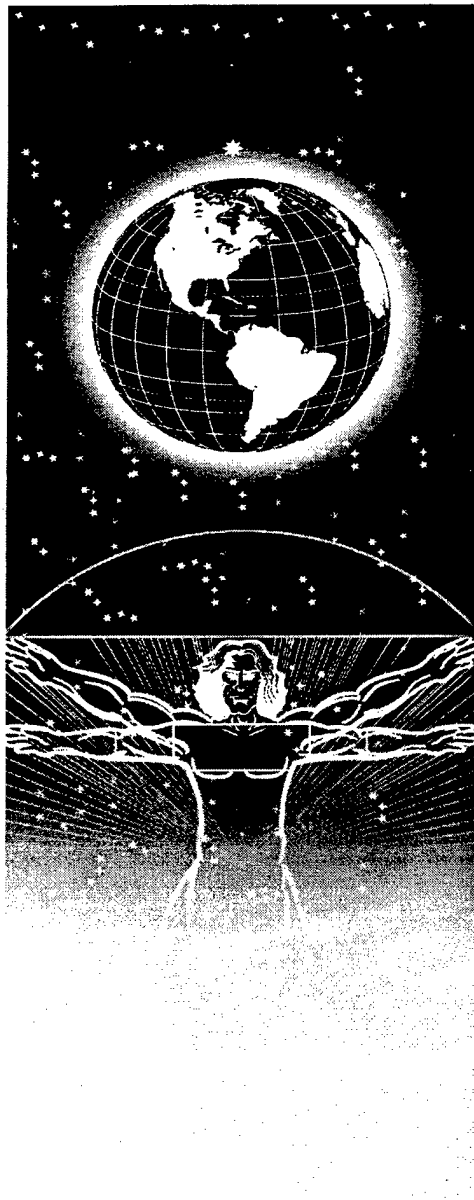AL/EQ-TR-1996-0023

UNITED STATES AIR FORCE
ARMSTRONG LABORATORY

In Situ Spectroscopic Environmental Analysis with Transportable Tunable Dye Lasers

Gregory D. Gillispie

Department of Chemistry
North Dakota State University
Fargo, ND 58105

February 1997

19981118 105

Environics Directorate
Environmental Risk
Assessment Division
139 Barnes Drive
Tyndall Air Force Base FL
32403-5323

DTIC QUALITY INSPECTED 4

NOTICES

This Technical Report is published as originally received under the SBIR Phase I Program and has not been edited by the technical editing staff of the Armstrong Laboratory Environics Directorate.

When Government drawings, specifications, or other data are used for any purpose other than in connection with a definitely Government related-procurement, the United States government incurs no responsibility or any litigation whatsoever. The fact that the Government may have formulated or in any way supplied the said drawings, specifications, or other data is not to be regarded by implication, or otherwise in any manner construed, as licensing the holder or any other person or corporation; or as conveying any rights or permission to manufacture, use, or sell any patented invention that may in any way be related thereto.

This report has been reviewed by the Public Affairs Office (PA) and is releasable to the National Technical Information Service (NTIS), At NTIS, it will be available to the general public, including foreign nationals.

This report has been reviewed and is approved for publication.

FOR THE COMMANDER:

BRUCE J. NIELSEN
Project Manager

MARK H. VANBENTHEM, Maj, USAF
Chief, Risk Assessment Technology Division

REPORT DOCUMENTATION PAGE

Public reporting burden for this collection of information is estimated to average 1 hour per response, including the time for reviewing instructions, searching existing data sources, gathering and maintaining the data needed, and completing and reviewing the collection of information. Send comments regarding this burden estimate or any other aspect of this collection of information, including suggestions for reducing this burden, to Washington Headquarters Services, Directorate for Information Operations and Reports, 1215 Jefferson Davis Highway, Suite 1204, Arlington, VA 22202-4302, and to the Office of Management and Budget, Paperwork Reduction Project (0704-0188), Washington, DC 20503.

1. AGENCY USE ONLY *(Leave blank)*	2. REPORT DATE February 1997	3. REPORT TYPE AND DATES COVERED May 1991 - September 1993

4. TITLE AND SUBTITLE

In Situ Spectroscopic Environmental Analysis with Transportable Tunable Dye Lasers

6. AUTHOR(S)

Professor Gregory D. Gillispie

5. FUNDING NUMBERS

F08635-91-C-0185

7. PERFORMING ORGANIZATION NAME(S) AND ADDRESS(ES)

Deparatment of Chemistry
North Dakota State University
Fargo ND 58105

8. PERFORMING ORGANIZATION REPORT NUMBER

AL/EQ TA-1996-0023

9. SPONSORING/MONITORING AGENCY NAME(S) AND ADDRESS(ES)

AL/EQA-OL
139 Barnes Drive, Suite 2
Tyndall AFB FL 32403-5323

10. SPONSORING/MONITORING AGENCY REPORT NUMBER

AL/EQ TR-1996-0023

11. SUPPLEMENTARY NOTES

Contracting Officer's Technical Rep: Mr Bruce Nielsen

12a. DISTRIBUTION AVAILABILITY STATEMENT

Approved for public release; distribution unlimited.

12b. DISTRIBUTION CODE

A

13. ABSTRACT *(Maximum 200 words)*

This report summarizes the efforts at North Dakota State University to implement laser-induced fluorescence spectroscopy as a means for sensitive detection of fuel and fuel related contamination. The direction of these efforts is upon in situ detection of polycyclic aromatic hydrocarbons in well monitoring or direct push, cone penetrometer testing (CPT). We discuss conventional approaches to fuel-related detection and the inherent weaknesses therein. Both laboratory and field studies involving the applications of our laser-based, time domain fluorescence instrument are presented. The principles of fluorescence spectroscopy pertinent to our concerns are outlined and discussed. Since light delivery and collection are based on fiber optics, the issues relating to fiber length, composite material, cladding, and wavelength dependence are presented. A review of our experimental methods and their relation to the results is provided, along with a discussion of the relevant concerns with interpretation of system performance. Data processing methods are presented, along with the results of the processing methods used during these studies. A presentation of wavelength-time matrices (WTMs) and contour plots data formats is given. Results from field studies are also presented.

14. SUBJECT TERMS

Laser-Induced Fluorescence, In Situ, Fuel Monitoring

15. NUMBER OF PAGES

106

16. PRICE CODE

17. SECURITY CLASSIFICATION OF REPORT	18. SECURITY CLASSIFICATION OF THIS PAGE	19. SECURITY CLASSIFICATION OF ABSTRACT	20. LIMITATION OF ABSTRACT
UNCLASSIFIED	UNCLASSIFIED	UNCLASSIFIED	UL

(The reverse of this page is blank.)

PREFACE

This report was prepared under the direction of Dr. Gregory D. Gillispie at North Dakota State University, Ladd Hall, Department of Chemistry, Fargo, ND 58105 for the United States Air Force (USAF) Armstrong Laboratory Environics Directorate (AL/EQ), Suite 2, 139 Barnes Drive, Tyndall Air Force Base, Florida 32403-5319.

This work outlines the construction and initial testing of a field deployable, wavelength tunable, time resolved fluorescence spectrometer capable of *in situ* fuel monitoring. It presents a discussion of the relevant spectroscopic considerations, major components of the instrument, data collection, analysis and display methods .

The AL/EQS project manager was Bruce Nielsen, Tyndall AFB.

EXECUTIVE SUMMARY

This report documents efforts by a research group at North Dakota State University to implement laser-induced fluorescence spectroscopy as a means for sensitive detection of fuel and fuel-related contamination. Attention is focused on *in situ* detection of polycyclic aromatic hydrocarbons in conjunction with either well monitoring or direct-push, cone penetrometer testing (CPT).

This work is a discussion of the current approach to fuel-related contaminant detection and the inherent cost and weaknesses of this approach. The sources of error with traditional approaches include sample collection, transfer, shipment, preservation, storage, and preparation. Each of these steps can negatively bias the data through loss of analyte via volatilization, degradation, transformation, or masking with impurities. The detection approach outlined in this work is based on the integration of a time-domain based, fluorescence measurement with cone penetrometer testing. The measurement is made via fiber optic light delivery and collection and involves a sapphire window interface between the spectrometer and soil environment. Both laboratory and field studies included in this report. The application is specific but not limited to condensed phases.

Section III describes the principles of fluorescence spectroscopy pertinent to our concerns. Examples of excitation and emission spectra of common PAH species are given to demonstrate the wavelength dependence of sensitivity and selectivity. Particular attention is given to the effects of the fluorescence decay process, the presence of fluorescence quenching agents, and lifetime determinations. Issues relating to fiber length, composite material, cladding, and wavelength dependence are discussed.

Section IV details the spectrometer developed at NDSU for fluorescence lifetime measurements of *in situ* soil samples. Emphasis is placed on laser system layout, the pump and dye laser assembly, the laser dye cells, and the remaining experimental components. The second part of this section discusses the method of operation and relevant concerns over interpretation of system performance results. Optimization of instrument performance by varying experimental layout, dye concentrations, pump energy, and other experimental factors is addressed. The need for making this approach more viable for long term site assessment and monitoring is also discussed.

Section V highlights the results of the research carried out under this contract. A discussion of fluorescence spectra, quantum yields, and fluorescence lifetimes is given. A brief review of our experimental methods and their relation to the results previously given is provided. Data processing methods are presented, along with the results of the processing of the data gathered during these studies. Data formats which depict wavelength-time matrices (WTMs) and contour plots are presented as are results from field studies.

(The reverse of this page is blank)

TABLE OF CONTENTS

Section	Title	Page

LIST OF FIGURES

(The reverse of this page is blank.)

LIST OF ABBREVIATIONS AND ACRONYMS

BTEX	Benzene, Toluene, Ethylbenzene, Xylenes
CCD	Charge Coupled Device (detector)
CPT	Cone Penetrometer Testing
DFM	Diesel Fuel Marine
DSO	Digital Storage Oscilloscope
EEM	Excitation Emission Matrix
EPA	Environmental Protection Agency
GC	Gas Chromatography
HPLC	High Performance Liquid Chromatography
Hz	Hertz (cycles per second)
ICCD	Intensified Charge Coupled Device
IR	Infrared
LIF	Laser Induced Fluorescence
MS	Mass Spectrometry
NDSU	North Dakota State University
Nd:YAG	Neodymium:Yttrium Aluminum Garnet (Laser)
ns	Nanosecond
PAH	Polycyclic Aromatic Hydrocarbon
PMT	Photomultiplier Tube
SCAPS	Site Characterization And Analysis Penetrometer System
SERS	Surface Enhanced Raman Spectroscopy
SLS	Synchronous Luminescence Spectroscopy
TCSPC	Time Correlated Single Photon Counting
TIR	Total Internal Reflectance
UV	Ultraviolet
WTM	Wavelength-Time Matrix

SECTION I

INTRODUCTION

A.   OBJECTIVE:

The objective of this program, conducted by North Dakota State University, Department of Chemistry, is to develop transportable tunable dye lasers for *in situ* spectroscopic environmental analysis. This technique will be used for sensitive detection of petroleum based contaminants in soil and groundwater.

B.   BACKGROUND:

Manufacturing, improper fuel storage and waste disposal procedures have caused extensive contamination of soil and groundwater. Thousands of hazardous waste sites contain fuels, solvents, and heavy metals.   In most cases, the nature and spatial extent of the contamination have not been adequately established.

Approximately one-third of contaminated sites have been created by spills or leakage of bulk petroleum distillates. Gasoline, diesel fuels, jet fuels, and heating oil are processed, transferred, and stored in such large quantities that comparatively small losses can easily lead to a serious problem. There are nearly 2 million regulated underground fuel storage tanks in the United States. The Environmental Protection Agency Office of Underground Storage Tanks has estimated that one-third of the total number are more than 20 years old, constructed from bare steel, not protected from corrosion, and have begun to break down.[1]

Gasoline service station sites with leaking underground storage tanks and/or transfer piping are found in almost every city. New standards for tank testing have been implemented, but substantial contamination has already occurred. The University of Tennessee concluded that corrective actions for leaking underground storage tanks could cost up to $67 billion, with about $46 billion in expenditures required before the year 2000. The Department of Defense estimates costs greater than $24 billion for cleaning up its installations.[2]

The aromatic hydrocarbon constituents of petroleum products are responsible for the major environmental threat. Petroleum distillates contain BTEX (benzene, toluene, ethylbenzene, and xylenes), naphthalenes, and polycyclic aromatic hydrocarbons (PAHs), such as anthracene, phenanthrene, and benzo[a]pyrene. Once in the ground, the fuel components are transported and dispersed in the vadose (unsaturated) zone and in the groundwater. The aqueous solubilities of 1800, 500, and 20mg/L for benzene, toluene, and naphthalene, respectively, make these pollutants a major cause for concern even though they may constitute only a fraction of a fuel's organic content.

The acute toxicity levels of benzene, toluene, and p-xylene for fish and shrimp are two to six mg/L, many times lower than their aqueous solubilities. Although the BTEX concentrations in polluted waters are usually much lower than the acute toxicity levels, chronic exposure to lower concentrations can still be detrimental. Studies have indicated that long -term effects of exposure to PAHs in the mg/L range include cancer, mutations, lowered feeding rates, lowered reproduction, and slowed growth rates for a variety of organisms.[3]

The sampling and chemical analysis activities performed during site characterization, monitoring, and remediation phases represent an estimated 35-65% of the total restoration costs at hazardous waste sites. Traditional methods of site characterization are time-consuming and often lead to insufficient or inadequate soil and groundwater data. The typical phased approach involves several steps which may be widely separated in time, including, investigation design, grid layout, soil boring, sampling (soil, soil gas, groundwater), off-site analysis, and data evaluation. Because of the high cost of sample collection and off - site analysis, sampling programs must choose between collecting an insufficient amount of data in the interest of lowering the cost, or, collecting an abundance of data, not all of which may be useful. Repeated rounds of sampling and analysis are common. The cost for each sampling location is high (typically $100 per linear foot), so a judicious choice of sampling locations is desirable. Other costs include shipping of samples to a laboratory, the actual analyses, standby time, and laboratory personnel.

A new technique that can reduce costs of characterization and monitoring phases by just 10% can have enormous economic impact. Reliable characterization/monitoring data will point out sites which do not need cleanup, either because the remediation costs relative to the

regained value are too high or because the damage has already been done and is no longer spreading.

1.   Soil Borings and Monitoring Wells

The standard method for determining subsurface petroleum contamination relies on a combination of soil borings and monitoring wells. In principle, the soil borings provide a vertical distribution of contamination at each probe location. A three-dimensional model of the contaminant plume can be constructed from a series of laterally distributed borings. However, conventional sampling with drill rigs is time consuming and expensive.

Development of a sampling plan begins with accumulation of data regarding soil type, direction of groundwater flow, history of previous site activities, and chemical data from previous sampling operations. Such information helps to identify contaminants that might be found, how many locations to sample, and the logical choices for analytical methods, but is often incomplete or nonexistent, in which case an empirical approach is necessary.

The three primary sampling approaches are: random, systematic, and judgmental.[4] They can be used independently or in combination, depending on the complexity of the study. Judgmental sampling is usually chosen when there is prior knowledge of the site activities and/or when a visual assessment can be made. It requires only a small number of samples, each of which is highly biased. A random sampling eliminates bias, but is costly in comparison because of the larger number of samples required. Systematic sampling uses a consistent grid or pattern to determine where to sample. Most often, a combination of the three is the best approach, but each study should be flexible enough to permit changes during field activities.

A high degree of uncertainty is associated with the sampling step itself. Only small portions of the core are sampled for laboratory analysis. The decision concerning where in the core to sample can be very subjective. Because each step in this process has the potential to introduce sufficient error to invalidate the results, care must be taken as the sample is collected, shipped, preserved, stored, and analyzed. The analyst is seldom the sampler, and usually has little or no contact with field personnel.

The advantage of monitoring wells is periodic sampling, making it possible to follow changes in contamination levels over time. After the water is withdrawn, samples must be analyzed by gas chromatography and similar techniques for detailed chemical information. However, there is an economic disadvantage of monitoring wells, because local, state, and/or federal statutes require and regulate periodic sampling even of clean wells.

2. Sampling Sources of Error

Significant sources of error in the sampling phase include sample collection, transfer, shipment, preservation, storage, and preparation. Activities involved in the individual steps are not necessarily mutually exclusive, nor are all six steps always necessary or carried out in the order given. Nevertheless, the analysis itself always lies at the end of a chain of events. Often the analyst is not a participant in the preliminary sampling steps, so the reliability of the final result is limited by the performance of others.

(a) Sample Collection. A representative set of samples must be obtained. The number of samples is usually subject to a budget-imposed upper limit. The larger the site, the higher the probability that a number of samples will miss localized hot spots. A well devised sampling plan takes into account past activities at the site. Field screening methods are attractive because they can provide cost effective real-time guidance for the selection of sampling locations. Alternatively, samples can be combined or pooled so fewer actual analyses need be performed. Unfortunately, combining/pooling increases the odds that a hot spot is missed as well as increasing the minimum detection limit. This practice is most useful if little or no contamination is suspected.

(b) Sample Transfer. In the conventional approach, the sample must be transferred from the sampling device to a container for shipment to a laboratory. This is a crucial step for volatile organic compounds. Excess manipulation or agitation of a groundwater sample can easily result in permanent loss of volatiles from the sample. The concentrations reported at the end of the sampling/analysis chain will suffer from negative bias (inaccurately low results). Experiments have demonstrated that concentrations may be under-reported by five times or more because of volatile loss.[5] The same risk is involved in pooling or

4

homogenizing samples. *In situ* analysis techniques have the potential of eliminating the sample transfer step.

(c)   Shipment, Preservation, and Storage. Shipping containers must be airtight to avoid volatile loss during shipment and storage.   To avoid oxidation/reduction processes of metals such as Cr(VI), sample pH must be controlled.

There is commonly a time lag, possibly as long as several weeks, between sample collection and actual analysis. During this interval, various chemical, physical, and biological processes may cause changes in the analyte concentrations. Volatiles are subject to release from solution or into the headspace of a solid sample; organics are subject to chemical reaction with oxygen or other species present in the sample; certain aromatics can undergo photochemical degradation; microbial degradation is also a concern. All of these processes introduce negative bias.

(d)   Preparation.   Most methods require manipulation (extraction, preconcentration, filtration, etc.) of the sample before the actual analysis. During any of these stages, chemical changes are potential sources of error. For example, volatiles can be lost during the extraction stage.

3.   Chemical Analysis of Soil and Water Samples

Analytical techniques capable of sensitively measuring aromatic hydrocarbons in soil and water include chromatography (gas, high performance liquid, and thin layer), mass spectrometry, and various spectroscopies including UV-visible or infrared absorption, Raman, and fluorescence. Gas chromatography with mass spectrometry detection (GC-MS) is used in many cases and is recommended by the EPA because it provides excellent speciation and essentially universal response to organic species.

4.   Field Screening Techniques

There is a growing interest in analytical techniques for field screening. Field screening methods in which the sample remains in its natural environment are referred to as *in situ* techniques and are faster and more economical than traditional analytical techniques.

Some of the intermediate steps, such as preservation, are eliminated. Priorities can be set on site, hot spots can be identified, and the need for a more comprehensive monitoring program or priority placement of the site can be quickly established. Samples showing a high probability of contamination are submitted for rigorous analysis.

Fiber optic spectroscopy, longpath Fourier-transform infrared absorbance, X-ray fluorescence, ion-mobility spectrometry, and immunoassays are typical field screening techniques. Further information can be found in the biennial proceedings of a series of international symposia on field screening methods.[6]

The least innovative field screening techniques are those in which samples are collected conventionally, but the measurement time is reduced for a more interactive approach to site assessment. Immunoassays, field GC and other methods carried out in mobile laboratories fall into this category. More innovative techniques substantially modify the sampling process. The ideal situation would eliminate the sampling step altogether. Long path or fence-line atmospheric monitoring by FTIR is one example. In the analysis of petroleum contamination in monitoring wells, a probe is dropped into a monitoring well making a measurement without withdrawing a discrete sample. Fiber optic spectroscopy carries light to the sample. The obvious tradeoff is speed and convenience vs. sensitivity and accuracy.

The application of fiber optics *in situ* has several advantages over indirect sampling techniques. Time and labor are minimized; standby time for expensive drilling services is decreased and sampling errors are avoided since the sampling process is eliminated. Fiber optic probes can produce three-dimensional plume assessment reducing costly results of erroneous water table and site disturbance. On-site and multiple site monitoring from a central, portable instrument is more efficient and economical.

Interest in fiber optic sensors for remote sensing and *in situ* analysis began about 1980. Fiber optics are suitable for chemical sensing applications for several reasons. They are resistant to temperature and humidity extremes and are immune to electromagnetic interference. The minimal size, the ability to transmit light over long convoluted paths, and safety in areas where environmental or electrical hazards exist are characteristic.

Fiber optics are often coupled with spectroscopic methods, such as Raman or fluorescence. Light is directed through the fiber optic to the source of contamination, at which point the light is absorbed or scattered. The fluorescence emission or Raman scatter is directed back through the same or separate fiber optics to a detector system. Fiber optic spectroscopy can be applied in either direct or indirect modes. Indirect methods (optrodes or fiber optic chemical sensors) are not likely to have the fast time response necessary for real-time data acquisition.

Cone penetrometers equipped with laser sensors are being used for characterization of subsurface fuel contamination. Efforts to incorporate spectroscopic devices into cone penetrometers followed soon after the first publication in 1985 on laser induced fluorescence spectroscopy over fiber optic cables.[7] During cone penetrometer testing (CPT), an electronically instrumented cone is continuously advanced into the subsurface at 2 cm/sec by adding sections of threaded pipe. The pushing force is provided by hydraulic rams in a specialized truck that weighs 20 tons or more. Standard CPT cones have angles of 60 degrees and base areas of 10 or 15 cm^2. An electrical cable passes through the string of push rods, connecting a control computer in the truck with sensors in the cone tip. The standard geotechnical sensors measure tip resistance and sleeve friction. Soil types can be categorized and empirically classified as a function of tip resistance and sleeve friction to tip resistance ratio. Soil conductivity and pore pressure are examples of other common geophysical measurements.

A sapphire (a crystalline phase of Al_2O_3) window has been incorporated in the side of a cone near the tip so that fluorescence measurements via fiber optics can be made.[8] The sapphire's hardness protects it from being scratched by sand and other materials encountered as the cone is pushed through the soil. Light transmitted by a fiber optic excites the soil sample through the sapphire window. Fluorescence associated with aromatic hydrocarbons and other species present in the soil is returned to the surface through collection fibers for detection. The "proof-of-concept" (qualitative validity) for this approach was achieved during a Tri-Service (Army, Navy, Air Force) program known as SCAPS (Site Characterization And Analysis Penetrometer System).[9]

C.   SCOPE

This report covers the work performed during research contracts F08635-89-C-0042 and F08635-91-C-0185 funded by the US Air Force. The research goals were:

a. Development of a transportable, wavelength tunable laser system suitable for field implementations of fiber optic fluorescence spectroscopy.

b. Investigation of the utility of time domain information that is attainable with the laser system.

c. Laboratory studies to characterize the spectroscopic behavior of aromatic hydrocarbons under conditions relevant to environmental samples (dissolved in groundwater, adsorbed on soil, etc.).

d. Field testing of the system

This system is based on frequency doubling the output of a visible, tunable dye laser pumped by a pulsed Nd:YAG laser. The tunable ultraviolet light is coupled into a fiber optic probe, which remotely delivers the laser light to the sample over distances of up to 50 meters. A portion of the fluorescence generated at the sample is returned through separate collection fibers to the detection system.   The signal is monitored for both temporal and intensity information.   Concentration and distribution of aromatic hydrocarbons in the sample is assessed according to the signal's dependence on excitation and/or emission wavelengths. Originally the development work was aimed at groundwater measurements with direct insertion probes, but cone penetrometer applications grew in importance over the course of the contracts.

Section II is an introduction to fluorescence principles with a discussion that focuses on previous work in fiber optic spectroscopy, especially fluorescence-based. The instrumentation that has been developed is described in Section III. Separate sections treat the dye laser characterization, the techniques for lifetime measurements, and the fiber optic probes. A data base of fluorescence and fluorescence excitation spectra (taken with a spectrofluorimeter), fluorescence lifetime data base for the same compounds, wavelength-time matrices (WTMs) for many different fuel types, and calibration curves that illustrate the sensitivity of the technique are included in Section IV,   APPARATUS.   The results of the initial field studies, for groundwater monitoring and cone penetrometry, are the subject of Section V.

SECTION II

HISTORY

A.   WHY FLUORESCENCE?

Fluorescence complements absorption spectroscopy. It offers greater sensitivity and, in conjunction with remote fiber optic sensing, is the method of choice for detection of trace aromatic species. The range of acceptable light transmission in optical fibers is 200-2500 nm. Spectroscopies that use light in this range include UV-visible absorbance, infrared absorbance, Raman scattering, and fluorescence. Of these, fluorescence has the desired combination of sensitivity, specificity, and applicability.

Electronic absorption (commonly referred to as UV-visible absorption) is associated with transitions between electronic levels. Energy from the absorbed photons raise the molecule from the ground electronic state to an excited state. Such electronic excitation is a prerequisite to subsequent fluorescence photon emission. Each organic molecule exhibits UV-visible absorbance, but perhaps at too short a wavelength for convenient study. Aliphatic hydrocarbons, for example, undergo electronic excitation for photons in the <200 nm range. UV-visible absorbance generally lacks sufficient sensitivity to be applied to field analysis and its capacity to speciate components is severely limited. There may be some applications to groundwater measurements.[10]

Chemical analysis by absorption spectroscopy relies on a combination of signal strength and characteristic structure. Because absorbance is so general, samples that contain many different chemical components (including all fuels) will yield spectra that are composites of all their components. Prominent spectral features increase the precision with which component contributions can be extracted by mathematical data processing. UV-visible absorption and fluorescence monitor electronic transitions which are not highly structured for solution samples.

In contrast, individual Raman and mid-IR bands, which carry molecular vibration information, may span as little as 0.1% of the usual spectral range and are therefore very specific. Unfortunately, IR and Raman are not extremely sensitive techniques.   Infrared

9

specific. Unfortunately, IR and Raman are not extremely sensitive techniques. Infrared measurements work well for high concentration samples (neat liquids, dispersions of solids in a nonabsorbing liquid mull, etc.) or for gaseous samples which have extremely narrow spectral features. Infrared absorbance suffers from an inability to directly analyze aqueous mixtures because of absorbance by the solvent.

In fluorescence and Raman spectroscopies, the detected signal intensity is proportional to the excitation flux. They are ideally zero-background experiments, although there is always a background contribution from physical scattering or solvent Raman scattering. Background scattering is a greater concern for studies involving soils than for groundwater. Fluorescence and Raman spectra usually represent small signals against an even weaker background, making high source radiant power desirable, especially for ultraviolet studies because of greater attenuation in the delivery fiber optic.

Raman spectroscopy has received considerable attention for fiber optic spectroscopy. Its excellent speciation capability resembles IR but has the advantage of using light in the visible region where fiber attenuation is low. Raman scattering, however, is usually an inefficient process such that any significant fluorescence, common to the majority of aromatic hydrocarbons, overwhelms the Raman signal. The best applications of Raman are likely for process control where concentrations are high enough to avoid the issue of sensitivity.

Two specialized forms of Raman spectroscopy, resonance Raman and Surface Enhanced Raman Spectroscopy (SERS), can yield the signal intensities needed to make Raman analysis feasible despite background complications. In resonance Raman the source wavelength lies in the electronic absorption region. For well documented[11] quantum mechanical reasons, the scattering signal is generally enhanced by several orders of magnitude. Resonance Raman's requirement for wavelength tunable excitation limits its analytical applications. Current research indicates that resonance Raman has strong potential[12,13,14], but a suitable method of calibration is an issue since the Raman signal depends on several parameters including detector angle and collection optics,[15].

SERS has also received attention as a possible PAH spectroscopic detection technique.[16] SERS exploits the tremendous increase in Raman scattering efficiency which

technique is known to provide excellent sensitivity for some species, especially pyridine, but most PAHs do not appear to exhibit the enhancement necessary for direct analysis at trace levels. Because dependence of the enhancement factor on surface morphology is the focus of much of the current research, and because of the fragile metal surfaces involved, SERS is unlikely for field applications.

B.   HISTORY OF LIF ON CONDENSED PHASES

In 1976, Schwarz and Wasik[17] reported one of the earliest attempts at quantitative analysis of PAHs in aqueous solutions using fluorescence. The excitation light from a deuterium lamp was wavelength-selected using a monochromator and the fluorescence emission was isolated with filters. Photon counting detection was used in this continuous excitation experiment. Detection limits in the 0.03 to 0.10 μg/L range were found for aromatic hydrocarbons including benzene, naphthalene, anthracene, pyrene, fluoranthene, and benzo[e]pyrene. Only benzo[e]pyrene failed to exhibit the expected linear relationship between fluorescence and concentration. Sound rationales were advanced for this exception.

Shortly thereafter, Richardson and Ando[18] published a similar study in which a pulsed laser source was employed. The main instrumental features were: (a) nitrogen-pumped and frequency-doubled tunable dye laser excitation source; (b) isolation of the fluorescence with filters; (c) signal processing with a photomultiplier tube and boxcar averager. The authors reported detection limits of 19 (benzene), 0.0013 (anthracene), 0.0044 (naphthalene), 0.0010 (fluoranthene), and 0.005 (pyrene) mg/L and a linear detection range over as much as a six-order-of-magnitude concentration variation. These numbers are to this day representative of what can be obtained for laboratory cuvette-type measurements.

This early fluorescence work demonstrated the excellent detection limits and linear quantitative behavior available with fluorescence techniques for direct study of aqueous samples. However, because of the broad, overlapping spectral features of aromatic hydrocarbons in aqueous solution, it was clear that multicomponent analysis would not be trivial. Visual or hand-calculated analysis of multicomponent spectra is effectively impossible for all but the most elementary and spectrally well-separated mixtures. Computer assisted structural interpretation of fluorescence spectra was investigated in 1976 by Miller and

11

Faulkner.[19] Although successful, this work focused on using peak locations, widths, and relative intensities for compounds that were separated from mixtures using HPLC. Multicomponent analysis from spectra alone was not accomplished. Miller and Faulkner did demonstrate, however, that large laboratory databases could be searched and matches found with tolerable consistency.

C.   MULTIDIMENSIONAL FLUORESCENCE FORMATS

Fluorescence, a multidimensional technique, is uniquely distinguished from other optical spectroscopies. The fluorescence intensity for a given compound (and solvent) is a function of the excitation wavelength and the emission wavelength. A pulsed excitation experiment also involves a time dimension. Accordingly, many attempts have been made to incorporate multidimensional fluorescence methods to extract more information. This is especially attractive for multicomponent mixtures such as fuels.

The most familiar multidimensional fluorescence presentations are the excitation-emission matrices (EEMs) introduced by Warner et al.[20] An EEM is a mapping of the fluorescence intensity as a simultaneous function of excitation and emission wavelengths. The data can be arranged in matrices in which the rows represent fluorescence spectra taken at various excitation wavelengths. The columns represent fluorescence excitation spectra taken at various emission monitoring wavelengths. The resulting data can be plotted in both three-dimensional and contour styles. The height or intensity of each point on the plot is a linear combination of the intensities for each individual component at that particular wavelength combination.   The use of EEMs for component analysis has been documented but the technique has not been applied on a regular basis.[21,22]

The synchronous luminescence spectrometry (SLS) method limits the amount of data and decreases the complexity of analysis. This method is actually a variation of EEMs in that a synchronous spectrum is a "cut" of an EEM plot from one corner to the other. The same cut can be accomplished directly with a scan in which a constant difference is maintained between the excitation and emission wavelengths. In favorable cases the spectrum has a profile similar to a chromatogram in which each peak represents an individual component.

A thorough explanation of the SLS and its relationship to EEMs is found in a review by Warner and McGown.[23] Early work generated excitement when a five component PAH mixture of naphthalene, phenanthrene, anthracene, perylene, and tetracene was analyzed.[24] The spectrum consisted of five well separated peaks representing each of the components. Previous work had only been applied to a fingerprinting of complex samples such as crude oil.

The optimal choice of wavelength interval has a dramatic effect on the synchronous spectrum and is directly related to the Stokes shift of the species involved. The fluorescence and absorbance spectra of different PAHs do not occur at equal wavelength intervals if the absorbances lie in widely separated spectral regions. Instead, PAH fluorescence is Stokes shifted by a near constant amount of energy. Researchers have developed a constant energy synchronous luminescence technique, in which there is a constant energy separation between the emission and excitation wavelengths throughout the scan. Constant energy scans make better use of the total fluorescence by involving more separate peaks of the spectrum.[25] When using constant wavelength difference techniques, the use of a 3 nm wavelength separation is a good compromise for molecules demonstrating a strong 0-0 transition. A 20 to 30 nm wavelength separation is used for PAHs in solution which do not exhibit a strong 0-0 transition at room temperature. The optimum wavelength separation for several compounds is quite different, but the energy separation is essentially the same.

While synchronous techniques have proven to be useful in reducing the complexity of an analysis, it is generally accepted that these techniques are essentially fingerprinting in nature. Caution should be used in trying to apply these techniques to multi-component analysis.[26]

The mathematics involved in the analysis and calibration of the matrix are not nearly as simple as the concept. Warner[27] developed a systematic procedure for the quantitative analysis of a multi-component fluorescent sample using EEMs. A complete mathematical treatment and examples of the effects of noise and spectral overlaps are provided.

In 1980, Ho[28] used another method, rank annihilation, which involves a six-component PAH solution which is varied with regard to constituents. The technique was demonstrated to be a powerful tool for EEM analysis.

A ratio method, used by Fogarty[29], requires that each component have a spectral region in which it is the lone emitter. Since this is not characteristic of many PAH mixtures the technique would undoubtedly fail. EEMs are obviously complex and signal-to-noise is an important consideration.

Wavelength-time matrices (WTMs) are an alternative multidimensional fluorescence method in which fluorescence time profiles are measured at a series of excitation and/or emission wavelengths. Because measurement of time domain data in fluorescence is a tedious process and severely limited in several ways, relatively little work has been reported on WTMs for multicomponent analysis. WTMs can, in principle, be performed with a single wavelength laser source. If the excitation wavelength can be varied, a three-dimensional approach becomes available. A motivation for this research was the development of more efficient approaches to the time domain information.

D.   FIBER OPTIC SPECTROSCOPY

Application of fiber optics to spectroscopy began with Raman work in the early 1980s. These studies were performed with visible excitation since attenuation of light within the fiber was minimal. An early review article on the application of fiber optics to chemistry defined the terms and concepts involved with fiber optics, along with discussion of the application possibilities.[30]

The simplest fluorescence probe configuration uses the same fiber for delivery and collection of the light. The collection efficiency (for equal collection cross-sectional area) is the highest theoretically possible, owing to the perfect overlap between the light delivery and collection acceptance cones. A disadvantage of the single fiber configuration is that extraneous light signals, either directed into or generated in the core, can produce an unacceptable background level. Extraneous light signals can originate from Raman scattering

14

from either the fused silica core, the cladding, or the fluorescence generated in the cladding by evanescent waves. Longer fiber lengths generate a higher level of extraneous signal, while the fluorescence intensity decreases. The detection capabilities of the single-fiber configuration tend to be severely degraded for long probes.

Measurements with probes longer than a few meters invariably involve separate delivery and collection fibers. Schwab and McCreery described a fiber optic probe for collection of Raman spectra.[31] Their probe contained a total of 19 fibers, each 200 μm in diameter. A central fiber carried excitation light from an ion laser to the sample. The 18 collection fibers at the probe end were arranged in two concentric circles (6 fibers in an inner ring and 12 in an outer ring) around the delivery fiber. At the detection end, the collection fibers were arranged in a vertical line to match the slit dimensions of the spectrometer. McCreery used fiber optics for both delivery and collection of light in a simple probe design for visible Raman spectroscopy.[32] An adjacently configured, two-fiber probe was developed and is still in use.

Schwab and McCreery used a similar design with six collection fibers adjacently arranged about one central excitation fiber.[33] Separate launch-collection fiber configurations have been shown to be less efficient arrangements for fluorescence light gathering than single fiber probes[34], or probes designed with fibers at 22° angles[35]. However, the rejection of scattered light from the excitation source in the adjacently arranged multifiber design is superior and is optically less complicated than the single fiber design. Probe construction is also simplified in the adjacent fiber arrangement. This saves time and reduces the overall size of the probe considerably. A recent summary of practical considerations in applying fiber optics to spectroscopy discusses optical fiber characteristics, constraints, and arrangements and provides an overview of the theoretical calculations that can be done to arrive at optimized coupling configurations.[36]

Fused silica fiber optics have sufficiently low attenuation such that an *in situ* arrangement can be employed even at ultraviolet wavelengths. This allows remote fiber optic fluorescence analysis of BTEX and other ultraviolet absorbing and emitting species. However, the attenuation increases sharply for wavelengths shorter than 300 nm, and along with the

15

demands of ultra-low detection limits, a high-power excitation source, such as a laser, is required.

1.   Laboratory Studies

Research groups have been actively exploring the viability of *in situ* laser induced fiber optic based fluorescence analysis since the mid 1980s. In 1983, T. Hirschfeld[37] first proposed that fluorescent dye tracers be monitored with fiber optics in the visible wavelength range. He suggested that classic Raman spectrometers be used to monitor the fluorescence owing to their fluorimeter-like design and higher overall efficiency in dealing with low power signals.

The first report of fiber optic fluorescence spectroscopy for analysis of aromatics in water was the 1985 publication of Chudyk, Carrabba, and Kenney[38] from Tufts University. The frequency-doubled output of a nitrogen-pumped dye laser (270 nm) or the fourth harmonic of a Nd:YAG laser (266 nm) was used as the excitation source. A fiber optic probe was used with two 600 μm fused silica fibers, one to deliver the laser light to the sample and the other to carry the fluorescence to a photomultiplier tube (PMT). The signal from the PMT was monitored with a boxcar integrator. Considerable effort was made to analyze launch efficiencies, fiber losses, and damage thresholds for launching the excitation beam. No attempt was made to incorporate time resolution into the technique.

The laser induced fluorescence of phenol and o-cresol were measured for a 25 meter delivery fiber. Emission spectra were first taken with a monochromator to determine the optimum filter in order to selectively monitor fluorescence and reject scattered light. These filters were then used with a PMT to construct log-log concentration curves. A nitrogen laser pumped dye laser was used with one meter fibers to analyze other priority pollutants, including toluene.

The concentration curves lack the expected linear relationship. The authors cited Beer's law to explain their poorly behaved log-log plots. However, Beer's law is an

absorbance concept which cannot account for the non-linear behavior of fluorescence signal intensity at the concentrations in this particular study.

In light of the poor plots, the reported detection limits of 10 and 1μg/L for phenol and o-cresol, respectively, may be in error. Other studies, including data presented here, have demonstrated that fluorescence behavior, including that obtained with fiber optic based measurements, displays the expected linear relationship over several orders of magnitude concentration range.[39]

The Tufts researchers have since followed separate paths in fiber optic spectroscopy. The Kenney group[40] has developed a quasi-tunable pulsed laser source based on Raman shifting the Nd:YAG laser harmonics in hydrogen and/or methane gas mixtures. A series of lines with an average spacing of 5 to 10 nm are produced throughout the ultraviolet and visible regions of the electromagnetic spectrum. Non-time-resolved fluorescence spectra are acquired for each wavelength and are combined to produce an excitation-emission matrix (Section V) for least squares multicomponent analysis.

Carrabba et al.[41] have devoted most of their attention to Raman spectroscopy. They used a holographic Bragg diffraction filter for Rayleigh line rejection. This filter provides a relatively high and flat transmission to within a few hundred cm^{-1} of the laser line. Solid, liquid, and surface-enhanced Raman spectra were observed with a compact spectrograph, incorporating a holographic filter. The possibilities of compact portable Raman systems for environmental monitoring is apparent.

A study by Chudyk et al.[42] emphasizing laser-induced fluorescence of aromatic groundwater contaminants addresses problems of fiber luminescence and cross-talk and the manner in which these effects, lead to inaccuracies in laser induced fluorescence measurements. A glass cut-off filter is incorporated to eliminate scattered excitation light and water Raman scatter.

Lieberman et al.[43] developed a pulsed-laser, fiber optic-based fluorimeter to determine fluorescence decay times of PAHs in sea water. This approach uses pulsed nitrogen laser excitation with an intensified diode array detector. Lifetimes are measured by

17

advancement of the detector gate, which is about 5 ns wide. The fiber probe contains a 2 meter long bifurcated seven-fiber bundle (six-around-one probe), each with a core diameter of 325 μm. A 10 meter length of 325 μm fiber delivers the light from the laser to the central fiber of the bundle. Much of the focus has been on diesel fuel marine (DFM), a fuel widely used by the Navy. DFM contains significant quantities of larger PAHs, such as anthracene and benzo[a]pyrene. The reported data was for these species dissolved in a solvent mixture of air-saturated sea water and a small volume of ethanol.

Niessner et. al.[44] have also used a nitrogen laser excitation source. Detection was carried out using a photomultiplier tube detector. Recording of the decay curves was undertaken with a boxcar integrator. The fiber optic probe consisted of two multi-mode, step-index quartz fibers (one excitation and one collection fiber) of 50 meter length with 600 μm core diameter. The best experimentally determined signal to noise (S/N) ratio was achieved if the collection fiber was angled at 11° to 16° from the delivery fiber with a separation of 0.1 to 0.2 mm between the tips of the two fibers. Some of the larger PAHs, such as chrysene, pyrene, and fluoranthene, were investigated. Each was dissolved in air-saturated ultra-pure water containing a small amount (less than 1% by volume) of acetonitrile.

Work involving phase-resolved fluorescence and laser sources can also be found in the literature. Bright and Litwiler[45] reported the lifetime determination of several large PAHs, e.g., pyrene and anthracene, in ethanol, using fiber optic phase-resolved spectroscopy. The UV line (351.1 nm) of a mode-locked argon-ion laser was used in conjunction with a multifrequency phase and modulation fluorimeter. Unfortunately, this system's output and that of other commonly available CW lasers lie at too long a wavelength for fluorescence excitation of aromatic compounds with fewer than three rings.

2. Fiber optic Fluorescence - Field Studies

In a continuation of his laboratory work, Kenney[46] used the same basic configuration in a cart design. Again, the only signal resolution technique used was spectral, with filters for separation of the excitation and emission wavelengths. Long-wave pass filters were used to block Rayleigh and Raman scatter but pass the longer wavelength fluorescence. Since Raman scattering of water occurs at or near the fluorescence emission maximum for a

large number of the benzene-type fluorophores targeted for this project, any filters which eliminate Raman scatter will greatly reduce the sensitivity of the technique. This is one of the key problems associated with a spectrally limited selection technique. Field testing was carried out on a very limited scale.

Although Kenney made several references to field analysis, no quantitative field data were actually offered. They found that laser intensity in the field was less stable than under laboratory conditions, probably due to temperature variations of the equipment. Laser power normalization, which is necessary to take fluctuations into account, was carried out by splitting 10% of the excitation fiber light through an excitation wavelength passing filter onto a PMT. This technique is questionable due to the highly variable nature of collecting scattered excitation light. Direct specular reflection from particulate matter can give differing intensities. The authors did not address this issue or its consequence on the data gathered.

However, one of the authors has recently reported a technique which uses evanescent waves. Coupling between the excitation fiber and a monitor fiber monitors the UV energy actually delivered to the probe[47]. This type of evanescent coupling is possible due to total internal reflection of the photons within the fiber. The photons actually travel outside the core for a short distance, some traveling into the adjacent fiber.

Further work by Chudyk[48] using the same basic instrument provided no additional technical developments, although some actual field data were reported. Total concentrations of detectable organics were apparently calculated from the fluorescence measurements (the approach was not specified) and compared to GC/MS data for the same sites. A plot of the data reveals a very poor correlation between the two techniques.

Other groups have had success in developing fiber optic fluorescence detection systems capable of field analysis. Inman and coworkers[49] developed a fiber optic based fluorimeter which employs a nitrogen laser excitation source. The authors, having recognized the benefits of temporal information as an additional parameter, implemented a time-gated polychromator in the form of an intensified linear photodiode array. The polychromator approach allows the entire emission spectrum to be acquired simultaneously. This is beneficial

in that the entire spectrum can be attained and is not affected by shot-to-shot intensity variations which occur during data acquisition.

The temporal resolution was accomplished by gating or "enabling" the detection array for short periods of time. The time window is gradually advanced until the signal has reached background levels. The resulting data form a two-dimensional emission-time array. The authors tested reference solutions of rhodamine, anthracene, and quinine sulfate in various standard solvents. Decay times compared favorably with those in the literature.

Decay lifetimes were also collected for sea water solutions. It was found that the lifetimes had, as expected, been shortened by oxygen quenching and matrix effects. However, the lifetimes of different species were still sufficiently different to suggest that gating would offer an improved capability to resolve individual components in mixtures. As is the case for much of the time-resolved studies, the actual implementation of this added temporal dimension remains largely undeveloped. No actual field data were collected although the unit is field ready according to the authors.

Another technique in use by Kenney[50] utilizes a Nd:YAG harmonic pumped Raman shifter to provide an array of UV wavelengths. The desired excitation wavelength is individually selected with a dispersive prism and launched into a 10-20 m excitation fiber. A separate collection fiber delivers the resulting fluorescence to a grating which disperses the fluorescence onto a linear diode array. EEMs are collected and mathematically massaged to account for the inconsistencies in excitation wavelength step size and the widely varying energies resulting from the Raman shifter source.

SECTION III

PRINCIPLES

A.   FLUORESCENCE PRINCIPLES AND NOMENCLATURE

Most polycyclic aromatic hydrocarbons (PAHs) fluoresce when irradiated with light in the proper wavelength range. Fluorescence is a process of photon (light) emission that occurs as molecules decay from a higher energy quantum state to a lower energy quantum state. The higher energy states are created by a prior act of photon absorption. The wavelengths of light required for excitation generally lie in the UV and visible spectral regions.

The fluorescence excitation spectrum is a plot of fluorescence intensity as a function of excitation wavelength, and is closely related to the molecule's absorbance spectrum.[51] The UV absorbance/fluorescence emission spectra for benzene, toluene, xylene, and naphthalene in aqueous solution are shown in Figure 1. Absorbance occurs at shorter wavelengths and represent the spectra shown to the left in each of the sub-figures below. The corresponding emission spectra are shown at longer wavelengths, adjacent to the absorbance spectra. Note that the individual spectra are highly overlapped with their own distinct and characteristic appearance. Unlike atomic spectroscopy, it is generally not possible to find a wavelength such that only one compound absorbs. Fluorescence is not as selective as other techniques, particularly many of the chromatographic methods.

Fluorescence emission generally occurs at longer wavelengths than the excitation, and is said to be *Stokes shifted* from the excitation wavelength. The emission spectra appear similar to the absorbance spectra and are highly overlapped. Furthermore, naphthalene is well separated from the BTEX. A general phenomenon is that the higher the molecular weight of an aromatic hydrocarbon, the longer its emission wavelength.

There are two very important points regarding fluorescence:
- The fluorescence spectrum of a particular molecule is independent of the excitation wavelength.
- Fluorescence lifetime is independent of the emission wavelength.

21

Fluorescence has several advantages over absorbance spectroscopy. The background signal is very low for solution fluorescence measurements in which the light passes through a homogeneous medium. A small signal is measured against an even smaller background resulting in greater sensitivity. Absorbance, however, measures a small change in absorbance from an already large signal and background. Fluorescence is also very compatible with examination of highly scattering samples in which the background signal is higher, for example, in cone penetrometry.

Under dilute solution conditions, the fluorescence signal exhibits linear dependence on analyte concentration. A plot of the log of the signal intensity vs. the log of the analyte concentration should exhibit a slope of one. In addition to unique excitation and emission spectra, each PAH has its own characteristic fluorescence lifetime in the range from one to several hundred nanoseconds. The fluorescence lifetime is defined as the time interval over which the fluorescence intensity decays to $1/e$ of its initial value.
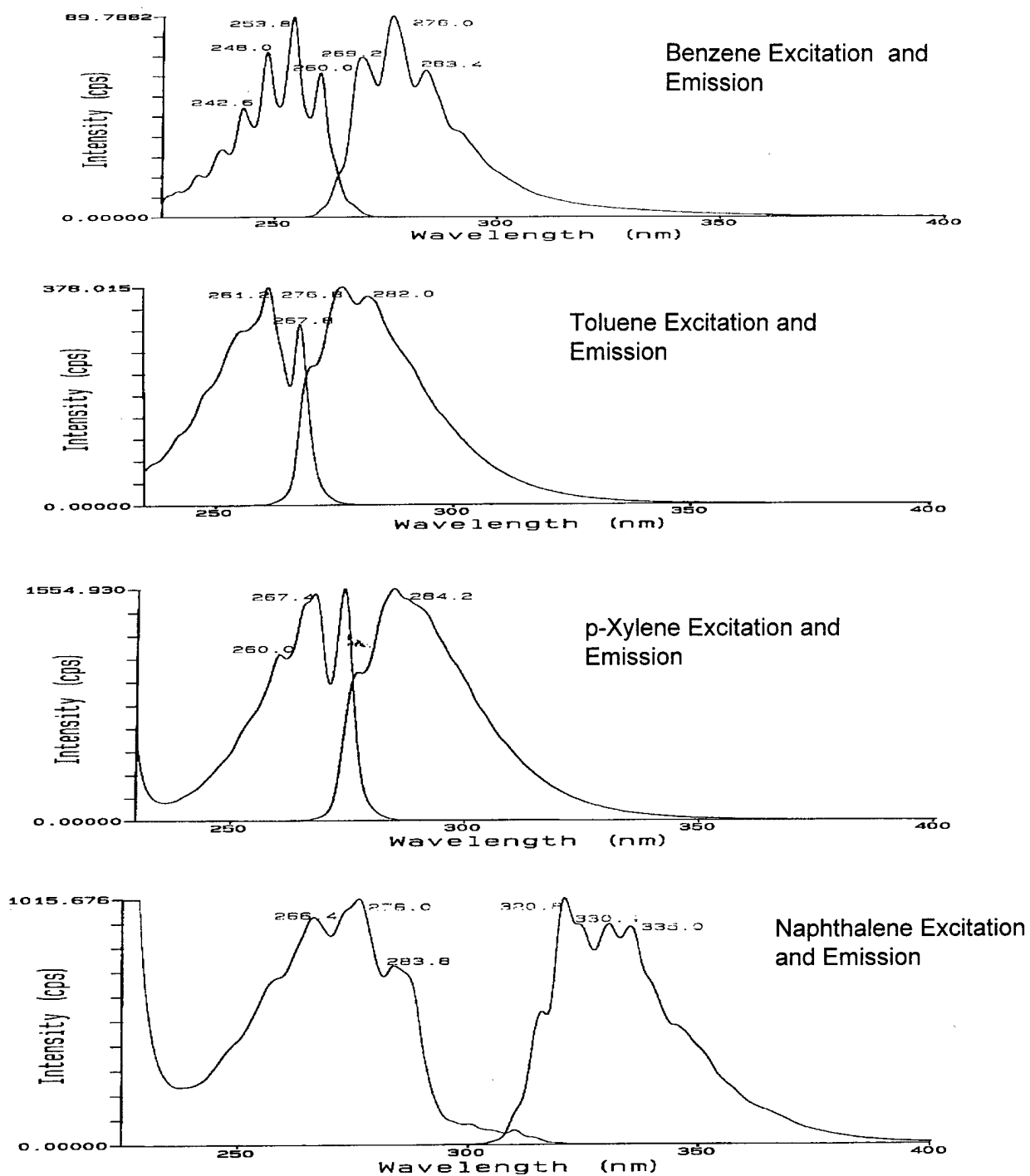
Figure 1: Excitation and emission spectra of benzene, toluene, p-xylene, and naphthalene in aqueous solution.

Fluorescence from molecules in condensed phases commonly occurs from the first excited singlet state, denoted in Jablonski notation as S_1. Often all the processes that contribute significantly to S_1 deactivation are kinetically first order (or pseudo first-order). In this case, the excited state population undergoes exponential decay, and the fluorescence lifetime is usually defined as the time interval over which the fluorescence intensity decays to 1/e of its initial value. The lifetime is the reciprocal of the sum of the rate constants for all the S_1 deactivation paths. The fluorescence lifetime is really the S_1 state lifetime; the same value should be obtained by any alternative technique, (e.g. transient absorption) which probes the excited state population. Fluorescence is generally used because the light produced is easily detected and monitored.

The principal S_1 decay paths of interest are fluorescence, intersystem crossing to the triplet states, internal conversion to the ground electronic state, and pseudo first-order quenching. For our experiments, the excited state population from which the fluorescence occurs is always created by photon absorption from the ground state, denoted S_0.

$$S_0 \xrightarrow{\;h\nu\;} S_n \to S_1 \qquad\qquad (1)$$
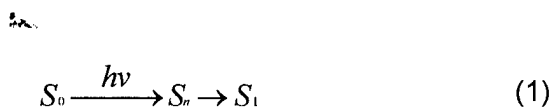
Excitation to a higher electronic state S_n (n > 1) is rapidly followed by internal conversion to S_1 on a "fast" time scale compared to the fluorescence. Internal conversion is a nonradiative transition that occurs from a low vibrational level of an upper excited state to a high vibrational level of a lower excited state (e.g., $S_2 \to S_1$ transition). Molecules that have undergone internal conversion lose their excess vibrational energy via collisions with solvent molecules. Similarly, molecules raised by photoexcitation to the upper vibrational level of S_1 quickly lose their excess vibrational energy by collisions with surrounding molecules. Both of these processes are commonly referred to as vibrational relaxation, and occur on a fast time scale (10^{-12} sec) compared to fluorescence (10^{-9} sec). As a consequence, fluorescence generally occurs only from a Boltzmann distribution of vibrational levels in the first excited singlet state. Thus, the fluorescence spectral distribution and lifetime are the same, regardless of the wavelength of the excitation source.

Equation (2) represents fluorescence, the deactivation of the excited state to the ground state with the production of light (hv).

$$S_1 \xrightarrow{k_r} S_o + h\nu \qquad (2)$$

The competing deactivation processes from the lowest excited singlet state are internal conversion to S_0 and intersystem crossing to T_1. In either case, the energy-conserving nonradiative transition is followed by solvent-assisted vibrational relaxation, which converts the electronic excitation into heat.

$$S_1 \xrightarrow{k_{nr}} S_o + heat \qquad (3)$$

To separate the internal conversion and intersystem crossing processes from S_1, additional information, e.g., the quantum yield of triplet formation, would be required. For simplicity here, we combine the individual intersystem crossing and internal conversion rate constants into a single nonradiative rate constant, k_{nr}.

The decay processes (equations 2 and 3) are intramolecular. However, under certain conditions, the excited state lifetime is sufficiently long for bimolecular (intermolecular) processes to occur. The significant processes involve quenching (Q) and are represented in simplified form as:

$$S_1 + Q \rightarrow S_o + Q \qquad (4)$$
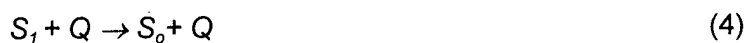
As long as the quenching process is irreversible and S_1 is not regenerated, equation (4) is adequate for our purposes.

The degree of quenching depends on the lifetime of the excited state, the type of solvent, the concentration of the solvent, and the temperature. Quenching increases when the

25

lifetime, concentration, and temperature increase and decreases when the viscosity of the solvent increases.

The fluorescence lifetime is the inverse of the rate constants of the radiative deactivation process (k_r), the nonradiative deactivation process (k_{nr}), any photochemical reaction process (k_p), the product of the quenching process (k_q) and the concentration of quencher [Q], (equation 5):

$$\tau_f = 1/(k_r + k_{nr} + k_p + k_q [Q]) \tag{5}$$

Another useful relationship involving the fluorescence lifetime is that between the fluorescence quantum yield and the radiative decay rate constant of fluorescence (equation 6).

$$\tau_f = \Phi_f / k_r \tag{6}$$

where Φ_f is the fluorescence quantum yield. The quantum yield is the ratio of the number of fluorescence photons to the number of photons absorbed. The excited state deactivates to the ground state via photon emission with rate constant k_r.[52]

The Stern-Volmer equation describes the effect of a quencher on excited state decay properties. For our purposes, it can be used to relate the lifetime in the presence of a quencher, τ, to the lifetime at zero quencher concentration, τ_0. This form of the Stern-Volmer equation is

$$\tau_o / \tau = 1 + \tau_o (k_q [Q]) \tag{7}$$

where k_q is the second order rate constant for quenching and [Q] is the concentration of the quencher.[53]

26

B. PRINCIPLES OF LIGHT TRANSMISSION IN FIBER OPTICS

Fiber optics are cylindrical waveguides used to direct light radiation in the ultraviolet, visible, and near- to mid-infrared spectral regions. Standard fibers have a concentric arrangement of core, cladding, and buffer regions. Light propagates through the core via total internal reflectance (TIR) at the core-cladding interface. The electromagnetic field of the light propagating in the core penetrates a few tens of micrometers into the cladding in the form of an evanescent wave. The function of the buffer is to prevent disruption of the core-cladding interface by water absorption, abrasion, and other processes.

A necessary condition for TIR is that the core must have a higher refractive index than the cladding. The numerical aperture (NA) of a fiber is related to its acceptance angle by,

$$NA = \sin \delta = \sqrt{(\eta_1^2 - \eta_2^2)}, \tag{8}$$

where δ is the half angle of acceptance and η_1 and η_2 are the core and cladding refractive indices, respectively.[54] The acceptance angle δ is defined by the ray of greatest angle that enters the core and undergoes TIR at the core-cladding interface; only those rays entering at angles less than δ are transmitted. The numerical apertures of plastic-clad silica fibers are in the range 0.23 to 0.48 with corresponding half angles of 13.3° and 28.7°. The numerical apertures of silica-clad silica fibers lie between 0.18 to 0.22 with corresponding acceptance angles of 10.4° and 12.7°.[55]

Numerical aperture, wavelength dependent attenuation, core diameter, and cost are the most important fiber parameters for spectroscopy. Most fibers used in spectroscopy are multimode step-index type, as opposed to small diameter multimode graded-index fibers used in telecommunications or polarization preserving (single-mode) fiber. Fibers with plastic, glass, or fused silica cores are available, but only fused silica will transmit sufficient ultraviolet light for fluorescence spectroscopy of aromatic hydrocarbons. Both plastic (polymer) and fused silica cladding materials are standard. Plastic cladding types are often differentiated into "hard" (usually some fluoropolymer) and "soft" (for example, silicone rubber) categories.

27

Light is attenuated by scattering, absorption in the core, or absorption of the evanescent wave in the cladding as it travels through the fiber. The shorter the wavelength of the propagating light, the greater the fraction of light loss per unit path length. The basic equation for the loss (L), expressed in units of decibels (dB), is

$$L \ (dB) = -10 \ log \ (I_{out} / I_{in}) \tag{9}$$

where I_{in} is input intensity and I_{out} is the output intensity.[56] Figure 2 shows representative data for plastic-clad silica and silica-clad silica fibers in the ultraviolet region. Attenuation in the ultraviolet region is higher than in the visible region, and the losses may be appreciable (50% or more) for probes longer than a few meters.

The core diameters of standard commercial fibers range from 25 to 1000 micrometers. It is generally advantageous to use a single large diameter fiber for delivery of excitation light, and a cross-section of fibers (a multifiber bundle) for fluorescence collection. Popular choices for core diameters are 200 μm or ca. 600 μm. A small cladding-to-core diameter ratio allows more compact packing of the fibers in a bundle. Typical clad to core diameter ratios are 1.1 to 1.5.

Fiber cost per unit length strongly depends on the choices of core material, cladding material, and core diameter. Silica-clad silica fiber is roughly three times more expensive than plastic-clad silica fiber for 200 μm core diameter and about five times more expensive for 600 μm cores. The cost of silica-clad silica fiber scales approximately with the square of the core diameter (proportional to the cross-sectional area); for instance, the cost is $2.05 for one meter of 200 μm fiber and $18.50 for a similar length of the same type of fiber with a 600 μm core diameter. The dependence on diameter is smaller for plastic-clad silica fiber. The costs per meter of 200 μm and 600 μm fiber are $0.74 and $3.65, respectively. These prices are as quoted by FiberGuide Industry (Stirling, NJ), which generally had the lowest prices of the companies consulted.

The velocity at which light travels through a fiber is given by the speed of light in vacuum divided by the refractive index of light in the medium at the specific wavelength. The refractive index of fused silica decreases with an increase in wavelength. The refractive index of fused silica at 265.2 nm is 1.50003, while the refractive index at 457.9 nm is 1.46498.[57] For a 1 meter probe, light at 265.2 nm takes 5.00 ns to travel through the probe, while light at 457.9 nm needs only 4.88 ns. The time shift between these two wavelengths is 0.12 ns. As the length of the probe increases, so does the length of time needed for the light to travel from one end to the other. It takes light at 257.9 nm 100 ns to travel through a 20 meter probe, while it takes the light at 457.9 nm only 97.7 ns. The time shift for these two wavelengths through a 20 meter probe is 2.3 ns.
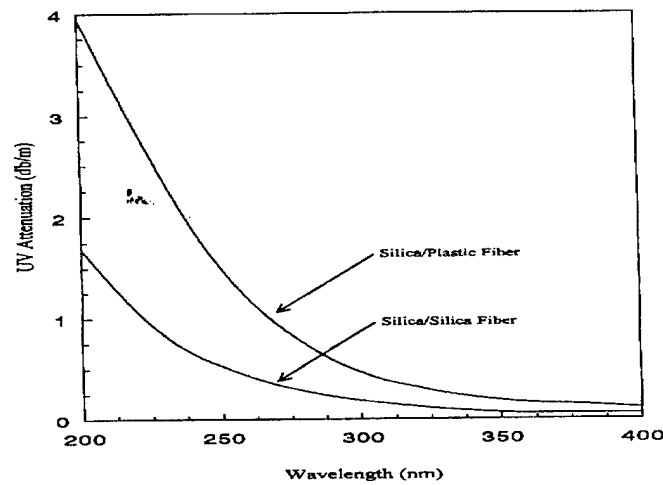

Figure 2: Signal attenuation through fiber as a function of wavelength.

SECTION IV
APPARATUS

A.   LASER SYSTEM LAYOUT

The instrumentation we have developed differs in two major ways from all of the other laser-induced fluorescence (LIF) units that have been proposed for field screening:

- the tunable laser source
- the incorporation of time-domain information

The Army and Navy rely on a fixed wavelength, nitrogen laser source (337 nm), which is limited in the range of compounds which can be excited for fluorescence. Ideally, a tunable excitation source can be wavelength optimized for specific situations in order to realize the multi-dimensional techniques. Kenny does achieve a measure of quasi-tunability with his Raman shifting source.[50] We anticipate future applications when the full tunability of our system will be critically important.

Compiled spectra (Appendix A), show that ultraviolet light is required to efficiently excite the fluorescence of the commonly occurring aromatic hydrocarbons. Almost all of the work reported in the literature has utilized the nitrogen laser, which has a single output wavelength at 337 nm. Unfortunately, this wavelength is too long to excite the aromatic hydrocarbons with only one or two rings. The nitrogen laser approach works reasonably well for aromatic hydrocarbons with compounds of higher molecular weight, or, "heavy fuels". Diesel fuel and coal tar are amenable to nitrogen laser excitation as is gasoline, although to a lesser degree. Along with a lower molecular weight, the solubility properties of aromatic hydrocarbons restricts the nitrogen laser approach in the detection of BTEX and naphthalenes.

The outputs of many CW (continuous wave) lasers occur at wavelengths too long for efficient excitation of aromatic compounds with less than three rings (see Appendix A for extensive compilation of spectral data). Pulsed lasers are required to supply the necessary ultraviolet light. Most of the excitation sources are inefficient for determining the fluorescence lifetimes of BTEX and small PAHs, which are major components of fuels, such as JP-4. The

fourth harmonic of Nd:YAG (266 nm) is an alternative that is worth consideration. The main limitation is that fiber transmission is much poorer at 266 nm than 337 nm. Depending on the length of the optical fiber, there may not be enough light exiting the fiber to perform the experiment.

Nitrogen, excimer, and Nd:YAG lasers have been the dominant lasers in the ultraviolet spectroscopy of PAHs in the laboratory environment. Each of these lasers is single wavelength such that any one wavelength can excite a select group of PAHs with high efficiency. A partial exception is the Nd:YAG laser which is capable of exciting PAHs at 266 nm and 355 nm, depending on harmonic generation crystal selection. To rely on these fixed wavelengths is tempting due to the simplicity of operation and extremely high energies available. However, because of the extremely inefficient excitation of many PAHs the sacrifice in speciation capability and sensitivity is a severe limitation.

The only available alternative for broad wavelength selection in the UV is the frequency doubled dye laser. With a combination of two dyes the majority of PAHs can be efficiently and semi-selectively excited. Dye lasers have had a reputation for being very difficult to align and maintain, preventing such systems from being deployed for field based applications.[58] However, dye laser technology has matured to routine laboratory uses with basic optical principles replacing the "art and magic". Our contention is for the feasibility of building a transportable dye laser capable of field application.

The results of our efforts to design and build a rugged, field portable laser system are described below. Details describing the relevant issues pertaining to the major components of this system are included. The following description covers the form as of the middle of 1993. The transportable dye laser system components are schematically indicated in Figure 3. The arrangement of the dye laser on a 2 x 4 foot optical breadboard is drawn approximately to scale at the top of the figure.

The system was assembled around an aluminum Uni-Strut frame bolted together in a configuration that results in efficient space utilization while allowing maintenance and future design modifications. To protect the unit from shock and vibration, a simple suspension system of bladders originally built for vibration isolation of milling equipment were purchased from a

local surplus supply store. The bladders were simple to install and are easy to maintain while providing for more than adequate mechanical shock protection. Casters are located under the frame to roll the instrument from lab to van. Inflation of the suspension bladders raises the frame to suspend the casters, which can be left in place during transport. This allows convenient movement of the system with no disassembly. The optical breadboard is covered with an opaque nylon cover to allow easy access to the breadboard.

1. DCR-11 Nd:YAG Laser

2. HG-2 Harmonic Generator

3. Dye Laser

4. Fiber Optic Probe

5. 0.32 Meter I.S.A. Monochromator

6. 200 MHz Tektronix 2440 D.S.O.

7. CyberResearch Expansion Chassis

8. Portable 80386 P.C.
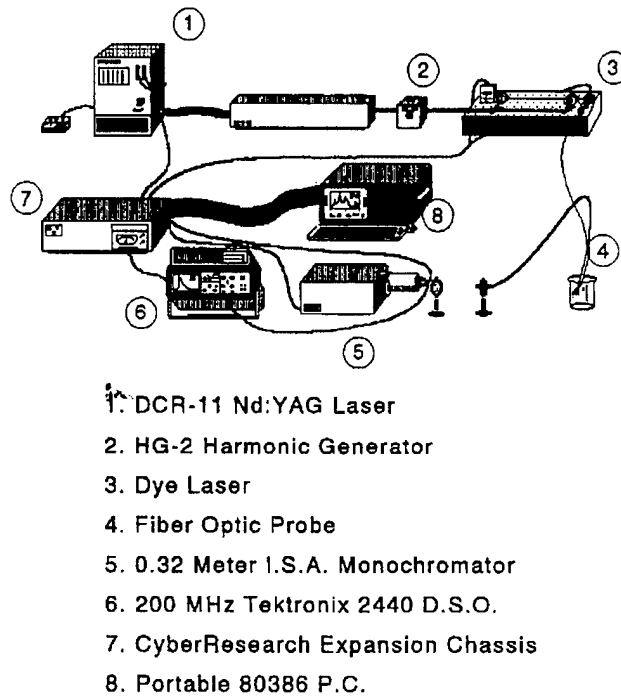
Figure 3: Component diagram of the spectrofluorimeter system.

1. Pump Laser

The dye laser is pumped by a Quanta-Ray GCR-12 Nd:YAG laser with 2nd, 3rd, and 4th harmonic generation capabilities. The laser is mounted on the breadboard beside the dye laser. No external cooling water is needed. The cube shaped power supply measures approximately 2 feet on each side and is powered with 240-208V single phase AC. The laser head is attached to the power supply by an 8 foot umbilical and measures $1 \times 1 \times 4$ feet including the harmonic generator. The laser can be operated either from a remote control panel

or via the control computer. Maintenance of the YAG laser consists of changing flashlamps, topping off the distilled water reservoir used to cool the flash lamp and rod along with changing the air cleaning and drying materials in the air filter.

The harmonic generator, located at the front of the laser head, is equipped with a heater to provide stable generation and keep the KDP crystals dry. Two separate KDP crystals are moved in and out of the beam path in various combinations and are rotated to yield the harmonic wavelengths mentioned above. Dry, clean air is pumped by a small internal pump at approximately 0.2 cubic feet/hour through the optical path of the laser and the HG-2 housing to keep the optics clean and dry.

2. Transfer Optics from Pump to Dye Laser

The output from the Nd:YAG is first turned down toward the breadboard with a Pellin-Broca dispersing prism. A turning prism turns the dispersed beam parallel to the breadboard. The selected pump wavelength (532 nm or 355 nm, depending on the dye used) is directed toward the dye laser cells and the residual Nd:YAG fundamental (1064 nm) is beam-blocked. Generation of sufficiently short wavelength light to excite the fluorescence of BTEX components requires 355 nm pumping of the dye laser. When the Nd:YAG is set up for 355 nm output, the 2nd harmonic at 532 nm and the fundamental at 1064 nm are simultaneously present. The fundamental and 532 nm beam (when pumping with 355 nm) are blocked with a carbon beam-block. About 20% of the pump beam is delivered into the oscillator cell. The remaining 80% is directed with a 90° fused silica prism upward through a 1 inch hole (drilled in a 2×4 foot optical breadboard on the top of the frame) and into an amplifier cell.

Tapped 10-24 holes are located on 1 inch centers across the entire breadboard. Optical components are fastened with machine screws to the table. The dye laser utilizes two home-built dye cells with a common dye reservoir and a 300 gph centrifugal pump for dye flow. The impeller is magnetically coupled to the motor and the impeller housing is composed of nylon with viton O-rings. This prevents any contamination of dye solution with pump materials.

3. Frequency Doubling and Fundamental Rejection

The output from the dye laser is frequency doubled in an angle-tuned and temperature stabilized KDP doubling crystal. Power levels are sufficiently high such that no focusing is necessary for efficient second harmonic generation. After doubling, the visible beam that remains is rejected with a colored glass filter. The UV light is focused on the end of the fiber optic probe. We use a gentle focus (f/20 lens) which greatly minimizes potential problems of fiber optic damage or generation of extraneous light in the fiber by nonlinear processes.

4. Fiber optic Probe

The probe has a conventional six-collection-around-one-delivery fiber configuration; all fibers are the 600 μm core diameter plastic clad silica fiber from Fiber Guide.

5. Detection System

The fluorescence collected by the fiber optic probe is imaged into a 0.32m monochromator (Instruments S.A. HR-320) and the dispersed radiation is converted to an electrical signal with a photomultiplier tube (EMI-9813) under a 1.80 kV bias. The PMT signal is carried by a coaxial cable to a Tektronix model 2440 digital oscilloscope for signal capture. The digital storage oscilloscope (DSO) samples at 200 MHz. The signal cable is terminated at 50Ω on both ends. This 500 megasample/sec DSO is capable of downloading complete waveforms, areas, averages, and intensity-at-time values, depending on the mode of operation. The DSO is capable of an equivalent time bandwidth of 300 MHz. With interpolation of points the maximum time resolution is one point every 200 picoseconds. 200 shots are averaged per waveform in a typical emission WTM experiment.

6. Control Computer

The entire system is under the control of a Gateway 2000®33 MHz 486 personal computer with a 220 Megabyte hard drive and 8 MB of RAM. The computer communicates via RS-232 with a stand-alone microprocessor that controls the stepper motors on the tuning mirror of the dye laser oscillator, the rotation stage on which the doubling crystal is mounted, and the leadscrew of the monochromator. Communication with the digital oscilloscope is accomplished with a GPIB bus.

7. Modifications for field operation

The current version of our field laser system occupies approximately 24 cubic feet and is easily loaded into a van for transport to remote sites. The volume could be reduced to under 16 ft^3 with existing technology at no sacrifice in performance. Electrical power (208 V single phase at 10A for the Nd:YAG, 120 V for the other components) in the field is supplied from a 5 kW gasoline-powered generator. The only difference between laboratory and field operation is the source of the electrical power.

Given the required ruggedness for field work, it was important to design, construct, and mount all components, in particular those of the dye laser, in a fashion that reduces the chance of vibration induced misalignment. This was accomplished with minimal sacrifice in performance by removing a number of luxury degrees of freedom found in commercial laboratory-based dye lasers. Size was also a concern so small components were chosen when available, although cost concerns limited the choice of some components. Some equipment was custom made in-house to reduce cost and/or to meet a specification not available on the retail market.

B.   PUMP AND DYE LASER PERFORMANCE

The heart of the system is a Quanta-Ray DCR-11 Nd:YAG laser equipped with an HG-2 harmonic generator. It generates 1064, 532, 355, and 266 nm wavelengths at energies of 275, 135, 60, and 30 mJ/pulse respectively. Pulse energies > 150 mJ at 532 nm and > 60 mJ at 355 nm are available at repetition rates up to 15 Hz, although pulse energies drop off at repetition rates above 10 Hz, which is the standard operating rate. The pulse width is 10 ns at full width at half maximum (FWHM).

Either the 532 or 355 nm wavelength light is used to optically pump various dye solutions. Pump wavelength selection is currently attained with a fused silica Pellin-Broca dispersing prism which also serves to turn the pump beam back into the horizontal plane. The prism is rotated on an axis parallel to the table and unwanted pump wavelengths are blocked with carbon beam blocks while the desired wavelength passes through a 1.5 cm hole in the beam block. Varying ratios of light are delivered to the oscillator and amplifier dye cells by use of beamsplitters.

With 355 nm pumping, a 100% reflective (at 0°) beamsplitter is rotated to 45° and is used to supply the oscillator cell with 50% of the pump laser power. The remainder is delayed by approximately four nanoseconds by directing the light down the table and back again with quartz prisms and finally delivering the light to the amplifier.

With 532 nm pumping, a 20% reflective (at 45°) beamsplitter is used to supply the oscillator with 20% of the pump beam and the remainder is again delayed before delivery to the amplifier cell. A 6 nanosecond delay is optimum, but 4 nanoseconds is sufficient and requires a less complicated delay line. The delay consists of steering the beam 2 feet down the table and reversing the beam direction back another 2 feet. The "donut" shaped YAG pump beam is converted into a thin line of light parallel to the table by a 76 mm focal length cylindrical lens for both dye cells. The cylindrical lens is followed by a 25 mm focal length plano-concave lens to fill the 4 cm wide face of the dye cells. This results in a 2 to 3 mm deep "cylinder" of excited dye molecules just inside the quartz face with each pulse of the pump beam.

The dye laser is diagrammed in Figure 4 and is built in a Littman grazing incidence configuration.[59] A 3° wedge prism is located 1.5 inches to one side of the oscillator cell. One surface of this wedge is positioned so that the surface reflects about 10% of the superradiant dye molecule emission back through the active dye volume. On the other side of the dye cell the pencil of stimulated emission strikes a two inch long, 2,440 groove/mm grating, located 2.5 inches from the other side of the cell, at near grazing incidence. The grating surface faces down, directing the dispersed beam down to a mirror positioned at variable angles with a stepper motor-controlled rotation stage.

For a given mirror angle, only a very narrow range of wavelengths is reflected back up to the grating and rediffracted back into the active volume. As these photons of selected wavelength pass through the excited region they stimulate emission of photons at the same wavelength. These selectively emitted photons are again partially reflected back through the cell by the 3° wedge and this cycle continues throughout the pump pulse duration in a cascading effect that creates a nearly monochromatic beam of photons. In this way, the mirror angle determines the wavelength. This monochromatic oscillator beam is then amplified by the amplifier cell to increase energy.
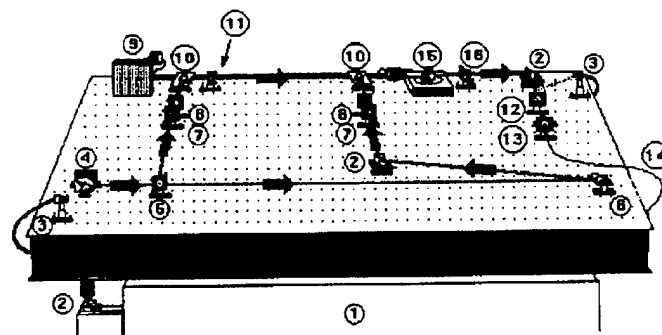
1. Nd:YAG Laser	9. Rotation Stage and Grating
2. 15 mm Quartz Prisms	10. Dye Cells
3. Photodiodes	11. 3 deg. Feedback Wedge
4. Pellin-Broca Dispersing Prism	12. 100 mm CVX Focusing Lens
5. Beamsplitter 20% at 45 Deg.	13. 5-Way Fiber Positioner
6. Quartz Prisms	14. 600 Micron Fiber Optic
7. Quartz Cyl. Lens (76 mm)	15. KDP Doubling Crystal
8 Quartz PCV Lens (-25 mm)	16. Visible Blocking Filter

Figure 4: Component diagram and experimental layout of the dye laser assembly.

The amplified beam emerging from the amplifier cell passes through a KDP doubling crystal. Laser beam doubling is dependent upon the angle of the crystal and the correct angle is attained by rotating the crystal on an axis normal to the optical table via the stepper motor-controlled rotation stage. Once the UV laser light of the desired wavelength is generated, it is separated from the visible dye laser beam with an Andover UG-5 or UG-11 visible blocking filter (UG-11 for longer wavelength use) and launched with a 50 mm focal length biconvex fused silica lens into a 600 µm, nylon-clad, silica fiber supplied by FiberGuide Industries. Positioning is accomplished with a Newport, five-way positioner.

Because of the significant attenuation of UV light in silica fibers, the system must supply relatively high levels of tunable excitation light. Table 1 shows both the best case energies and the average, everyday energies used during data acquisition with the current dye laser system.

TABLE 1. PULSE ENERGIES OF TUNABLE EXCITATION SYSTEM

Pump Wavelength	Pump Energy	Dye Laser Energy	Ultraviolet Energy
532 nm Best Case	50 mJ/pulse	15 mJ/pulse	4 mJ/pulse
532 nmAve. Exp.	50 mJ/pulse	5 mJ/pulse	0.5 mJ/pulse
355 nm Best Case	25 mJ/pulse	10 mJ/pulse	1 mJ/pulse
355 nm Ave. Exp.	25 mJ/pulse	2.5 mJ/pulse	0.3 mJ/pulse

Another important aspect of the laser is long-term stability. If a system is to perform with consistency, the source must operate in a stable fashion during analysis and must be easily returned to acceptable performance levels if drift has occurred. This was the case with the fundamental Nd:YAG beam of 1064 nm. The harmonically generated beams of 532 and 355 nm required occasional (less than daily) adjustment to return to optimization from a maximum drift $\leq$ 10%. Dye laser performance, however, was not as stable. A slight adjustment of the feedback optics was occasionally necessary to bring energies back up to acceptable levels from occasional misalignment which caused energy losses of up to 75% in 24 hours. These high drift rates were the exception, rather than the norm, with drifts of 10-20% per day being much more common. These energy drifts could have many origins:

- Actual physical "bumping" is suspected in the worst cases, as the optics protection systems were often not in place to allow for design improvements and adjustments.
- Some components are not as rugged as possible because of time restrictions and personnel shortage.
- Thermally induced expansion and contraction of the Uni-Strut chassis and an "economy grade" optical table are suspected of causing optical misalignment induced energy drifts in the 10-20% per day range.

Quantitative measurements were not always necessary during readjustment. Instead, tuning was done by visually monitoring the UV beam with a fluorescent card. The initial tuning of the dye laser following assembly or after optical design changes can take several hours. "Tweaking" of the instrument afterward to optimize performance takes very little time. A rigorous long term stability study was not pursued in light of the numerous higher priority studies.

The actual UV light generation of the system displayed satisfactory stability in the short term with maximum drifts of approximately 10-20% during concentration curve acquisition and Time-Wavelength array acquisitions (less than ten minutes). This is easily handled by energy normalization of the data such as temperature stabilization or pulse averaging.

Crystal temperature variation due to absorption of the beam directly affects doubling efficiency. When a "cool" crystal is tuned and the beam is passed through it, a slow warming occurs along with a loss of some doubling efficiency. Temperature stabilization of the crystal or a dedicated crystal positioner would solve any short-term energy fluctuations.

The averaging capability of the digital storage oscilloscope compensates for the shot-to-shot variation of the laser pulse energies. As averaging of the pulses continues, signal quality quickly reaches a "smooth" profile in 10-20 shots. From that point on, profile quality improves at a considerably slower rate and only under conditions of extremely low analyte concentration does continued averaging appear to be necessary or even desirable as this increases acquisition time. For any condition, the pulse reaches an apparent "steady state" after 20-30 seconds (200-300 shots).

C.   DYE LASERS CELLS

The first version of the transportable tunable laser utilized conventional transversely pumped, flowing dye cells. These were used through the first field studies at Tinker AFB in August 1991. Following the Tinker studies, we evaluated and switched to Bethune-type prism cells. Bethune cells use total internal reflection (TIR) to create a highly uniform illumination of a circular cross-section of dye passing through a small diameter bore, drilled parallel to the vertex of a right angle prism. Although the basic design was reported over ten years ago,[60] prism cells are offered only as options by the commercial dye laser manufacturers. The few publications citing their use show them employed as either amplifier cells or in broad band oscillators. We have found that prism cells also offer excellent performance as oscillators. Both open and closed cavities have been used successfully. Bethune cells can eliminate several optical elements found in conventional cells.

Commercial manufacturers, including Lumonics and Continuum, offer Bethune cell options on their dye lasers only as amplifiers. Bethune cells are often thought to be too inefficient for use in oscillator configurations. Since Bethune cells operated as tunable laser oscillators had not been satisfactorily evaluated for our needs, we proceeded with our own evaluation.

Pulse energy, pulse duration, conversion efficiency, bandwidth (or bandpass), polarization, beam quality, divergence, level of amplified spontaneous emission, shot-to-shot stability, and long term stability are parameters of a dye laser's overall performance. Beam quality, polarization and bandpass are relevant because the visible output of the dye laser must be frequency-doubled to the ultraviolet region of the spectrum and high beam quality, linear polarization, and narrow bandpass enhance this non-linear conversion process. The following variables affect Bethune cell dye laser performance:

- input pump energy
- dye concentration
- bore size
- length of irradiated area in prism cell
- type of diffraction grating
- oscillator configuration (open vs. closed)
- reflectance of output coupler (closed configuration)
- oscillator cavity length
- optical delay of pump pulse to amplifier
- pulse repetition rate vs. dye flow rate

The relationship between these parameters is complicated and non-linear in nature. For example, decreasing the bandpass of the output by increasing the oscillator cavity length results in increasing the lasing threshold which in turn lowers the overall conversion efficiency. A slight angular deviation of an optic in one dimension may only decrease the laser output by a few percent while the same deviation in another dimension may cause lasing to cease altogether.

The Bethune dye laser configuration promised to be a robust and durable design and was thus considered better suited for use in the NDSU field transportable instrument. The initial efforts to characterize the Bethune style design focused on determining the laser's conversion

40

efficiency which is measured as the ratio of output to input energies. The characterization in terms of conversion efficiency relied on measurements of pulse energy as a function of input pump energy. Plots of this type yield slope efficiencies and thresholds for laser action.

The main activity in the dye laser characterization focused on conversion efficiency and tuning range, the determining factors for applicability of the system to field screening methods. Another goal was to develop and establish procedures that can be used in the future to evaluate other dyes, pump lasers, and cavity configurations. Evaluations were performed for three different dyes: R6G, C500, and C460. The former two are used in the double dye laser system built for Tinker AFB, allowing us to examine both 532 nm pumping (R6G) and 355 nm pumping (C500). C460 was chosen since preliminary work had been done using a Lumonics excimer laser as a pump source (308 nm).

D. EXPERIMENTAL

1. Equipment

The pump laser was a Spectra-Physics GCR-11 Nd:YAG. The dyes were purchased from Exiton and the solvent used was Mallinckrodt™ brand spectroscopic grade methanol. A Molectron J25 power meter was utilized to measure the pump pulse energies and the dye laser oscillator and amplifier output energies. When needed, a negative lens was placed in front of the power meter to expand the pulse energy across a larger surface area of the detector to avoid damage. Software was written specifically for this project in Microsoft QuickBasic using the Professional Development edition.

The diffraction grating and tuning mirror in the dye laser oscillator cavity were stripped from a commercial dye laser. Because the instrument could not be readily retrofitted with Bethune prism cells, the wavelength tuning module and hand control pad were taken from a Lumonics HyperDye-300 dye laser and mounted on an optical table. The grating has 2400.4 lines/mm and is at approximately an 86.1° angle of incidence. The oscillator cavity has an overall length of 33.5 cm: the tuning mirror to grating distance is 55 mm, 175 mm from center of grating to oscillator cell, 45 mm cell width, and 60 mm from cell to the end element (a wedged window as partial reflector in closed configuration and full reflector in open configuration). The

41

amplifier cell was also a Bethune type cell, placed 32 cm from the oscillator cavity. The oscillator cell and amplifier cell each have bore diameters of 1.6 mm.

The prisms cells were fabricated in-house and the prism cell mounting fixtures were custom machined. The cells and mounting fixtures are similar to those commercially available. Because commercially available cells were too easily broken, improvements were made in the interest of strength and durability. A prism cell is made by drilling a hole in one right-angled prism and in two quartz disks, then affixing the disks to the prism. The disks provide a convenient holding surface for the prism and a means of preventing dye leakage.

2. Prism Manufacture

The UV grade quartz 90° prisms and disks were supplied by Esco Products, Inc. We typically use knife edge prisms, 15 or 20 mm in width. A knife edge finish is preferred over a beveled (chamfered) edge for several reasons. When machining, the placement of the drill is critical, visual perception of the edge of the prism is more precise when there is no chamfer present. Chipping and breakage occurs to a larger degree with a beveled edge especially in the area between the drilled hole and the edge nearest to and parallel with the drilled hole. It is necessary to resurface the prism end faces after machining. Conversion efficiency is adversely affected because of the small amount of pump light that is lost out the flattened prism vertex. This occurs because the 45° angle of incidence needed for total internal reflection has been lost with the beveled edge.

The drills were purchased from Lunzer Industrial Diamonds, Inc. The drill bits are referred to as diamond plated core drills and consist primarily of high precision tubing with diamond grit impregnated on its side and end. The drills were mounted in nuts that connected to a specially designed "Water-Swivel" (also supplied by Lunzer) with a 1/2" drive shaft that fits into any drill press or milling machine. The Swivel permits coolant under pressure to pass through the inside of the hollow drill while rotating. Plain tap water may be substituted for the drilling coolant, but it must be delivered under high pressure. For 1-3 millimeter diameter holes the water should be supplied at 90 psi. A high pressure delivery source was fabricated out of a portable air tank connected to an air compressor. It is imperative that the drill remains

unplugged. As the drill passes through the quartz prism, the material protruding up into the center of the drill may break free and clog the drill. This shortens the lifetime of the drill significantly.

The choice of the bore diameter depends on the beam dimensions of the dye laser pump source. Ideally the beam height should be four times the bore diameter and the beam width should equal the width of the prism hypotenuse face.

The end faces of the prisms and the disks must be resurfaced after drilling to remove any small chipped regions from around the hole. Diamond grit sanding disks obtained from Hi Tech Diamond Products were used to ensure that the opposing faces remain parallel.

Several methods have been used to fasten the disks to the prisms. One method employed a two component epoxy supplied by Master Bond, Inc.. After mixing the epoxy, the pieces were aligned and glued by stacking them on stainless steel hypodermic tubing, which was covered with Teflon® tubing. The Teflon® tubing ensured that the prism cell would not stick to the alignment pin in the event that epoxy seeped to the bore interior during assembly. The epoxy was advertised as having outstanding resistance to organic solvents, but our experience found that prolonged exposure to the methanol in combination with periodic UV irradiation would turn the clear epoxy a dirty yellow-brown color, followed by glue failure.

Another method of attaching the disks to the prisms was provided by Vitta Corporation and utilized a glass transfer tape. The transfer tape consists of a thin Borosilicate film. The tape is applied between the pieces which are then aligned with a precision stainless steel hypodermic tubing mounted vertically on a piece of stainless stock. Another piece of stainless is placed atop the quartz assembly to provide a greater static pressure at the prism/disk surfaces. The entire assembly is then slowly heated to 900°C and held for two hours. The quartz disks become permanently fused to the quartz prism. This method of attaching the disks is more effective than the gluing technique, but is more difficult. The transfer tape is quite hard to work with and has a limited shelf life.

Figure 5 depicts the Bethune cell assembly. Buna o-rings were used to seal the dye circulatory system and to hold the prism cell unit. The prism cell holders were made as two

"halves" with the prism cell sandwiched between. Several holding jigs were necessary for machining. One jig holds the prism vertex parallel to the mill spindle axes. Another jig holds the disks for drilling and sanding. A third jig used for positioning the drill on the prism end has a guide that indicates the bisection of the 90° angle. The operator must visually assess the distance from the vertex.
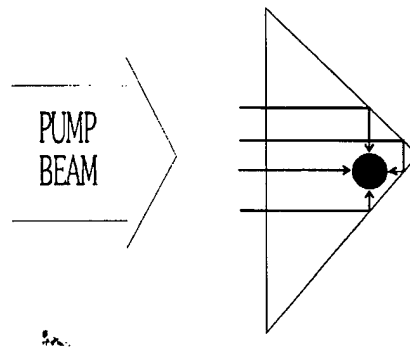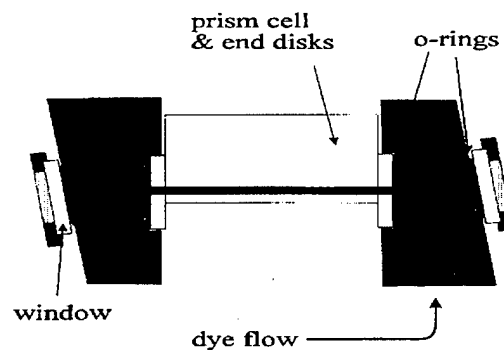

Cut-away view of prism cell holder.

Figure 5:Cut-away views of Bethune cell assembly. Top: directional control of impinging light into the dye cross-section. Bottom: end-cap assembly and flow of dye solution.

44

3.   Alignment Process

The alignment process follows these steps:

a) Observe back-reflection off prism face for proper beam position relative to entry into Bethune cell. Back-reflection should be coincident   with   incoming beam.

b) View into prism bore while slowly turning up pump intensity. Look for indication that dye concentration is neither too concentrated (cross section not fully illuminated) nor too dilute (full illumination does not change intensity with increasing pump power).

c) Place full reflector 1-8 inches from side window for feedback, and align reflector until "brighter" circular images with intensified concentric circle(s) appear. If the image is not round, dilute dye concentration.

d) Place the grating in the beam path.

e) Align the grating until the reflected beam image appears "clipped".

f) Place the tuning mirror normal to the first-order diffraction.

g) View back-reflection off the grating against the side of the prism holder.

h) Align until the back-reflection is on the same plane as the beam exiting the prism.

I) Slowly rotate mirror so that the back-reflection goes back through the prism.

j) Replace first mirror with wedge window for closed configuration.

4.   Methodology

The first systematic study was the variation of output coupler reflectance for a given concentration and pump energy. This was done to assess whether different output couplers required different optimum dye concentrations for maximum conversion efficiency. Both open and closed cavities were examined simultaneously. The input pump energy was varied by holding the Nd:YAG energy constant and inserting a variety of beamsplitter combinations into the Nd:YAG beam path to achieve the desired pulse energy at the Bethune cell face.

The testing cycle began with a low C500 dye concentration and a small amount of C460. The first beamsplitter combination was placed in the Nd:YAG beam path and the

pump energy was measured with a power meter, fine adjusting the Nd:YAG as needed to compensate for power drifting. The appropriate optic (wedge, partial reflector or mirror) was then inserted into the oscillator cavity and aligned to give the maximum energy output at the peak of the dye tuning range (approximately 505 nm). The maximum output was monitored using a power meter. A laser tuning curve was then generated by stepping the tuning module in 5 nm increments and averaging the power meter response over 50 (eventually 30) laser shots. The pump energy was then decreased to the next value by inserting the appropriate beamsplitter combination in the Nd:YAG beam path, and fine adjusting the energy.

A variety of tuning curves was generated, each corresponding to different pump energies for the same feedback optic/dye concentration combination. The final step was placement of the next feedback optic in the oscillator cavity. The entire cycle was then repeated. After all feedback optics had been tested, the dye concentration was increased by adding a small amount of dye powder to the circulator. The entire cycle was repeated using the new dye concentration.

Next, the optimal C500 concentration was determined for the open configuration and for one closed configuration (using the wedged window as output coupler). As before, the optical elements were changed after altering the pump energies, the dye concentration was then increased and the process repeated. It was determined that the optimum dye concentration for maximum output was the same for both the open and closed configurations.

The C460 and R590 optimum concentrations were determined in the closed configuration by changing the dye concentration and monitoring the output energy at a selected wavelength (Figure 6). The tuning control module was set to a wavelength near the dye's maximum gain (corresponding to the peak of the dye's tuning curve). The dye concentration was increased, while keeping the pump pulse energy constant. The C460 dye was pumped at 355 nm with a pulse energy of 16 mJ and monitored at 460 nm. The R590 dye was pumped at 532 nm with a pulse energy of 18 mJ and monitored at 590 nm.
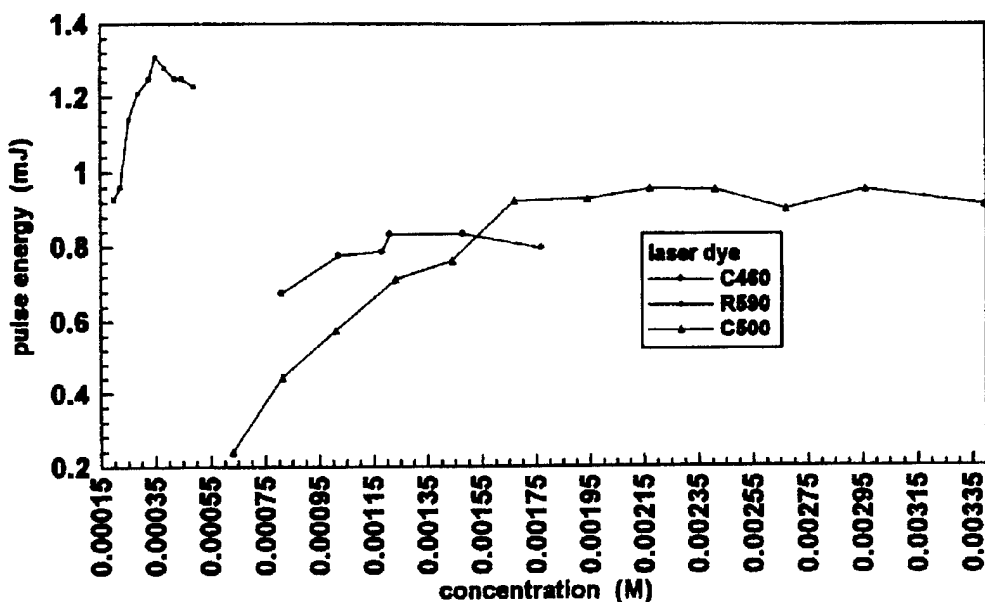
Figure 6: Oscillator outputs for C460 and R590 laser dyes over a range of dye concentrations.

5. Fiber Probe Assembly

After the excitation beam has been generated, it is launched into the excitation fiber and exits the homemade probe illustrated in Figure 7. The probe consists of Torr-Seal brand epoxy, glass tubing, heat shrink tubing, and fibers. Six detector fibers surround a central excitation fiber in the standard arrangement. Side-by-side two-fiber probes can be built for testing applications where fluorescence intensity is sufficient to yield acceptable signal levels.[61] In the six-around-one probe the return bundle is arranged in a vertically stacked orientation for launching into a stepper motor controlled, 0.32-meter Instruments SA monochromator equipped with 1800 groove/mm grating. A 2-inch, 30 cm focal length fused silica lens is used to focus the collection fiber light on the slit. A Thorn EMI model 9813B photomultiplier tube (PMT) was used for signal amplification.

Excitation
Fiber

Emission
Fibers

overlap
regions

End - On
View
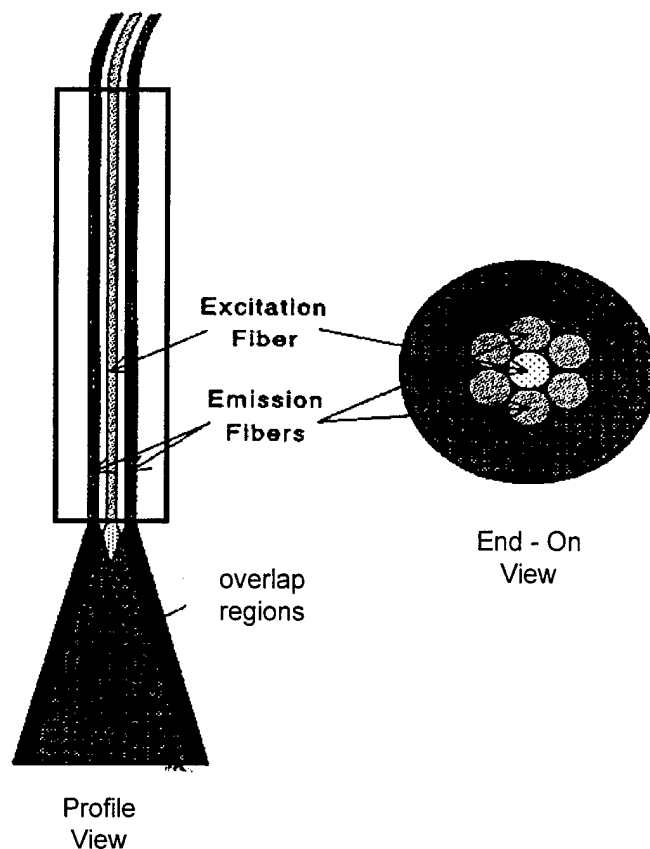
Profile
View

Figure 7: Schematic diagram of the probe.

Profile view of overlapping cones of acceptance; end-on view of geometric efficiency
of the six-around-one arrangement.

The performance of the current probe design was quite satisfactory. The design affords good rejection of both molecular and particulate scatter and allows fluorescence to be gathered at a level which yields excellent detection limits. The design facilitates consistent assembly with a minimum of time and effort, a minimum of materials and no need for alignment mechanisms. Polishing of the probe to a flat finish is easily accomplished by free hand on a low cost rock polisher. If any damage occurs to the surface, the probe can be ground away to a fresh surface and quickly polished. With angle sensitive arrangements, an entirely new probe would have to be assembled. Finally, the very slim probe design can be inserted into very small diameter spaces or well casings (<0.25 inches).

Torr-Seal epoxy appears to have excellent durability even after long-term, intermittent exposure to water. We did note some piston-like movement, in which the core and cladding move in and out of the buffer (protective jacket surrounding the fiber), apparently because the epoxy swelled after absorbing water. This does not appear to affect performance, because the degree of pistoning is nearly the same for each fiber such that the geometric relationship between the fibers is maintained. This is not the case for any other arrangement.

Pistoning can be avoided by removal of the fiber buffer from the epoxied region. Attachment of a small quartz window onto the probe protects it from direct exposure to solution. This was done on highly concentrated JP-4 jet fuel-water solutions and on neat JP-4 jet fuel. At these concentrations, absorption of the laser beam occurs in such a short distance from the excitation fiber that the resulting fluorescence occurs outside the cone of acceptance of the collection fibers. The quartz window allows the beam to expand before contacting the highly absorbing solution, allowing the fluorescence to occur within view of the collection fibers.

A 2-3mm wide laser beam was launched into the probe with a quartz lens and a five-way positioner. A jawed holding device taken from a mechanical lead pencil held the fiber in place within the positioner. This allowed easy cleavage of a new surface in case of energy induced or accidental damage. Average launching efficiencies were 10% for cleaved surfaces. Efficiencies of 60% were achieved with polished ends. Cleaved launch surfaces were used for convenience throughout the experiments and to avoid additional delay time needed to mount and polish fibers. Future designs will incorporate a short launching section of fiber composed of either a permanent polished standard fiber or a polished tapered fiber. This section will be terminated with a conveniently accessible coupling device to enable switching between various probe designs.

E.   RESULTS OF DYE LASER OPERATION

1.   Matching Pump Beam Width to Bethune Cell Width

To couple the maximum energy from the pump source into the Bethune cell, the physical dimensions of the pump beam should be equal to the width of the prism and the height of the beam four times the diameter of the hole drilled in the prism. A pump beam height greater than four times the hole diameter results in wasted pump photons. A pump beam

height less than four times the diameter leads to asymmetric pumping of the dye volume. Underfilling causes the profile of the output beam to change such that the output is no longer a symmetric circular beam. The advantage of using the Bethune prism to obtain superior beam quality is then lost. The dynamics involved for a pump beam that is narrower than the prism cell are subject to a variety of effects. The most prominent effects are believed to be dead volume absorption, length of the lasing medium, and gain saturation.

Dead volume is the region of unpumped, and therefore unexcited, dye molecules. Rather than being excited and emitting radiation, the dye molecules absorb a fraction of the radiated emission, raising the lasing threshold and lowering the lasing efficiency. There are benefits to having longer regions of active gain. A systematic study would include a variety of prism cell widths, each having lengths of equal dead volume. Saturation effects should also be considered. A high pump energy flux over a relatively small dye region may result in excess pump photons that are never absorbed by the dye molecules, again resulting in an overall lower conversion efficiency. This may also be the process involved when the ratio of output to input pulse energies begins to decrease as the pump energy is continually increased.

The diameter of the input beam with respect to the bore diameter of the prism must be considered when amplifying with Bethune style dye cells. Amplification with prisms having greater diameters than the oscillator prism results in distortions in the profile of the oscillator beam. The gain of the laser dye is controlled by the absorption of the pump beam by the dye molecules, which falls exponentially as the pump beam penetrates into the dye medium. For moderate to high dye concentrations the region surrounding the outer perimeter of the drilled hole provides considerably greater gain than the region lying along the axis of the bore. Looking into the end of the amplifying cell while it is being pumped, a donut-like image is observed which results from the majority of the pump beam being absorbed around the circumference of the hole. Thus an increase in amplification occurs when the oscillator beam is deviated from the center of the amplifier bore toward one edge. The amplified beam is distorted because of nonsymmetrical amplification. In this series of experiments the oscillator and amplifier cells had equal bore diameters.

When studying the C460 dye, the pump beam of the Nd:YAG was roughly 7 millimeters in diameter. Expansion of the pump beam to nearly 17mm in diameter was

accomplished by placing a plano-convex lens approximately 3 focal lengths from the prism face. The pump beam filled the entire image of the bore. A 47% reduction in the lasing threshold was obtained but the actual reduction of the threshold is more dramatic. By enlarging the pump beam with the plano-convex lens, a large amount of the pump energy is wasted. The region of the beam falling outside of the 6.5 millimeter image on the prism face (four times the bore diameter) is never absorbed by the dye, raising the apparent threshold. Thus, the 47% reduction is a lower limit.

In all subsequent studies, a cylindrical lens expanded the pump beam only in the horizontal dimension to match the length of the bore in the prism. In the horizontal dimension, at a distance greater than 2 focal lengths from the lens, the beam expands. In the vertical dimension, the beam is unchanged. A more systematic study would require single beamsplitters capable of delivering the desired pump energy and confining of the pump beam to specific boundaries with the use of a mask or similar device. Several of the pump energies used in the C500 dye laser utilized several beamsplitters placed in the main YAG beam path simultaneously. The multiple pump beams were of different energies and resulted in the dye being inhomogeneously excited along the length of the bore. By using a mask, the pump beam can be shaped to the exact dimensions of the image on the prism face, allowing for critical measurement of the pump energy incident on the dye volume.

2.   Oscillator Cavity Alignment

The alignment of the grating plays an important role in a Littman grazing incidence configuration. If the ruled lines of the grating are not perpendicular to the plane of incidence of the laser beam, a misalignment results. If the laser is in alignment at one end of the dye's tuning range, lasing may cease prematurely at the other end of the spectrum. A slight adjustment of the tuning mirror will restore lasing at the expense of a decreased range at the other end of the spectrum. There is a certain degree of difficulty in achieving proper alignment, although a slight misalignment may be desirable. For example, the tuning module used in these experiments was manufactured with the grating slightly skewed. The laser was intended for use with a wide variety of dyes. If the grating and mirror were in perfect alignment, for certain wavelengths, it may have been possible for the light reflecting off the mirror to undergo

51

a diffraction off the grating back onto the mirror and establish a competing cavity, adversely affecting the oscillator behavior.

Figure 8 shows the effect of optimizing the dye laser output to favor either the longer or shorter wavelength end of the tuning range for each dye. Maximum output, efficiency, is obtained by optimizing the alignment of the oscillator cavity to give maximum pulse energy when at the maximum gain region of the dye. The oscillator cavities for the C460, C500 and R590 dyes were optimized to give maximum output when the dye laser tuning module was adjusted to 460 nm, 505 nm and 590 nm respectively.
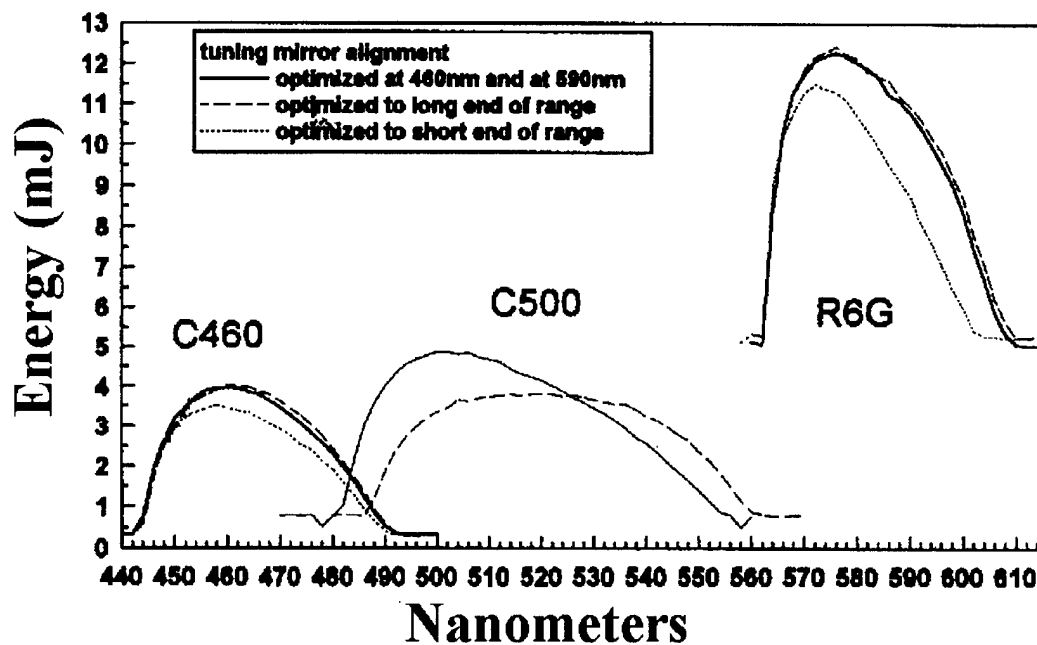
Figure 8: Dye laser output

3. Effect of Different Output Couplers On Tuning Range

When constructing a dye laser oscillator, several design parameters and performance characteristics came into play for both open and closed configurations. The closed configuration has two paths for light loss. Radiation passes through the output coupler

(partial reflector), or, some of the light that strikes the grating experiences diffraction and falls on the tuning mirror. The remaining light experiences reflection off the grating and is lost.

The open cavity configuration replaces the partial reflector with a full reflector and all radiation is lost via reflection off the grating. The open cavity has the benefit of a lower lasing threshold and higher efficiency, but the closed cavity has the benefit of lower amplified stimulated emission (ASE). The optical elements used to make the cavity, such as the grating and the output coupler, also contribute to the performance.

The type of grating employed affects the output in a number of ways. An obvious parameter is the bandpass of the output. A higher groove density results in narrower bandpass. The type of grating and its positioning also contribute to efficiency and should effect the level of amplified stimulated emission (ASE), depending on the oscillator configuration. When used at very high angles of incidence, the diffraction efficiency of a grating becomes low. (The ratio of the amount of light diffracted to the amount of light reflected becomes low.) This raises the lasing threshold and should increase the amount of ASE for the open configuration. Manufacturers often compensate by using the grating at lower angles of incidence and inserting a beam expanding device between the oscillator and grating in order to illuminate a larger number of grooves. The grating itself also makes a difference. For example, a holographic grating probably operates less effectively than a ruled grating that is blazed for a particular wavelength. The tuning module used had a fixed grating at a fixed angle of incidence.

Changing the reflectivity of the output couplers in the closed configuration had no substantial effect on the tuning range of the dye. The relative amplitude of the tuning curve changed for each output coupler, but the overall shape remained the same.

The C500 dye concentration of 16mJ gave the maximum output energy in both the open and closed configurations (Figure 9). The tuning range slowly broadens as the optimum concentration is reached and that output of the closed configuration is more dependent on concentration than is the open configuration.
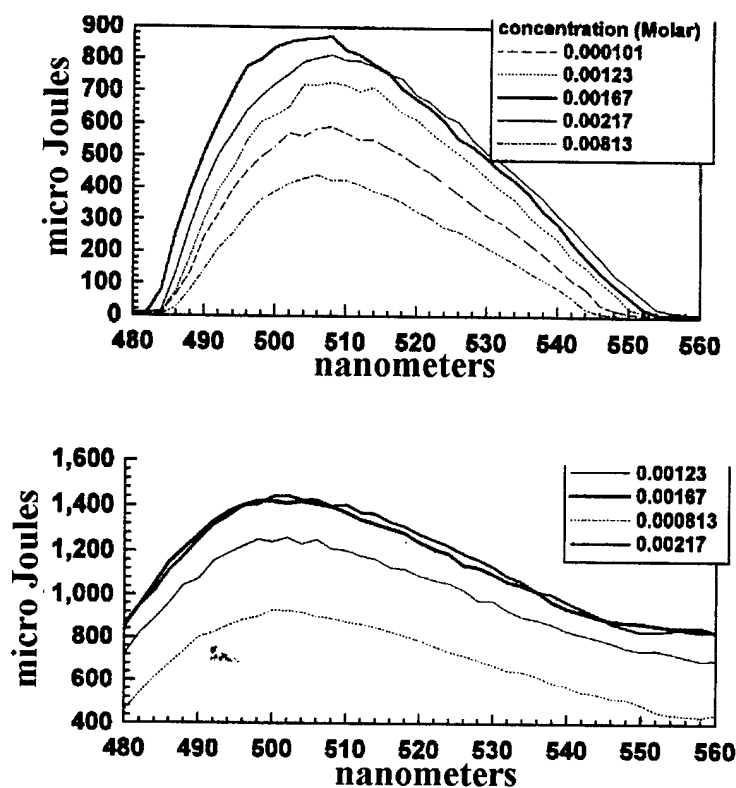
Figure 9: Tuning ranges of closed (top) and open (bottom) configurations.

4.   Conversion Efficiency Dependence On Concentration And Pump Energy

Figure 10 shows a graph of oscillator conversion efficiencies as a function of concentration for the C500 dye laser over a variety of different pump intensities. Both open and closed configurations are presented. The conversion efficiency is determined by the pump intensity and the dye laser pulse energy at the wavelength of maximum output as measured with the power meter. Nominally, the output was measured at 505 nm. As the concentration exceeds the optimal, the conversion efficiency falls off more rapidly for the closed configuration. The conversion efficiency for the open configuration plateaus earlier than the closed. It also appears that the conversion efficiency in both configurations plateaus earlier for greater pump energies. Determination of peak conversion efficiencies for the C460 and R590 dyes were

54

performed at single pump energies, 16 for C460 and 18 mJ for R590, in closed configuration. The effect of altering the pump delay to the amplifier cell is graphed for C500 dye in Figure 11.

This study considered only the pulse energy of the laser output. Literature searches of previous studies implementing Bethune cells as broadband oscillators indicate that near gaussian profiles of the beam cross-section are possible, but at low concentrations. As the dye concentration increases, the beam profile flattens until eventually the beam is ring-like. Even if the oscillator output was not ring-like, it would be possible to create a donut beam upon amplification. This was observed on the C500 dye laser. The amplified output had enough intensity to view the image of the beam against a graphite beam block. By diluting the dye concentration in the amplifier cell, the beam pattern can be seen to change from a bright ring image to a filled-in circular image. Figure 12 describes a measure of the amplified stimulated emission (ASE) for the output of the C460 dye laser using a spectrograph equipped with a CCD.
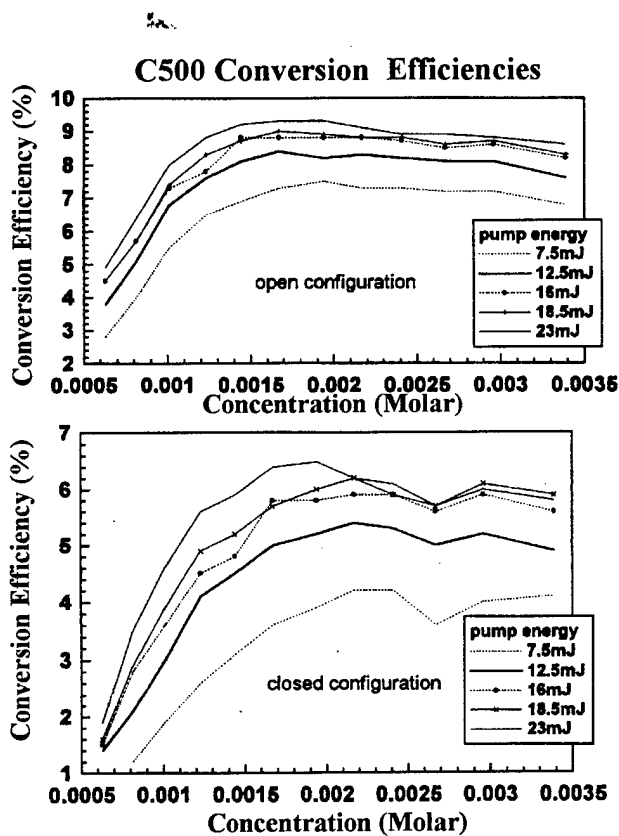
Figure 10: Peak conversion efficiencies for the C500 oscillator
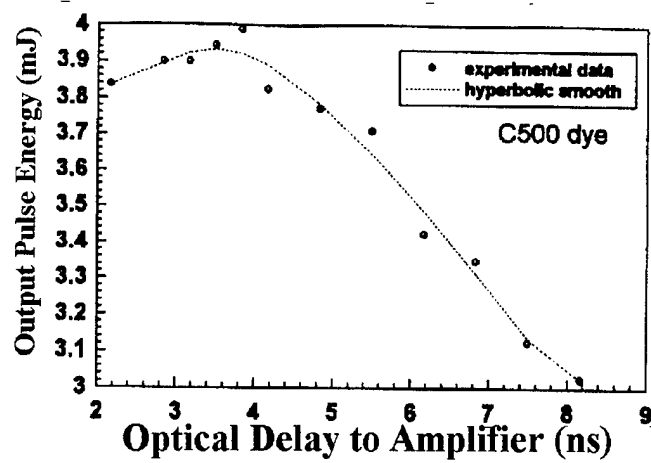
Figure 11: Effect of pump delay to amplifier cell.
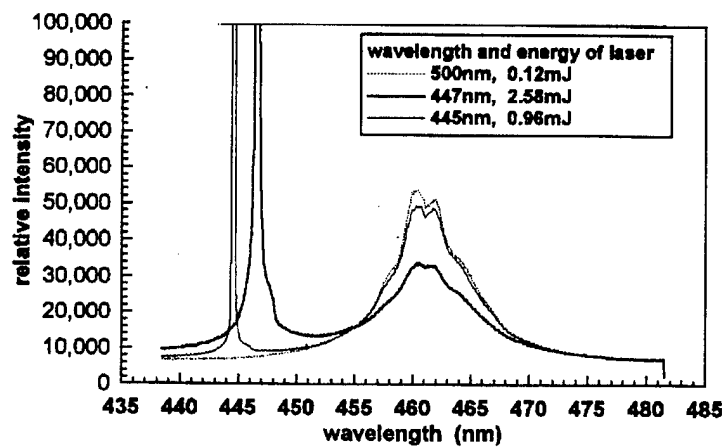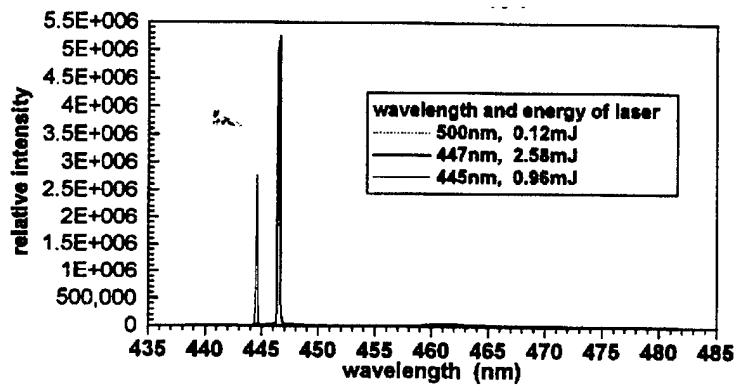
Figure 12: C460 Laser Output with CCD. (Bottom shows expanded vertical scale.)

SECTION V

SPECTROSCOPIC RESULTS

Four different environments were investigated: air-saturated and deoxygenated alkane solutions and the corresponding air-saturated and deoxygenated aqueous solutions. Research goals were: (1) Generate a database of fluorescence lifetimes for BTEX and naphthalenes in aqueous solution; (2) Establish the accuracy and precision of lifetimes measured with a digital oscilloscope and fiber optic light delivery and collection; (3) Assess the effect of dissolved oxygen, naturally occurring anions, e.g., chloride or sulfate, and humic substances on lifetimes.

A.   EXPERIMENTAL METHODS

We have assembled a database of fluorescence and fluorescence excitation spectra for approximately 25 aromatic hydrocarbons in aqueous solution. The spectra were acquired with a standard spectrofluorimeter equipped with a xenon arc excitation light source, double monochromators for both excitation and emission wavelength selection, and single photon counting detection.   Concentrations of the analytes were kept sufficiently low so that reabsorbance effects on the spectra were negligible. The spectra were corrected for both intensity variation as a function of excitation and the wavelength response of the detection system.

Figures 13, 14, and 15 summarize the data by plotting the mean fluorescence wavelength and full-width at half maximum for all the compounds in the database. There is a general trend of fluorescence intensity distribution shifting to longer wavelengths with increasing size of the molecule. These figures represent the excitation efficiency for individual compounds, but do not show the excitation efficiency of one compound relative to another.
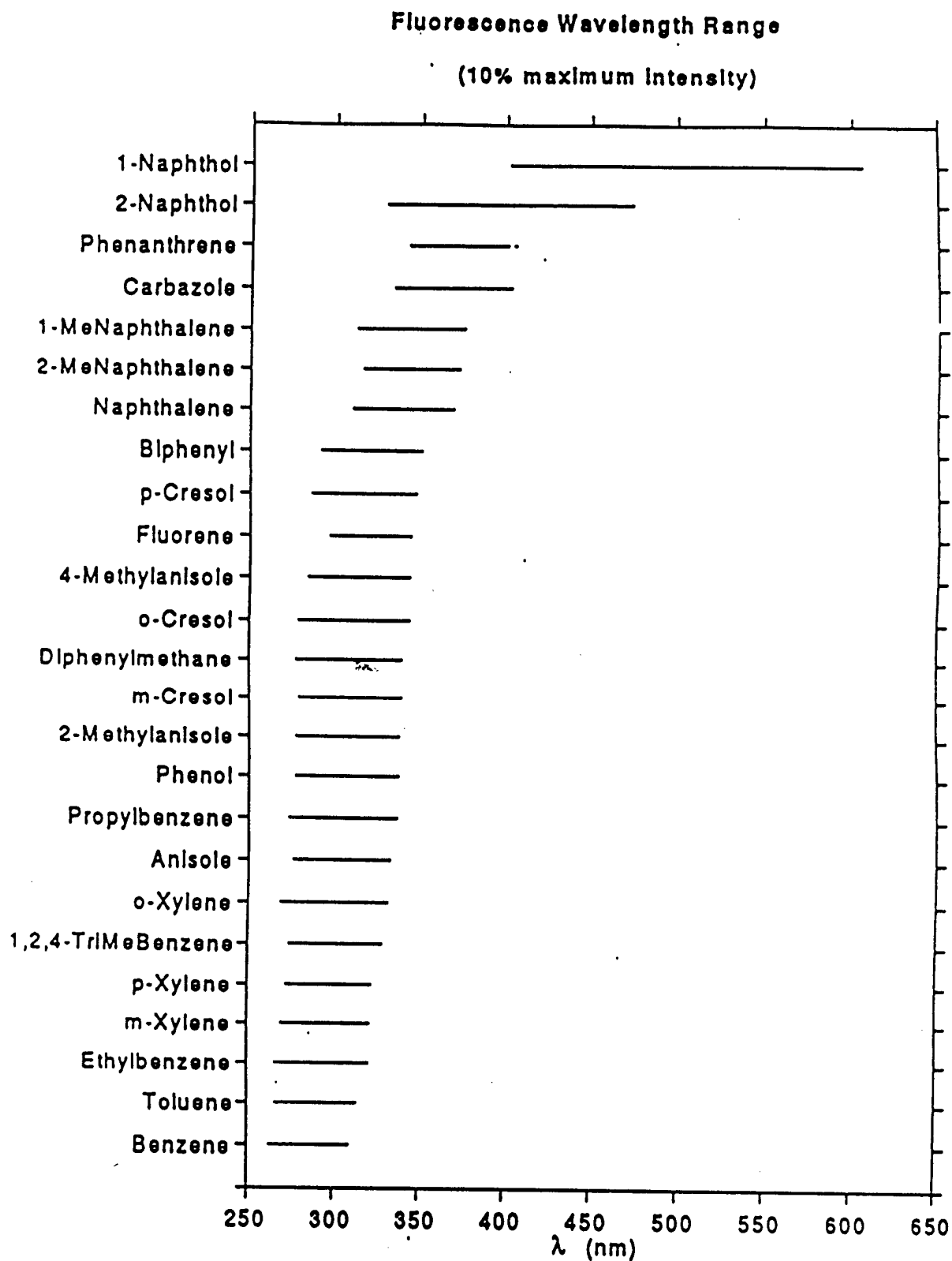
Fluorescence Wavelength Range

(10% maximum Intensity)

Figure 13: Fluorescence wavelength range (10% maximum).

Fluorescence Wavelength Range
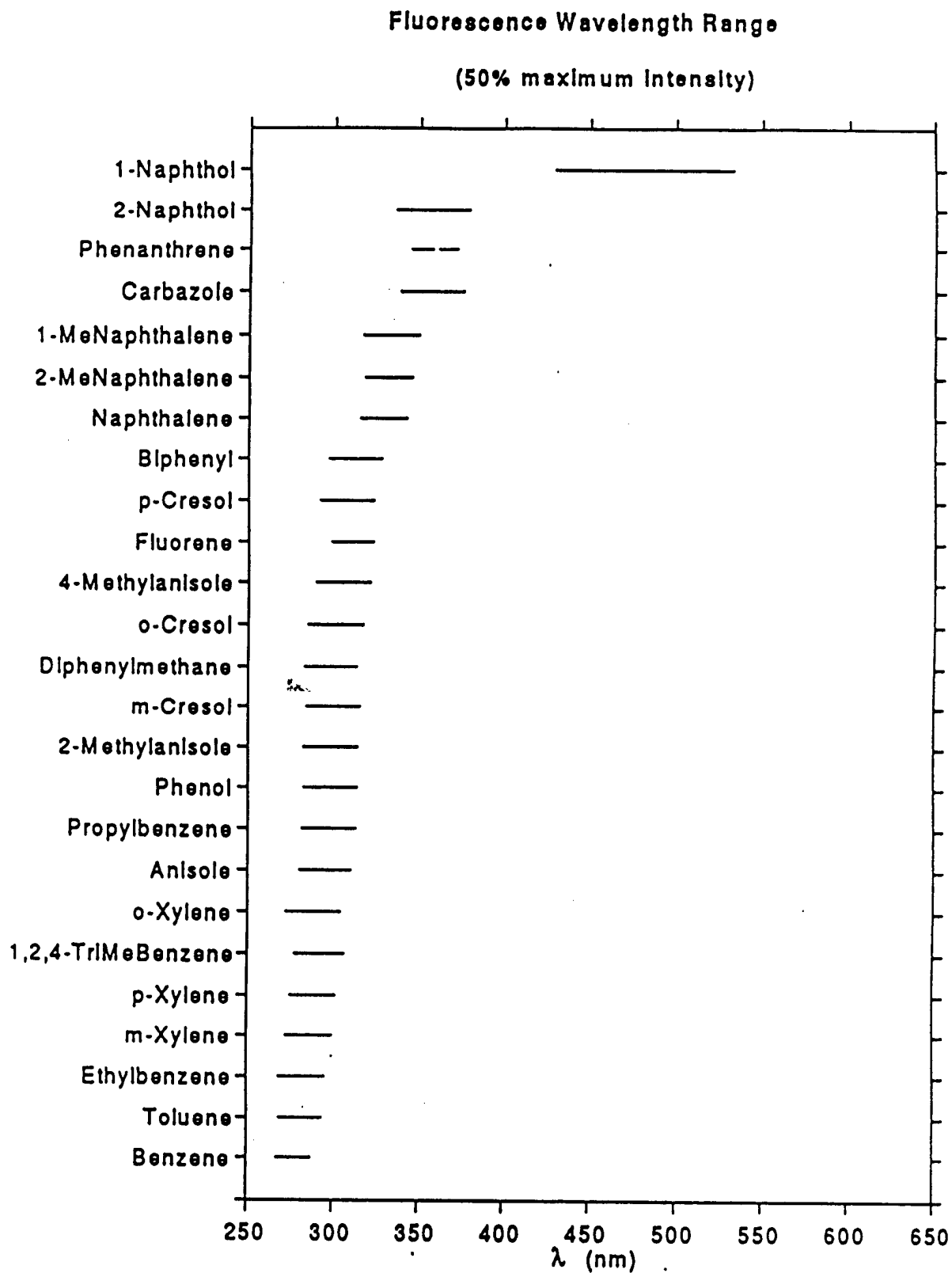
(50% maximum Intensity)

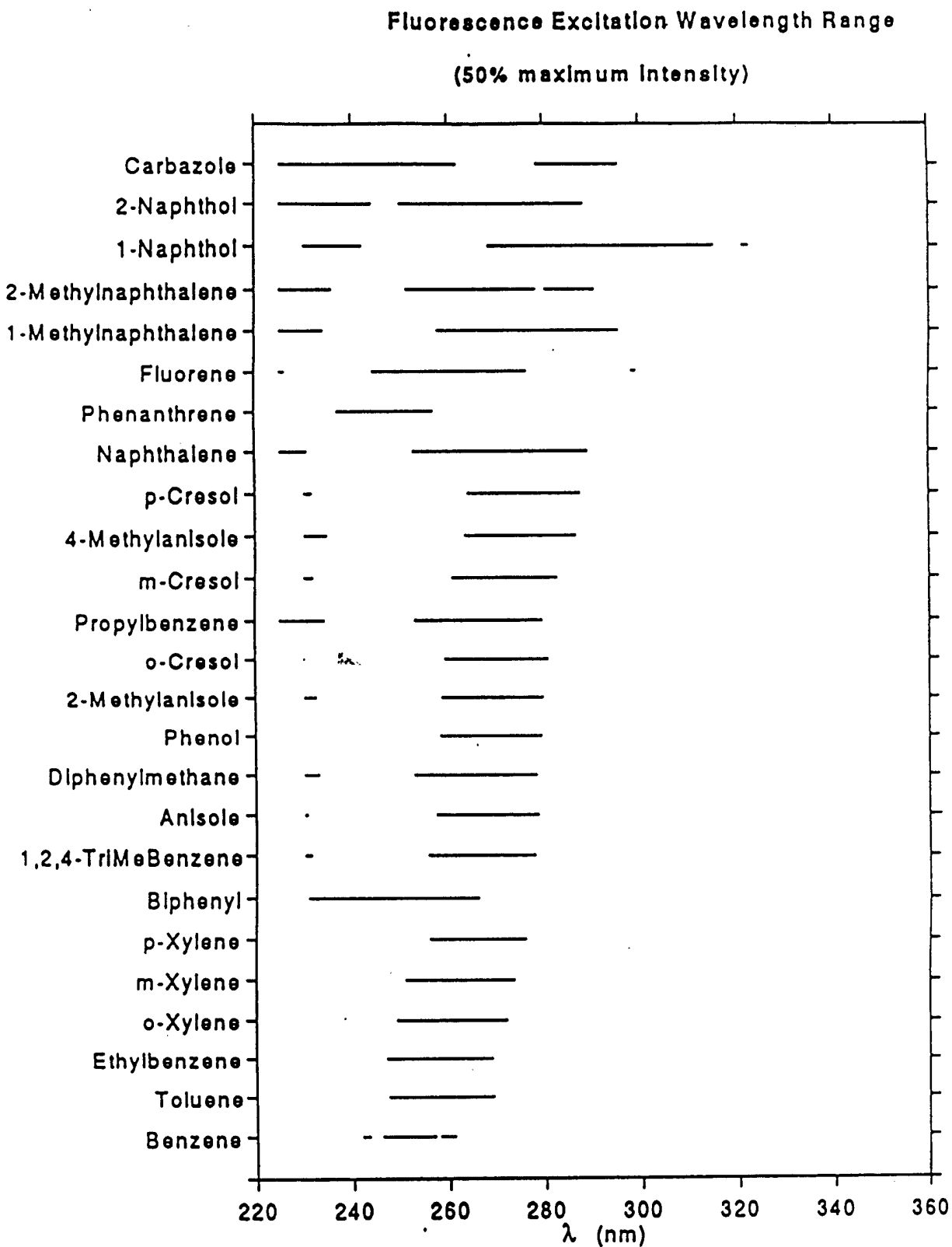Figure 14: Fluorescence Wavelength Range (50% maximum).

Figure 15: Fluorescence Excitation Wavelength Range (50% maximum).

By selecting the emission wavelength, we can achieve an initial form of class detection. The BTEX components can be selected with a choice of emission wavelength less than 300 nm. The phenols pose a minor interference in this region. A 320-350 nm wavelength region is appropriate for optimization on naphthalenes.

The spectral variation between the organic and aqueous solvent environment is expected to be small, shifts on the order of 10 nm or less. On the other hand, photophysical parameters (fluorescence quantum yield and lifetime) are more dependent on solvent. Substituent effects are small, but not inconsequential. If the spectral properties of the various derivatives are very similar, they can be treated as one compound.

Full details on the laboratory instrumentation can be found in the M.S. thesis of Roxane Meidinger (North Dakota State University, 1993). Lifetimes were determined with 266 nm excitation from the 4th harmonic of a Nd:YAG laser. The laser was operated at 10 pulses per second and less than 100 μJ/pulse were delivered to the sample at the terminus of the fiber optic probe. Spectral grade cyclohexane was used as received. Water was passed through an activated charcoal filter to reduce fluorescence background to negligible levels. Absorbances of the samples at the 266 nm excitation wavelength were kept below 0.1/cm to eliminate reabsorption effects. Oxygen was removed by bubbling nitrogen through the solutions for approximately 6 minutes before measurements were made for oxygen quenching characterization. The fluorescence detection system consisted of a 0.3m monochromator, photomultiplier tube, and digital oscilloscope.

Measurement of accurate fluorescence lifetimes requires that any impurity background fluorescence be eliminated. Organic solvents were spectroscopic grade heptane, hexane, or cyclohexane. The absence of interfering fluorescence from these solvents was confirmed with a spectrofluorimeter. Figure 16 shows the emission spectra of water samples excited at 266 nm in the spectrofluorimeter. A Raman peak is observed at 294 nm for both tap water and distilled water, and the intensity is the same to within experimental error. Tap water exhibits appreciable fluorescence of comparable magnitude to the Raman scattering throughout the ultraviolet and into the visible. We attribute this signal to naturally occurring humic materials. Even distilled water shows some elevated background that can be removed by filtering through

activated charcoal. The distilled water for the aqueous solutions was routinely triple-filtered through activated charcoal to remove any interfering impurities.
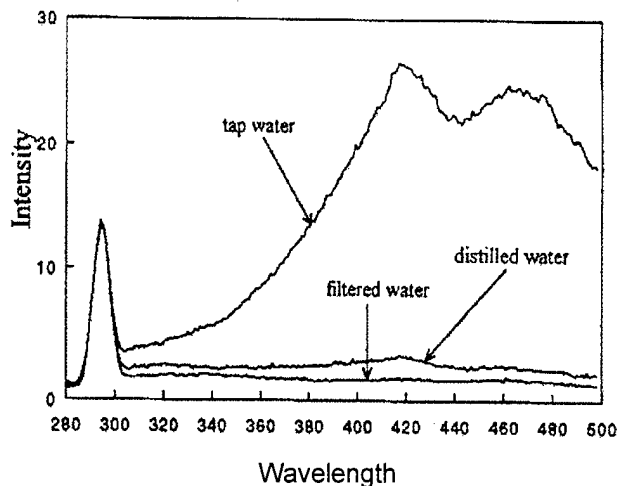

Figure 16: Emission spectra of water samples (tap and distilled) at 266 nm.

Each sample was adjusted to an absorbance of 0.10 ± 0.01 at the 266 nm excitation wavelength. An efficient method for removing oxygen is required for measurement of deoxygenated sample lifetimes. Methods to deoxygenate solutions include; freeze-pump-thaw cycles,[62] inert gas sparging,[63] and carbon dioxide sparging with dry ice.[64] The freeze-pump-thaw method was attempted first, but eliminating air leaks occurring through the fiber optic probe was difficult. Nitrogen sparging proved to be faster and more convenient. Efficiency was confirmed by the measured lifetime of pyrene in degassed cyclohexane.

The sample holder in Figure 17 was a 3-necked 100 mL distillation flask (Kontes, model 2955550-0100, Houston, TX).   The fiber optic probe, sealed inside a 14/20 ground glass thermometer adapter, was positioned in one neck of the distillation flask. A second port was covered with a rubber septum. A hypodermic syringe passing through the septum into the solution delivered nitrogen sparging gas from a cylinder. The third port was held open for gas venting.
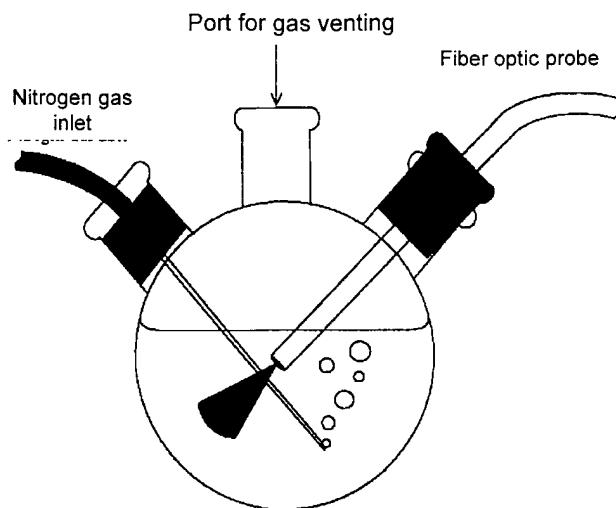
Figure 17: Distillation flask.

For any given molecule, the data were first acquired for an air-saturated solution. The sample was deoxygenated and the measurements repeated. Each 50 mL sample was deoxygenated by bubbling nitrogen gas through it for 6 minutes before data collection. During the data collection, a steady stream of nitrogen was flowing across the top of the sample to prevent oxygen from reentering the system and quenching the fluorescence. Solvent evaporation during the sparging period yields a substantial cooling effect, as much as 10 degrees. Since the fluorescence lifetimes are themselves a function of temperature, we later added a constant temperature bath to keep the solution temperature at $25 \pm 0.1C$.

Most of the solutes of interest are less soluble in water than in organic solvents. Therefore, methanol stock solutions were used to prepare the actual samples for measurement. A small amount (less than 0.1% by volume) of the concentrated methanol solution was added to air-saturated water, the solution was mixed, and the laser waveforms were acquired. The effect of the methanol on the aqueous solution fluorescence lifetimes was investigated. The lifetime of naphthalene in air-saturated water is 36 ± 1 ns. Methanol was added in 100 μL increments to the 50 mL sample and the lifetime determinations repeated after each addition. The lifetime values were constant within experimental error for additions up to 1000 μL (ca. 2% methanol by volume). None of the solutions used for this study contained more than 300 μL methanol.

Oxygen is the major cause of fluorescence quenching, but other species found in water are potential quenchers. A study was carried out to determine the effect of common anions on the fluorescence lifetimes of water samples. Degassed 1M aqueous sodium salt solutions of Br^-, Cl^-, SO_4^{2-}, CO_3^{2-}, and HCO_3^- were used. Naphthalene was the target analyte. The procedure for collecting these data was similar to that described for deoxygenated aqueous solutions. The salt solutions were sparged with nitrogen before the naphthalene was introduced into the sample.

The laser excitation time profile and the fluorescence decay profile were measured for every combination of solvent and solute. The first step was to set the emission monochromator wavelength at the maximum of the fluorescence spectrum. The slits were adjusted so that the trace on the oscilloscope screen was nearly full scale at 50 mV/div amplitude setting. The monochromator wavelength was then adjusted close to 266 nm to give an excitation waveform of nearly the same intensity as the emission. This step measured the laser pulse profile. The monochromator was then returned to the fluorescence maximum for the measurement of D(t). Next the sample was deoxygenated. Removal of oxygen led to enhancement of the fluorescence signal in longer-lived fluorescence. The slit widths on the monochromator were minimized in order to keep the same amplitude setting as the air-saturated solutions. If the oscilloscope time base was not changed, the same laser profile was used for both air-saturated and deoxygenated solutions in a given solvent.

Multiple acquisitions of the excitation waveform were downloaded to the control computer and averaged to improve the signal-to-noise ratio. A standard practice of collecting three acquisitions of 1000 laser shots each was adopted. After the laser data were collected, the monochromator was returned to the compound's emission wavelength, and multiple acquisitions of the decay profile were acquired. A set of three such emission profiles were collected, each having the same laser excitation profile. A 10 Hz repetition rate takes about five minutes to acquire the three acquisitions of 1000 shots each.

The computer averages the fluorescence data points and saves them along with the average laser emission as a "life" file with an .LIF extension to the file name. Each file contains a header with oscilloscope settings, date, and user-supplied comments. The computer also determines the variances of the fluorescence and laser data sets and stores them in the file.

The LIF files are processed with a computer program[65] to determine the lifetime of the sample. The program uses the phase plane method to find a lifetime approximation as input to the Marquardt least squares fitting routine. A baseline offset and time shift are also incorporated into the software. The program generates lifetimes and chi-square values and reports these with the scaling factor, time shift, and baseline offset. The least squares fitting is a deconvolution approach that works by iterative convolution. The parameters of the modeling equation are varied until the chi-square calculated for the model is a minimum. A Marquardt algorithm is used to achieve faster and more automated data analysis.

B.   DATA PROCESSING

Fluorescence lifetimes, τ, were recovered from the excitation and fluorescence intensity-time profiles, $E(t)$ and $F(t)$. Two main approaches were investigated: a Marquardt convolute-and-compare analysis and the phase-plane method of Demas.[66] We found that the phase plane method, which is fast and computationally simple, gave results of comparable quality to those from the Marquardt analysis.   Therefore, only the phase-plane method is discussed here. The sample decay is given in equation (10):

$$D(t) = Ke^{-kt} \int_{x=0}^{x=t} \exp(kx) E(x) dx \qquad (10)$$

where k is equal to $1/\tau$ and K is the proportionality constant to scale the amplitudes of the excitation profile and the sample decay.   The derivative of equation (10) with respect to time yields:

$$dD(t) / dt = K[E(t) + (-1 / \tau)\exp(-t / \tau) \int_0^t E(x)\exp(x / \tau)dx] \qquad (11)$$

$$= KE(t) - (1 / \tau) D(t)$$

Integration of equation (11) yields the equivalent form of equation (10) which is shown in equation (12):

$$D(t) = K \int_0^t E(x)dx - (1 / t) \int_0^t D(x)dx \qquad (12)$$

which can be rearranged to yield:

$$S(t) = (-\tau) W(t) + k\tau \qquad (13)$$

and:

$$W(t) = (-1/\tau)Z(t) + K \qquad (14)$$

where,

$$Z(t) = \int_0^t D(x)\,dx \ / \ \int_0^t E(x)\,dx \qquad (15)$$

and

$$W(t) = D(t) \ / \ \int_0^t E(x)\,dx \qquad (16).$$

A plot of $Z(t)$ versus $W(t)$ has a linear slope equal to $-\tau$ and an intercept of $K\tau$. A plot of $W(t)$ versus $Z(t)$ yields a linear slope of $1/\tau$ and a y-intercept of K. The integrals are evaluated by the trapezoidal rule. Demas recommends the W versus Z plot because most of the uncertainty is placed into the dependent variable; he characterizes the integrations of both the numerator and denominator in equation 5-7 as a form of "signal averaging."

In this procedure, the initial portion of the W versus Z plot is very noisy. The denominators will be very small until $E(t)$ has moved away from zero and these points are of no value in the linear fit. $D(t)$ lags behind $E(t)$ so the numerators are also very small. Similarly, the numerators are very uncertain until $D(t)$ is significant. These factors lead to obvious curvature in the plots. We found that reliable results required that the portion used for the linear fit begin at about the peak of the fluorescence decay. This eliminates a lot of the data. For long lifetimes, the result is not greatly different from making a simple log I versus t plot.

We found the superior procedure used equation (12) to perform a linear regression. All the data are treated equally. If weighting factors are not used, the data should be excluded prior to the laser pulse since this contains no useful information. Similarly, there is no useful information after $F(t)$ has returned to zero. By trial and error, we found that stable results were obtained if we used all the data for which $F(t)$ is greater than 5% of its maximum value. This procedure was easily implemented into code.

Goodness of fit is indicated by chi-square the sum of squares of the weighted or unweighted residuals. When weighted residuals are used for the calculation, the value is referred to as a reduced chi-square. The following equation is used to calculate chi-square, χ^2:

$$\chi^2 = \sum \sigma_i^{-2} (y_i - f_i)^2 / n \qquad (17)$$

where σ_i is the standard deviation for the ith data point, y_i are the experimental data points, f_i are the calculated points of the fitting curve, and n is the number of data points minus the number of parameters to be calculated. The weighting factor emphasizes or weights more heavily the more accurately known points. For unweighted calculations, σ_i^{-2} is set to one.[67]

Demas et al.[68] evaluated errors in the phase plane method for deconvolution of luminescence lifetime data. They found similar accuracy and precision for weighted and unweighted fits. Since the unweighted fits are easier to do, they recommended that unweighted fits be used rather than the weighted least-squares fitting of the phase plane plots. We used the phase plane method to choose the initial point for least-squares fitting to reducing the overall convergence time.

The temporal width of the frequency-doubled laser pulses is 5 to 7 ns (FWHM) and the pulse repetition rate is 10-15 Hz. The digital oscilloscope samples each decay curve at 500 megasamples/sec, in which a point on the waveform is acquired every 2 ns. If the fluorescence signal is strong and the molecular lifetime long, the fluorescence temporal profile can be generated from a single laser excitation pulse. More often multiple laser shots are acquired, either to improve signal-to-noise for trace analysis or to yield enough data points to adequately define the decay curve. For time bases shorter than 50 ns/division, the oscilloscope automatically goes into an equivalent-time sampling mode to provide 50 sampling intervals per division. We typically use time bases of 10 or 20 ns/div, which results in 0.2 or 0.4 ns sampling intervals, sufficient to determine lifetimes down to 1 ns.

On an individual trigger, the scope provides eight bits of vertical resolution for a maximum of 255 available counts per channel, far less than the 10,000 or more counts per channel typical for lifetimes determined by time-correlated single photon counting. Signal averaging increases the effective number of bits. Moreover, the limitation to eight bits for real-time data capture is not limiting here because the statistical fluctuation in the PMT pulse amplitudes exceeds the digitization uncertainty. We are currently characterizing the data

acquisition statistics and exploring new approaches to optimize signal-to-noise and are confident that fluorescence lifetimes can be conveniently and accurately determined with this class of digital oscilloscopes. For deoxygenated naphthalene (*vide infra*) our day-to-day lifetime reproducibility is 41 ± 1 nanoseconds.

Representative signal-to-noise levels for waveforms acquired with a few hundred laser shots (ca. 30 seconds of actual measurement time) are illustrated in Figure 18. The anthracene solution was deoxygenated by nitrogen bubbling to eliminate quenching of the fluorescence by dissolved molecular oxygen. The effect is not great; the fluorescence lifetime of anthracene in air-saturated water at room temperature is 4.42 ns, compared to the value of 5.51 ns when the oxygen is removed. Oxygen quenching is more significant in organic solvents. Using naphthalene as an example, lifetimes of 119 ns (deoxygenated) and 9 ns (no purging) in heptane solvent are found, considerably different from the values of 96 ns and 16 ns, respectively, reported by Berlman.[69] Two opposing sources of error appear in Berlman's data, inadequate deoxygenation which reduces the observed lifetimes, and too high a solute concentration, which results in radiation trapping and artificially elevated lifetime values. The fluorescence lifetimes of the BTEX components, 2.4 ns for benzene, 5.3 ns for toluene, 11.9 ns for p-xylene, in air-saturated aqueous solution are comparable to the excitation pulse duration.

C. FLUORESCENCE LIFETIMES

1. Lifetime Data

The fluorescence lifetime determinations require separate measurements of the laser excitation and fluorescence emission temporal profiles. The duration of the Nd:YAG laser excitation pulses is about 6 ns. Since this is comparable to or even greater than some of the lifetimes of interest, deconvolution methods are necessary to extract the intrinsic molecular decay properties. Laboratory work to produce even more accurate temporal profiles continues, but the major problems of using a digital oscilloscope in this mode have been solved. The quality of our data for fitting calculated and observed fluorescence profiles for anthracene is shown in Figure 18.
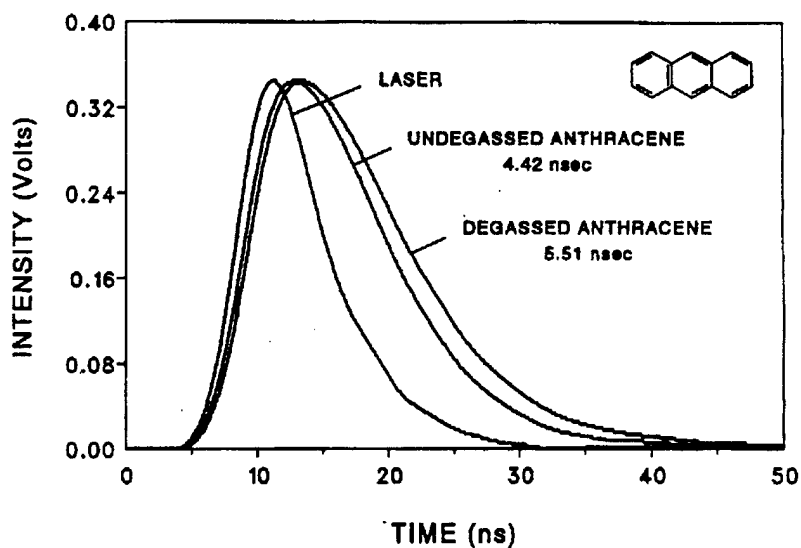
Figure 18: Observed fluorescence profiles for anthracene.

Fluorescence lifetime data for oxygen-free aqueous solutions is shown in Table
2. The only literature values for comparison are those for benzene reported by Luria et al.[70]

TABLE 2. LIFETIMES OF PAHS IN DEOXYGENATED WATER

Compound	Fluorescence Lifetime (ns)
benzene	2.5
toluene	4.9
ethylbenzene	4.5
o-xylene	6.1
p-xylene	11.1
propylbenzene	3.8
1,2,4-trimethylbenzene	8.6
naphthalene	40.3
1-methylnaphthalene	30.3
2-methylnaphthalene	24.6

2. Quenching Effects

Oxygen efficiently quenches fluorescence because its ground state has a triplet spin. The fluorescence lifetime is consequently a function of all conditions that affect either the oxygen concentration or its diffusion rate. For solution conditions, the most important factors are temperature, solvent polarity, viscosity, and the partial pressure of oxygen over the solution. Natural groundwater also contains other potential quenchers, including metal cations and anions such as hydrogen carbonate, sulfate and chloride.

Quenching effects on excited-state decay properties are conveniently determined by comparing the fluorescence lifetimes in the presence and absence of a quencher. The fluorescence lifetime in the absence of quencher, τ_0, is represented as,

$$\tau_0 = 1/(k_r + k_{nr}) \tag{18}$$

where k_r is the first-order rate constant for radiative emission and k_{nr} is the nonradiative decay rate constant. In the presence of quencher, the lifetime, τ, is further reduced according to:

$$\tau = 1/(k_r + k_{nr} + k_q[Q]) \tag{19}$$

in which $[Q]$ is the concentration of quencher and k_q is a second-order rate constant. Equations (18) and (19) can be combined into the Stern-Volmer equation:

$$\tau_0/\tau = 1 + \tau_0\, k_q[Q] \tag{20}$$

a) Oxygen. Equation (20) indicates that a plot of $\tau_0/\tau-1$ versus τ_0 should give a straight line passing through the origin if the quenching efficiency per collision is the same for all compounds in the study and the quencher concentration is fixed. Berlman[71] presented a graph of this type for the oxygen quenching of many different aromatic hydrocarbons in cyclohexane solution. We repeated much of Berlman's work and generally find longer lifetimes than he did for deoxygenated organic solutions. The trend is most obvious for molecules with long lifetimes, e.g., naphthalene and its methyl derivatives. Berlman's value for naphthalene in degassed cyclohexane is 96 ns, compared to 115 ns in our work.

The likely explanation is that our deoxygenation procedure is more effective than Berlman's. We tested degassing efficiency with pyrene, because its unusually long-lived lifetime makes it extremely susceptible to oxygen quenching. For a cyclohexane solution purged by nitrogen gas bubbling for six minutes, we found a pyrene fluorescence lifetime of 458 ± 15 ns, in good agreement with literature values.

The graphs of equation (20) for data taken for water and heptane solvents are shown in Figure 19. Our correction of Berlman's organic solvent data doesn't affect his conclusion that quenching efficiency per collision is nearly the same for all the compounds; fluoranthene is a notable exception for its near immunity from oxygen quenching.
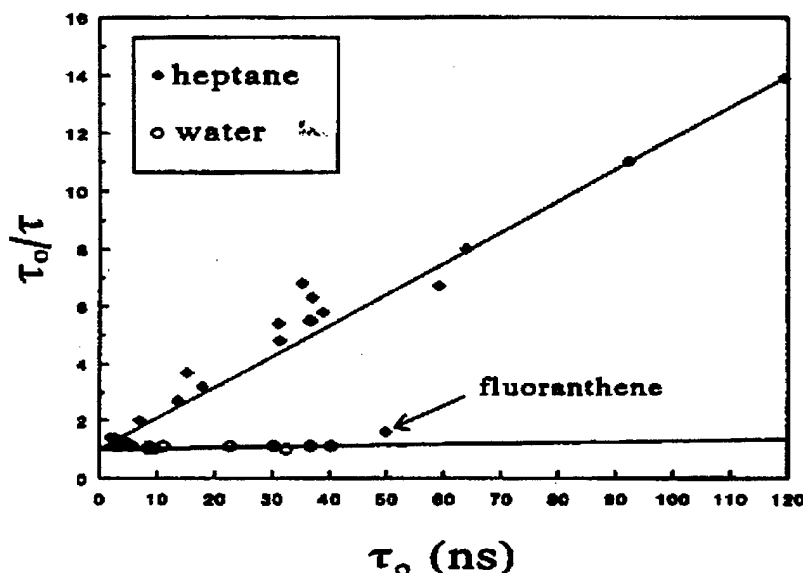
Figure 19: Quenching of analytes in heptane and water solvents.

The oxygen quenching for air-saturated *aqueous* solutions is nearly negligible. The slope of the line through the data is 40 times smaller than for the heptane solvent quenching line. Only for the longest-lived compounds could the effect even be discerned. For example, the lifetime of naphthalene increases only about 10% (from 36 to 40 ns) when the oxygen is removed. Pyrene is the most sensitive probe. Our value of 127 ns for an air-saturated distilled water solution of pyrene agrees well with Lieberman's report[72] of 129 ns in

air-saturated sea water. Oxygen removal extends the pyrene fluorescence lifetime to 194 ns. The aqueous solution quenching was calculated with just the naphthalene and pyrene data.

The nearly negligible fluorescence quenching by oxygen in aqueous solution compared to organic solvents is explained by the data of Table 4. First, note that the solubility of oxygen in water is an order of magnitude lower than in aliphatic solvents. This accounts for the majority of the difference. A secondary contribution arises from the higher viscosity of water, which in turn means a slower diffusion-controlled rate constant, k_d. The product of the oxygen solubility and k_d (Table 4, final column) is a measure of oxygen quenching in a given solvent under air-saturated conditions, if the quenching efficiency per collision is independent of solvent. Our data show this to be a good approximation.

TABLE 4. SOLVENT DATA RELEVANT TO THE QUENCHING EFFICIENCY OF OXYGEN

Solvent	Molar Solubility [a]	Viscosity [b] (cP)	k_d ($M^{-1} s^{-1}$)	$k_d[O_2]$ (s^{-1})
cyclohexane	2.28×10^{-3}	0.98	6.7×10^9	1.5×10^7
heptane	2.69×10^{-3}	0.42	1.6×10^{10}	4.3×10^7
hexane	3.02×10^{-3}	0.31	2.1×10^{10}	6.3×10^7
water	2.56×10^{-4}	1.00	6.6×10^9	1.7×10^6

[a] Calculated using data from reference 7 for organic solvents and reference 8 for water;
[b] Reference 9.

There is an intrinsic solvent dependence of τ_o. Consider the lifetime data in Table 5 for naphthalene in air-saturated and deoxygenated cyclohexane, heptane, and water. The lifetimes in degassed cyclohexane and heptane are identical to within experimental error. The only definite conclusion is that the ratio of radiative and nonradiative decay rate constants is the same in both solvents. In principle, both k_r and k_{nr} could be affected proportionately by a change from cyclohexane to heptane solvent, but there is no reason to expect that to be the case. However, the shorter τ_o value in water requires that either the radiative decay rate is lower or the radiationless decay rate is higher than in the aliphatic solvents. It is likely that k_{nr}, determined predominately by intersystem crossing, is faster in water than in the organic solvents.

TABLE 5. FLUORESCENCE LIFETIME OF NAPHTHALENE IN DIFFERENT SOLVENTS

Solvent	Lifetime (ns) undegassed	Lifetime (ns) degassed
cyclohexane	16.7	120
heptane	9	119
water	36	40

b.) Dissolved Ions. The prospects for quantitative fluorescence measurements under field conditions are enhanced by the demonstration that oxygen has only a minor effect. However, dissolved ions in natural waters are also potential quenchers. Just as oxygen can enhance the intersystem crossing rate, so can other species via the phenomenon known as the "heavy atom effect." The incorporation of high atomic weight atoms in a molecule is well known to enhance spin-orbit coupling between the S_1 and T_1 states and thereby speed-up intersystem crossing; the phenomenon is referred to as the internal heavy atom effect. The presence of high atomic weight atoms in the solvent or in ions dissolved in solution gives rise to an analogous external heavy atom effect. Because of relatively high concentrations in natural waters, chloride and sulfide are the most likely quenchers. We also studied bromide because it will provide an upper-limit to the magnitude of the heavy atom effect, although its concentration in natural waters is quite low.

We measured the fluorescence lifetime of naphthalene in deoxygenated aqueous solutions containing different concentrations of dissolved sodium salts. The data in Tables 4 and 5 show that there is a marked lifetime decrease with increasing bromide ion concentration. Chloride ion has a much smaller effect. Even for 1 MNaCl, only about 20% of the fluorescence is quenched and the effect is barely noticeable at 0.1 M quencher concentration. The Stern-Volmer plots in Figure 20 clearly reveal the expected linear relationship.
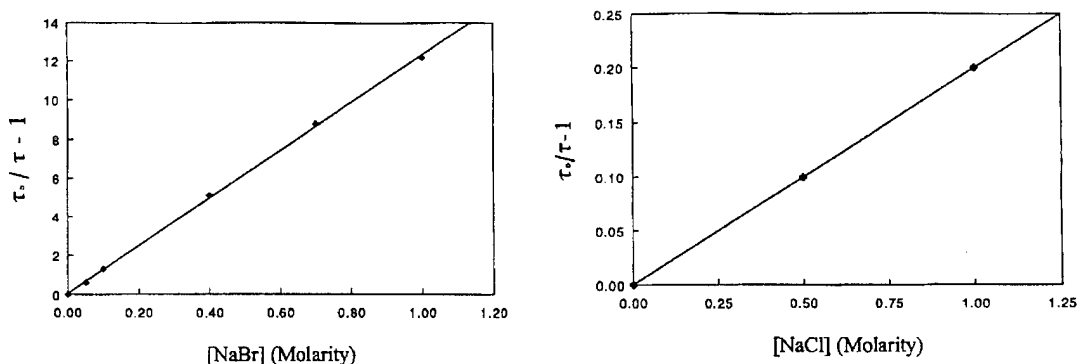
Figure 20: Quenching of Naphthalene by Cl⁻ and Br⁻ Ions.

TABLE 6. ANION EFFECT ON NAPHTHALENE FLUORESCENCE LIFETIME

Concentration [M]	Lifetime (ns) in NaCl(aq)	Lifetime (ns) in NaBr(aq)
0	40.3	40.3
0.05		26.4
0.1	40.1	18.1
0.4		6.8
0.5	35.2	
0.7		4.2
1.0	32.9	2.9

The lifetime of naphthalene in oxygen-free water is 40 ns with an experimental uncertainty of about 1 ns. The concentration of quencher that reduces the lifetime by an amount equal to the uncertainty defines an approximate threshold for the quenching effect to be considered significant. For our data, the quenching of naphthalene by Br⁻ is insignificant at concentrations below 0.02 M ($\approx$ 2000 mg/L) while the limit for Cl⁻ is about 0.1 M ($\approx$ 6000 mg/L). Since these values are much higher than levels normally found, these ions should not interfere with lifetime data from groundwater environments.   Stumm and Morgan report chloride concentrations of 4 to 20 mg/L for groundwater in a variety of environments.[73] Faure[74] gives the concentration of Br⁻ in streams at 20 mg/L while Krauskopf[75] reports a concentration of Br⁻ in seawater of 67 mg/L.

74

c.) Humic Substances.   Humic substances are formed by bacterial and chemical degradation of plant tissue. High concentrations of these species are commonly found in soil and in groundwater and their effect on aromatic hydrocarbon fluorescence must be determined. Even tapwater can show an appreciable humic fluorescence, as is illustrated in Figure 16. The signal in distilled water is much lower, but can be reduced still further by passing the water through a charcoal column. We examined the fluorescence of naphthalene in charcoal filtered, distilled water and in water which had been equilibrated with uncontaminated soil from Tinker AFB. A large humic substance fluorescence was observed in the 400-500 nm range for the latter sample. In addition, the naphthalene fluorescence was reduced substantially. The naphthalene fluorescence lifetime was determined and a value of approximately 35 ns was found in each case. Since the lifetime was not affected in the presence of humic materials, the reduction in fluorescence intensity must be due to static quenching. This is consistent with previous reports in the literature.

Gauthier et al.[76] measured the fluorescence of aqueous solutions of phenanthrene, anthracene, and pyrene and found that the fluorescence intensity decreased with an increase in humic materials. Concentrations near the solubility limit were used to maximize fluorescence relative to background from the humic material. The PAHs they investigated have moderate solubilities in water. An interesting note is that PAHs with lower solubilities tend to bind strongly to humic substances so that the humic concentrations required for the binding constant measurements are lower. Williams[77] also predicts that the quenching mechanism for dissolved humic materials is static. Fluorescence lifetimes of 1-naphthol, napropamide, and fluoranthene in aqueous solutions were determined and found not shortened with increasing humic acid concentration.

Quenching of fluorescence by oxygen or anions in solution is of only minor consequence and does not pose a problem for quantitative *in situ* fluorescence analysis. The fluorescence lifetimes of benzene, toluene, p-xylene, and naphthalene are significantly different, so lifetime data will likely prove helpful for speciating these compounds. Humic substances represent a greater complication.

D.   DATA FORMATS

1.   Wavelength-Time Matrices (WTMs)

We collect our data and assemble them as wavelength-time matrices (WTM), analogous to the excitation-emission matrices popularized by Warner and coworkers.[78] A WTM is a set of fluorescence decay profiles at a series of emission or excitation wavelengths. Examples of emission wavelength-time matrices are shown in Figure 21 for benzene, toluene, p-xylene, and a benzene/p-xylene mixture for which the relative concentrations were adjusted to give equal intensity contributions. The relatively high degree of vibronic structure in benzene and the lifetime ordering p-xylene > toluene > benzene are clearly evident. The lifetime comparison would be even more dramatic if the excitation pulse duration were shorter since the observed decay for benzene (and to a lesser degree for toluene) is dominated by the excitation temporal profile.

The data of a WTM can be processed in several ways, one of which is contour diagrams of the type shown in Figure 21. Note the tilt of the contours such that the fluorescence at longer wavelengths appears to occur earlier in time relative to the laser pulse than the shorter wavelength signal. The fluorescence lifetime of an emitter in solution does not depend on the monitoring wavelength, so the contour features (e.g., the peaks for benzene) ought to line up perpendicular to the time axis. Why they do not is a consequence of differential transit time of light at different wavelengths as it passes through 20 meters of optical fiber. The propagation velocity of light is greater at longer wavelengths owing to lower refractive index of the silica core. Allowance for this effect will be factored into future data.

Compared to the single component benzene data, the benzene peaks in the mixture are not as prominent and the presence of the p-xylene extends the contours to both longer wavelength and longer time. Time and wavelength regions can be identified for the presence or absence of a given component. For this mixture the signal at short wavelength, less than 270 nm, is attributable to benzene, while the signal at long time, greater than 30 ns, is predominately that of p-xylene. These positions fall in low intensity tails of the WTM. A more complex sample would not be as clear. In such cases, extensive mathematical processing of the data will be required.
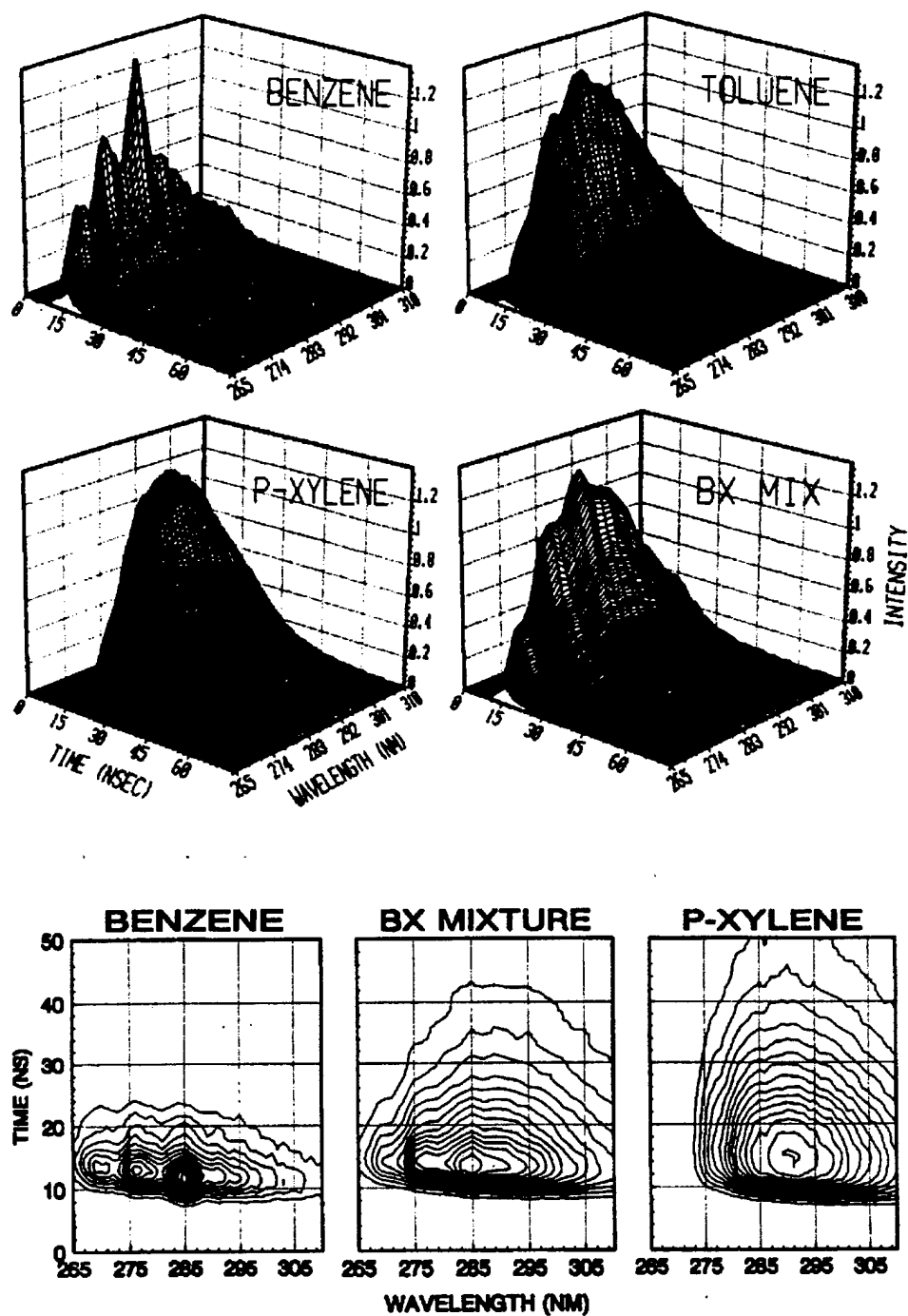
Figure 21: WTM's and corresponding contour diagrams for benzene, toluene, p-xylene and benzene/p-xylene mixtures.

An alternative process cuts the intensity-wavelength plane perpendicular to the time axis, which generates the equivalent of the fluorescence spectrum at a specific time relative to the laser pulse. Examples drawn from the benzene-xylene mixture WTM are shown in Figure 22. The cut at 15 ns, relative to an arbitrary time zero, lies along the ridge of the WTM nearly coincident with the peak intensity of the laser pulse. It is dominated by the contribution from the shorter-lived benzene; 20 ns later the benzene fluorescence has entirely, but the p-xylene emission persists and is verified by the superimposed time profile for p-xylene. The signal-to-noise ratio is quite good although these time-resolved fluorescence spectra have actually been assembled from a series of separate fluorescence decay profiles. This type of time-resolved fluorescence spectrum can also be generated with an intensified charge-coupled device (ICCD) detector.
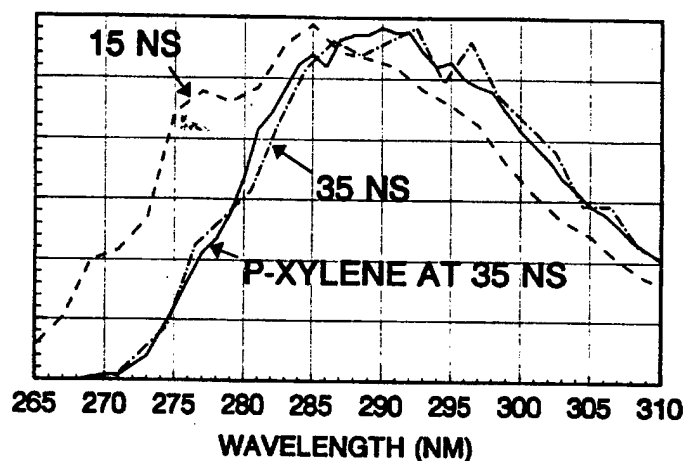
Figure 22: Time resolved views of benzene/p-xylene mixture from WTM

2. Field Studies

The NDSU transportable laser system was driven from Fargo, ND to Tinker AFB, OK in August, 1991 for a nine-day field trial. During this period *in situ* monitoring well measurements were made at a site of known fuel contamination. The primary purpose of the demonstration was to identify potential difficulties for field operation, although analytically relevant data were also obtained. The results are highly encouraging. During approximately

50 total hours of actual measurement under generator power, no down-time was caused by laser system problems despite daily temperatures in excess of 90°F. The transport van was not air-conditioned or shaded while the measurements were made.

The major contaminant at the Tinker site is toluene. Samples bailed immediately after the fiber optic determination were submitted for conventional gas chromatographic (GC) analysis. Three-dimensional representations of the plume derived from the GC and fluorescence data are shown in Figure 23. The two plumes are similarly shaped, with the GC values generally higher by a factor of 3-4. We believe there are two likely causes. One is high water turbidity that limits penetration depth of the laser light and collection of fluorescence. We will correct the data for turbidity in the future. The second factor is that the GC analysis required preconcentration by extraction. It is likely that toluene adsorbed on soil particles may have been dissolved in the extraction medium.
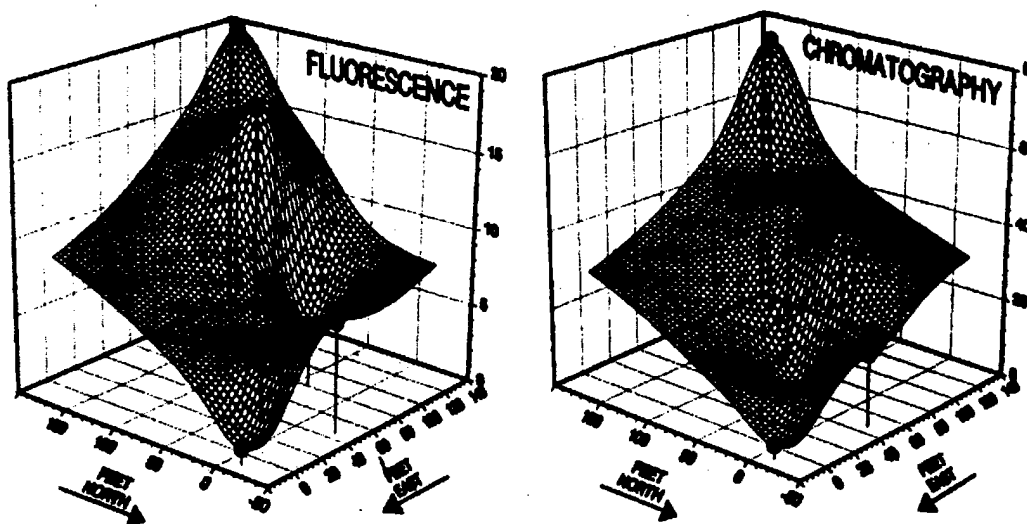
Figure 23. 3-D plume depictions at Tinker site which show the comparison between fluorescence and GC analysis.

REFERENCES

[1] P. Cruver, Environmental Protection. 1992, 25(12), pp. 56-57.

[2] see reference 1.

[3] J. M. Neff, "Polycyclic Aromatic Hydrocarbons in the Aquatic Environment," Applied Science. Essex, England, 1979.

[4] L. Keith, "Environmental Sampling and Analysis," Lew: Chelsea, 1991: pp. 7-23.

[5] A. D. Hewitt, T. F. Jenkins, and C. L. Grant, "Collection, Handling, And Storage: Keys To Improved Data Quality For Volatile Organic Compounds In Soil," American Environmental Laboratory, February, 1995, p. 25.

[6] (a) First International Symposium on Field Screening Methods for Hazardous Wastes and Toxic Chemicals Las Vegas, NV, 1989. (b) Second International Symposium on Field Screening Methods for Hazardous Wastes and Toxic Chemicals Las Vegas, NV, 1991.

[7] Chudyk, W.A., M. M. Carrabba, and J. E. Kenney, Anal. Chem. 1985, vol. 57, pp. 1237-1242.

[8] Lieberman, S.H. and G. A. Theriault, "Rapid, Subsurface, In Situ Field Screening of Petroleum Hydrocarbon Contamination Using Laser Induced Fluorescence Over Optical Fibers," Second International Symposium on Field Screening Methods for Hazardous Wastes and Toxic Chemicals. Las Vegas, NV: 1991; Abstract 82.

[9] Bratton, W.L., J. D. Shinn II and J. L. Bratton, "Air Force Site Characterization and Analysis Penetrometer System for Fuel-Contaminated Sites," Proceedings of the Third International Symposium on Field Screening Methods for Hazardous Wastes and Toxic Chemicals. 1992.

[10] Haas III, J.W., E. Y. Lee, C. L. Thomas and R. B. Gammage, Proceedings from the First International Symposium on Field Screening Methods for Hazardous Wast Site Investigations. pp. 105-108, 1988.

[11] J. Behringer, Raman Spectroscopy, Theory and Practice. Szymanski, Editor, Plenum Press, New York, 1989.

[12] Asher, S.A., Anal. Chem. 1984, vol. 56, pp. 720-724.

[13] Marley, N.A., C. K. Mann and T. J. Vickers, Appl. Spectrosc. 1984, vol. 38, pp. 540-543.

[14] Marley, N.A., C. K. Mann and T. J. Vickers, Appl. Spectrosc. 1985, vol. 39, pp. 638-643.

[15] Gerrard, D.L. and H. J. Bowly, Chemical Analysis of Polycyclic Aromatic Compounds. T. Vo-Dinh., Editor, Wiley, New York, 1989, Chapter 14.

[16] Vo-Dinh, T., Chemical Analysis of Polycyclic Aromatic Compounds. T. Vo-Dinh, Editor, Wiley, New York, 1989, Chapter 15.

[17] Schwarz, F.P. and S. P. Wasik, Anal. Chem. 1976, vol. 48, pp. 524-528.

[18] Richardson, J.H. and M.E. Ando, "Sub-Part-per Trillion Detection of Polycyclic Aromatic Hydrocarbons by Laser Induced Molecular Fluorescence," Anal. Chem. 1977, vol. 49, no. 7, p. 955.

[19] Miller, T.C. and L. R. Faulkner, Anal. Chem. 1976, vol. 48, pp. 2083-2088.

[20] Warner, I.M., G. D. Christian, E. R. Davidson and B. J. Callis, Anal. Chem. 1977, vol. 49, pp 564-573.

[21] Warner, I.M., G. Patonay and M. P. Thomas, Anal. Chem. 1985, vol. 57(3), pp. 463A-483A.

[22] Ho, C.N., G. D. Christian and E. R. Davidson, Anal. Chem. 1980, vol. 52(7), pp. 1071-1079.

[23] Warner, I.M. and L. B. McGown, Anal. Chem. 1988, vol. 60, pp. 162R-175R.

[24] Vo-Dinh, T., Anal. Chem. 1978, vol. 50, pp. 396-401.

[25] Inman, E.L. and J. D. Winefordner, Anal. Chem. 1982, vol. 54, pp. 2018-2022.

[26] Latz, H.W., A. H. Ullman and J. D. Winefordner, Anal. Chem. 1978, vol. 50, pp. 2148-2149.

[27] see reference 21.

[28] see reference 22.

[29] Fogart, M.P. and I. M. Warner, Anal. Chem. 1981, vol. 53, pp. 259-265.

[30] Chabay, I., Anal. Chem. 1982, vol. 54, pp. 1071A-1080A.

[31] Schwab, S.D. and R. L. McCreery, Anal. Chem. 1984, vol. 56, pp. 2199-2204.

[32] McCreery, R.L., M. Fleisschmann and P. Hendra, Anal. Chem. 1983, vol. 55, pp. 146-148.

[33] see reference 31.

[34] Louch, J. and J. D. Ingle, Jr., Anal. Chem. 1988, vol. 60, pp. 2537-2540.

[35] Keny, J.E., G. B. Jarvis, W. A. Chudyk and K. O. Pohlig, Anal. Instrum. 1987, vol. 16, pp. 423-445.

[36] Webb, M.J., Spectroscopy. 1989, vol. 4, pp. 27-34.

[37] Hirschfeld, T., T. Deaton, F. Milanovich and S. Klainer, Optical Engineering. 1983, vol. 22, pp. 527-531.

[38] Chudyk, W.A., M. M. Carrabba and J. E. Kenny, Anal. Chem. 1985, vol. 57, pp. 1237-1242.

[39] Richardson, J.H. and M. E. Ando, Anal. Chem. 1977, vol. 49, pp. 955-959.

[40] Taylor, T.A., X. Hong and J. E. Kenny, "Laser Fluorescence EEM Instrument for In-Situ Groundwater Screening", Second International Symposium on Field Screening Methods for Hazardous Wastes and Toxic Chemicals, p. 797, Las Vegas, NV, 1991.

[41] Carrabba, M.M., K. M. Spencer, C. Rich and D. Rauh, Appl. Spectrosc. 1990, vol. 44 (9), pp. 1558-1561.

[42] Chudyk, W., K. Pohlig, L. Wolf and R. Fordiani, <u>Proceedings of SPIE-The International Society for Optical Engineering.</u> 1172, pp. 123-129, 1989.

[43] Inman, S.M., P. Thibado, G. A. Therault and S. H. Lieberman, <u>Anal. Chim. Acta.</u> 1990, vol. 239, pp. 45-51.

[44] Niessner, R., U. Panne and H. Schroder, <u>Anal. Chim. Acta.</u> 1991, vol. 255, pp. 231-243.

[45] Bright, F.V. and K. S. Litwiler, <u>Anal. Chem.</u> 1989, vol. 61, pp. 1510-1513.

[46] Ghiggino, K.P., A. J. Roberts and D. Phillips, <u>Springer Ser. Chem. Phys.</u> 1979, vol. 6, pp. 98-100.

[47] Xu, H. and J. E. Kenny, <u>Appl. Spectrosc.</u> 1991, vol. 45, pp. 429-434.

[48] Chudyk, W., K. Pohlig, N. Rico and G. Johnson, <u>Proceedings from the First International Symposium on Field Screening Methods for Hazardous Waste Site Investigations.</u> pp. 99-102, 1988.

[49] Inman, S.M., P. Thibado, G. A. Theriault and S. H. Lieberman, <u>Anal. Chim. Acta.</u> 1990, vol. 239, pp. 45-51.

[50] Taylor, T.A., H. Xu, D. B. Wheeler and J. E. Kenny, A Poster from The Second International Symposium on Field Screening Methods for Hazardous Wastes and Toxic Chemicals: Meeting Program 57, 1991.

[51] Gillispie, G.D., "Spectroscopic Characterization of Polymers, 1. Fluorescence Principles", in <u>ACS Advances in Chemistry Series No. 236, Structure-Property Relations in Polymers.</u> Urban, M.W., Editor, 1993, pp. 89-127.

[52] see reference 51.

[53] Demas, J.N., <u>Excited State Lifetime Measurements.</u> Academic Press, New York, 1983.

[54] Fiber attenuation data provided by FiberGuide Industry of Stirling, NJ for Superguide G and PCS UV-Vis fiber.

[55] see reference 54

[56] see reference 54

[57] Thompson, B., <u>Optics Guide 5.</u> Section 3, p. 6, Melles Griot, Rochester, 1990.

[58] see reference 38.

[59] Littman, M.G., <u>Proceedings of SPIE-The International Society for Optical Engineering.</u> vol. 912, pp. 56-66, 1988.

[60] Wright, W. and I. S. Falconer, "A Transversely Pumped Prismatic Dye Cell For High Power Dye Lasers", <u>Opt. Commun.</u> vol. 67, pp. 221-224, 1988.

[61] Schwab, S.D. and R. L. McCreery, <u>Anal. Chem.</u> 1984, vol. 56, 2199-2204.

[62] Luria, M., M. Ofran and G. Stein, <u>J. Phys. Chem.</u> 1974, vol. 78(19), pp. 1904-1909.

[63] Birks, J.B., Photophysics of Aromatic Molecules, Wiley-Interscience, London, 1970.

[64] Matsuzawa, S., A. Wakisaka and M. Tamura, Anal. Chem. 1990, vol. 62, pp. 2654-2656.

[65] St. Germain, R. W., North Dakota State University at Fargo, personal communication, 1992.

[66] see reference 53.

[67] Dellonte, S., V. Raffaelli and F. Barigelletti, Gassetta Chimica Italiana. 1984, vol. 114, pp. 375-378.

[68] see reference 73.

[69] see reference 62.

[70] see refrence 68.

[71] see reference 62.

[72] Inman, S.M., P. Thibado, G. A. Theriault and S. H. Lieberman, Anal. Chim. Acta. 1990, vol. 239, pp. 45-51.

[73] Stumm, W. and J. J. Morgan, Aquatic Chemistry, Wiley-Interscience, New York 1981.

[74] Faure, G., Principles and Applications of Inorganic Geochemistry. pp. 173-174, MacMillian, New York, 1991.

[75] Krauskopf, K., Introduction to Geochemistry. p. 263, McGraw Hill, New York, 1979.

[76] Gauthier, T.D., E. C. Shane, W. F. Guerin, W. R. Seitz, and C. L. Grant, "Fuorescence Quenching Method for Determining Equilibrium Constants for Polycyclic Aromatic Hydrocarbons Binding to Dissolved Humic Materials", Environ. Sci. Technoll. vol. 20, pp. 1162-1166, 1986.

[77] Williams, S., The University of Pennsylvania at Philadelphia, personal communication, 1992.

[78] see reference 20.

APPENDIX A

COMPILED SPECTRA of PAHs/BTEX SPECIES

(The reverse of this page is blank.)

Benzene .8\4 m284
Benzene 4\.8 x243

—— BENZX.SPT
— — BENZM.SPT

276.0

283.4

269.2

260.0

253.8

248.0

242.6

Wavelength (nm)

Intensity (cps)

89.7882

0.00000

400

350

300

250

87
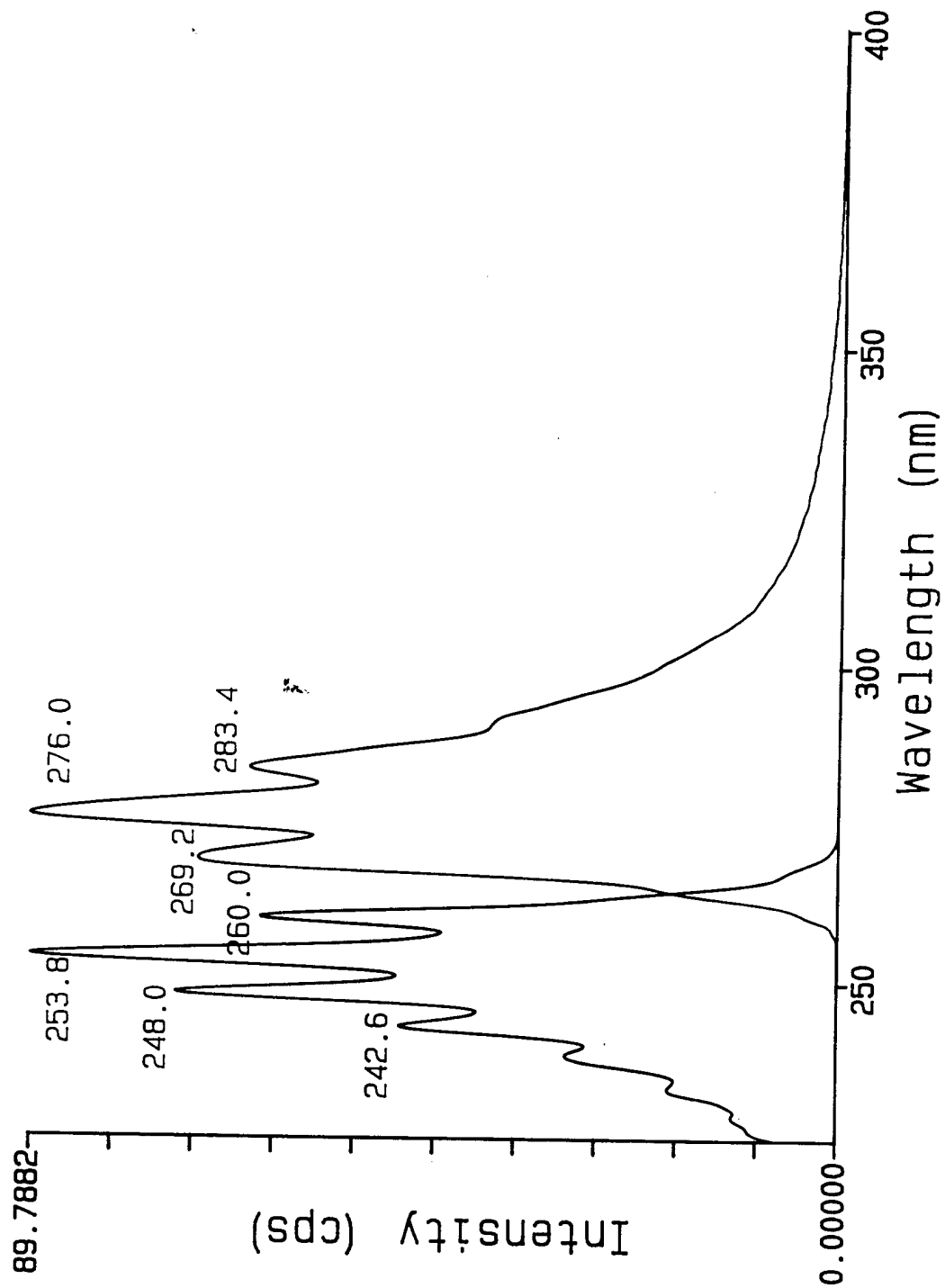
TOLUEX.SPT   Toluene .5\4 m282
TOLUEM.SPT   Toluene 4\.8 x255

261.2 276.8 282.0
267.8

Intensity (cps)
378.015
0.00000

Wavelength (nm)
250   300   350   400
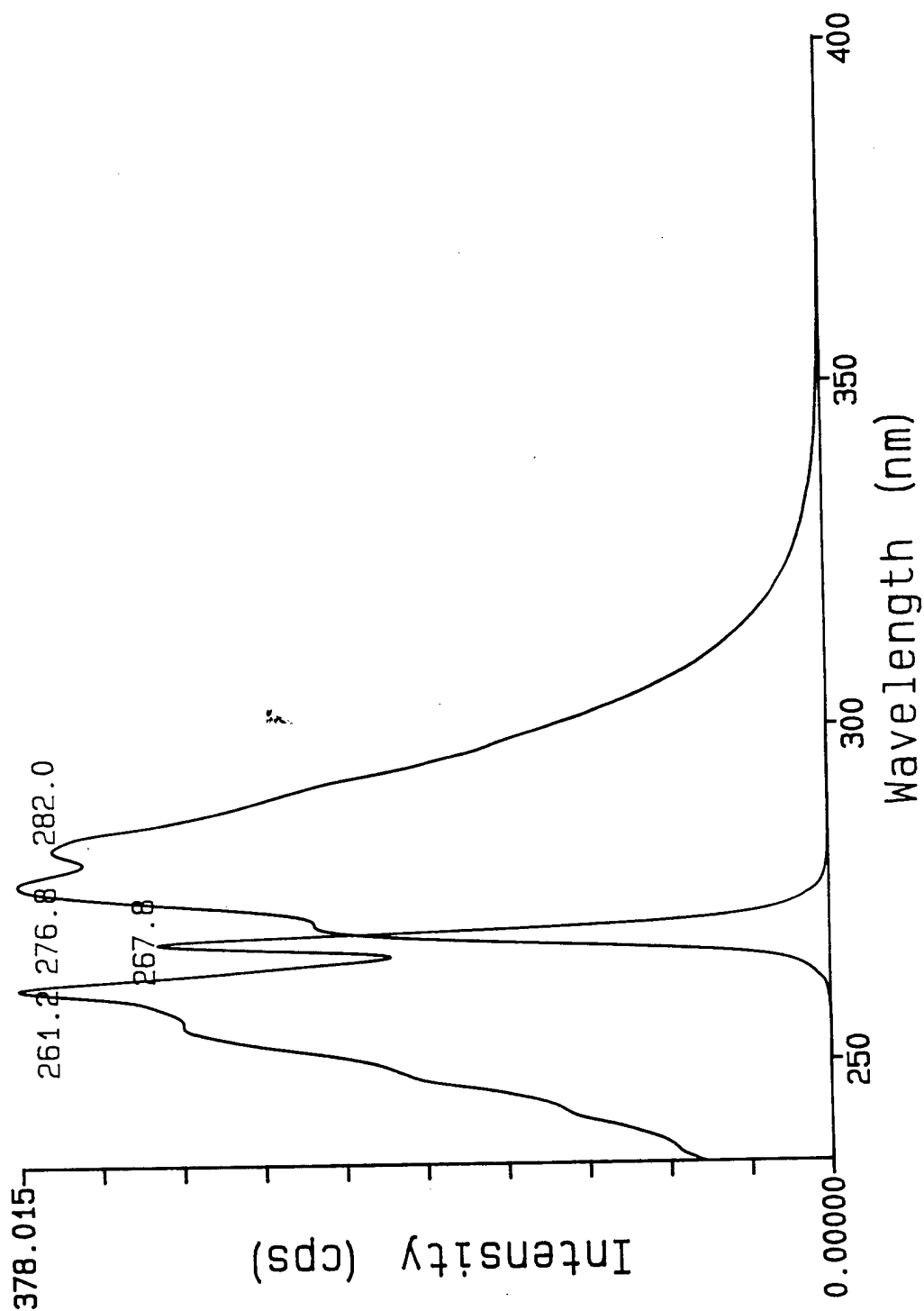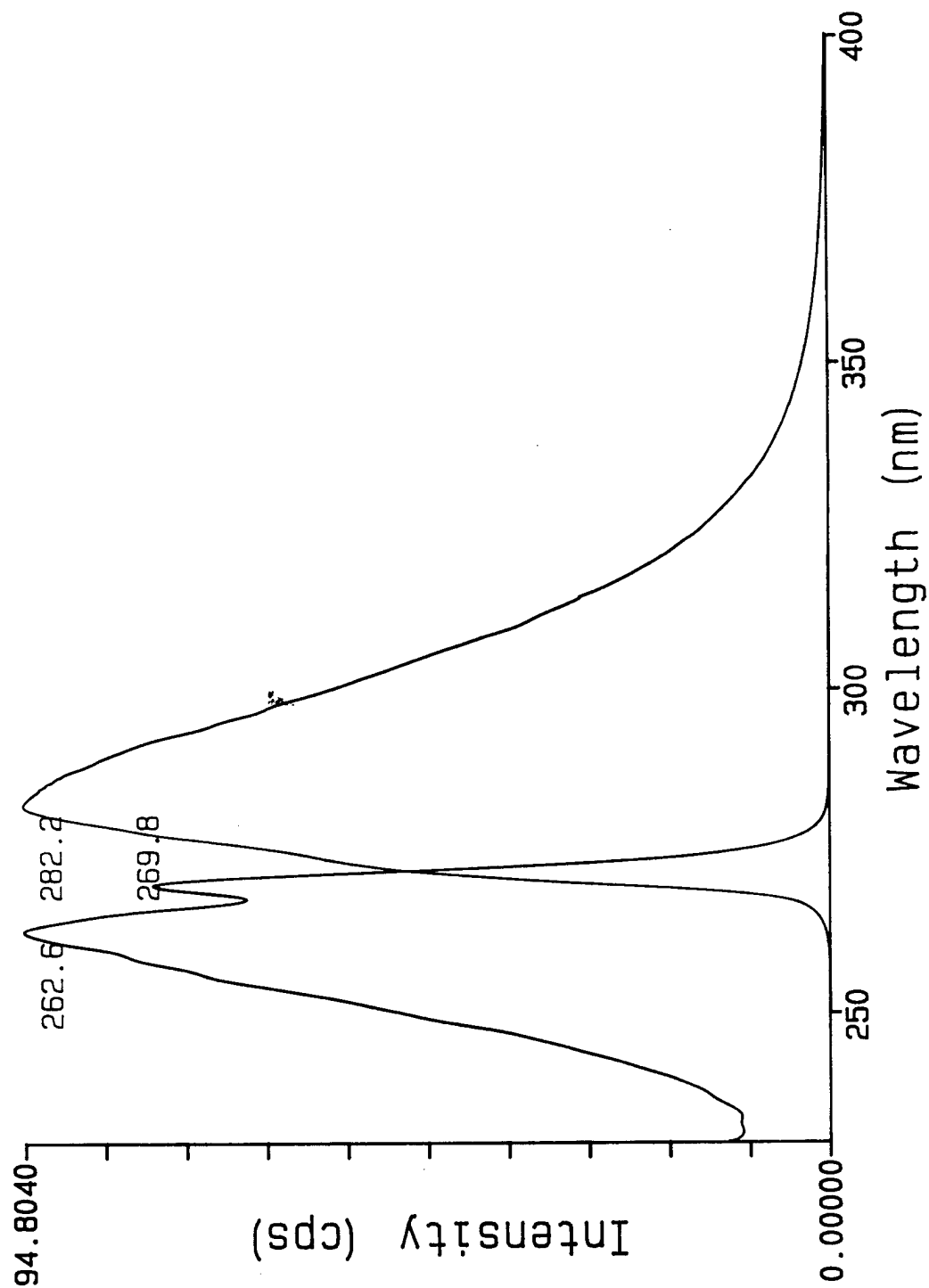
m-Xylene .7\4 m290
m-Xylene 4\1 x264

- - MXYLX.SPT
—— MXYLM.SPT

282.2
271.4
264.0

Wavelength (nm)

Intensity (cps)

350.115

0.00000

p-Xylene .6\3 m300
p-Xylene 4\.8 x260

—— PXYLX.SPT
—— PXYLM.SPT

284.2
267.4
260.0

Wavelength (nm)
Intensity (cps)
1554.930
0.00000

91
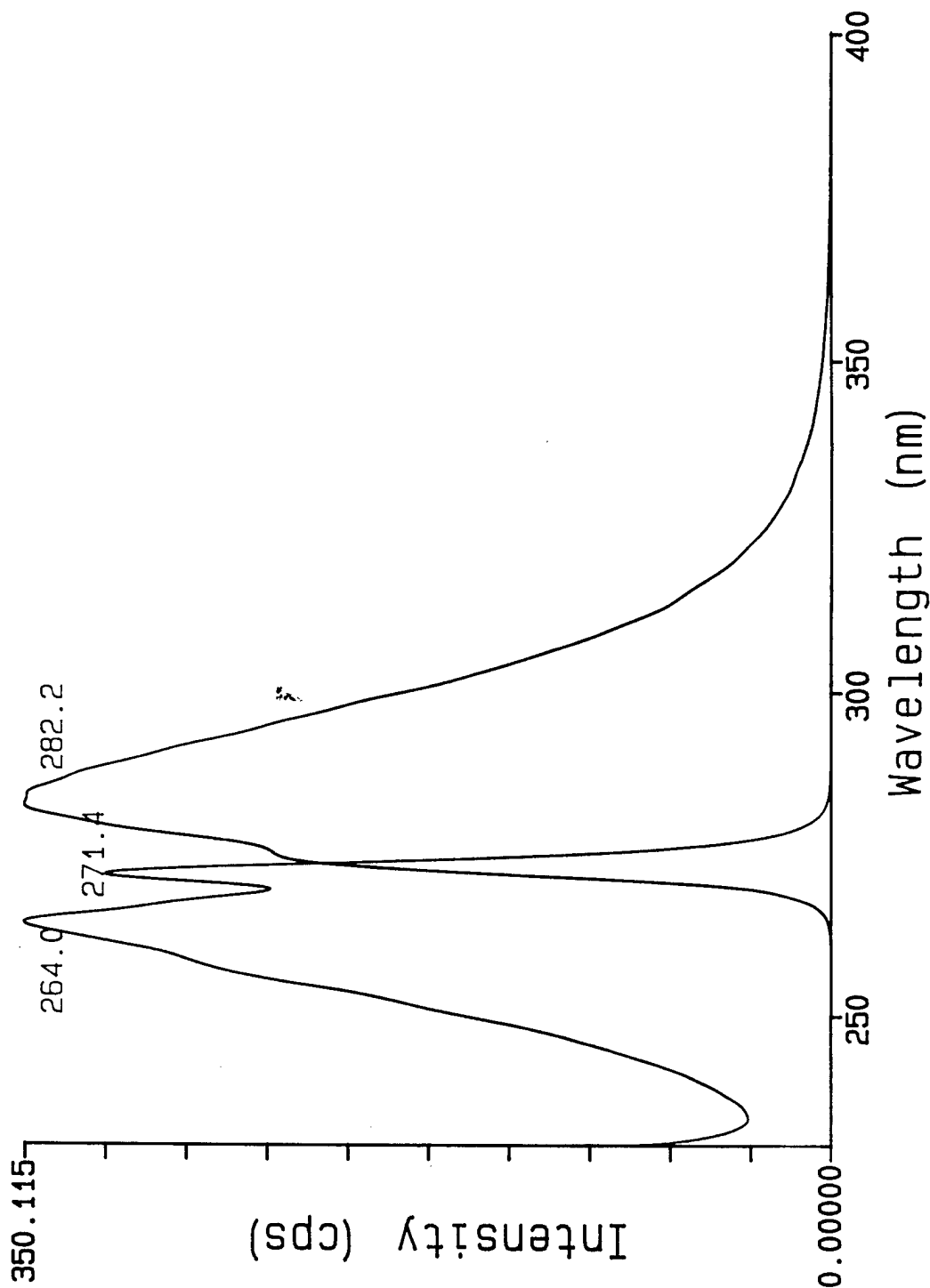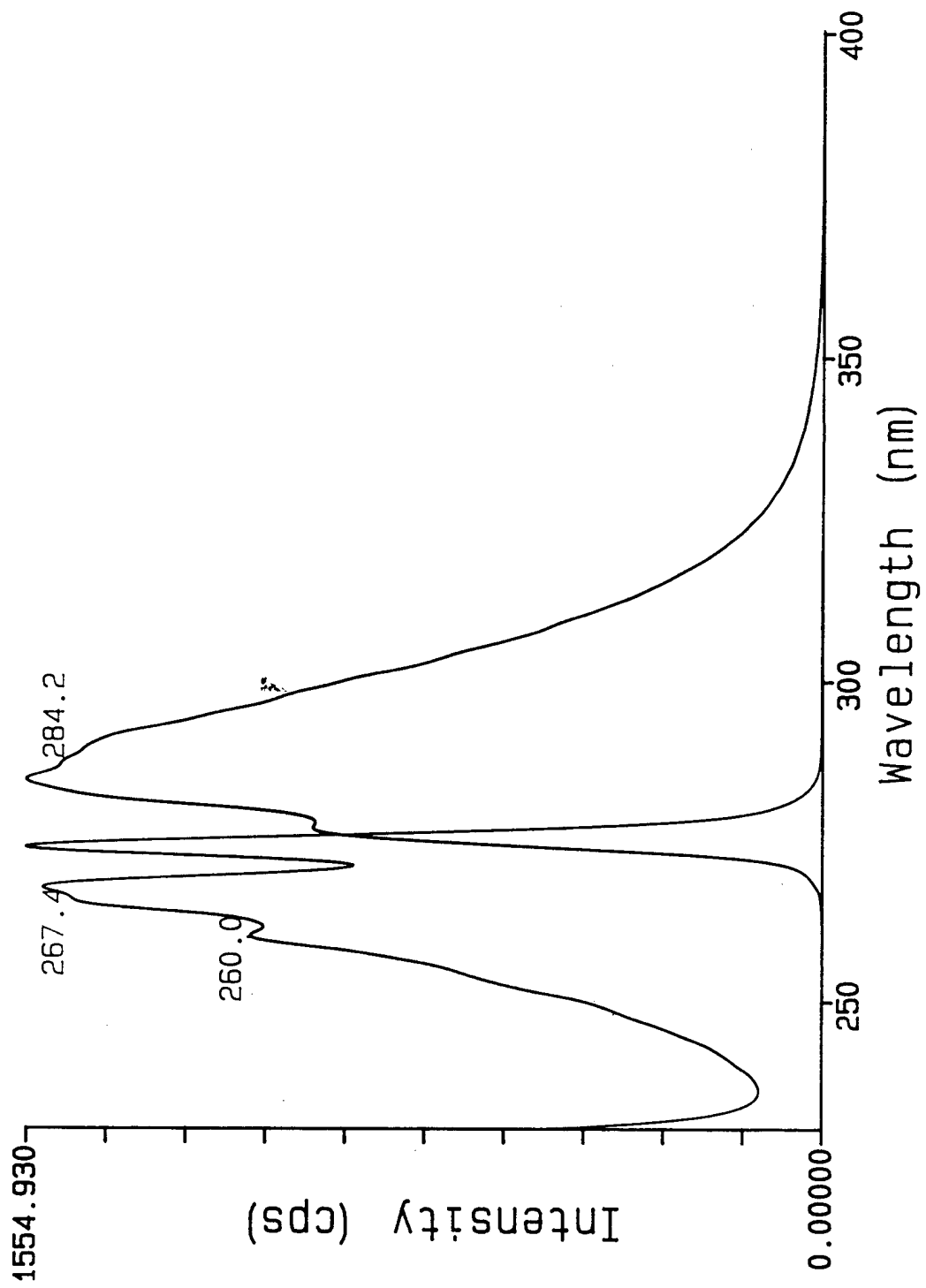
ETBENZX.SPT Ethylbenzene .8\4 m279
ETBENZM.SPT Ethylbenzene 4\.8 x264

281.8
276.0
267.2
260.4

Wavelength (nm)

Intensity (cps)

111.849

0.00000
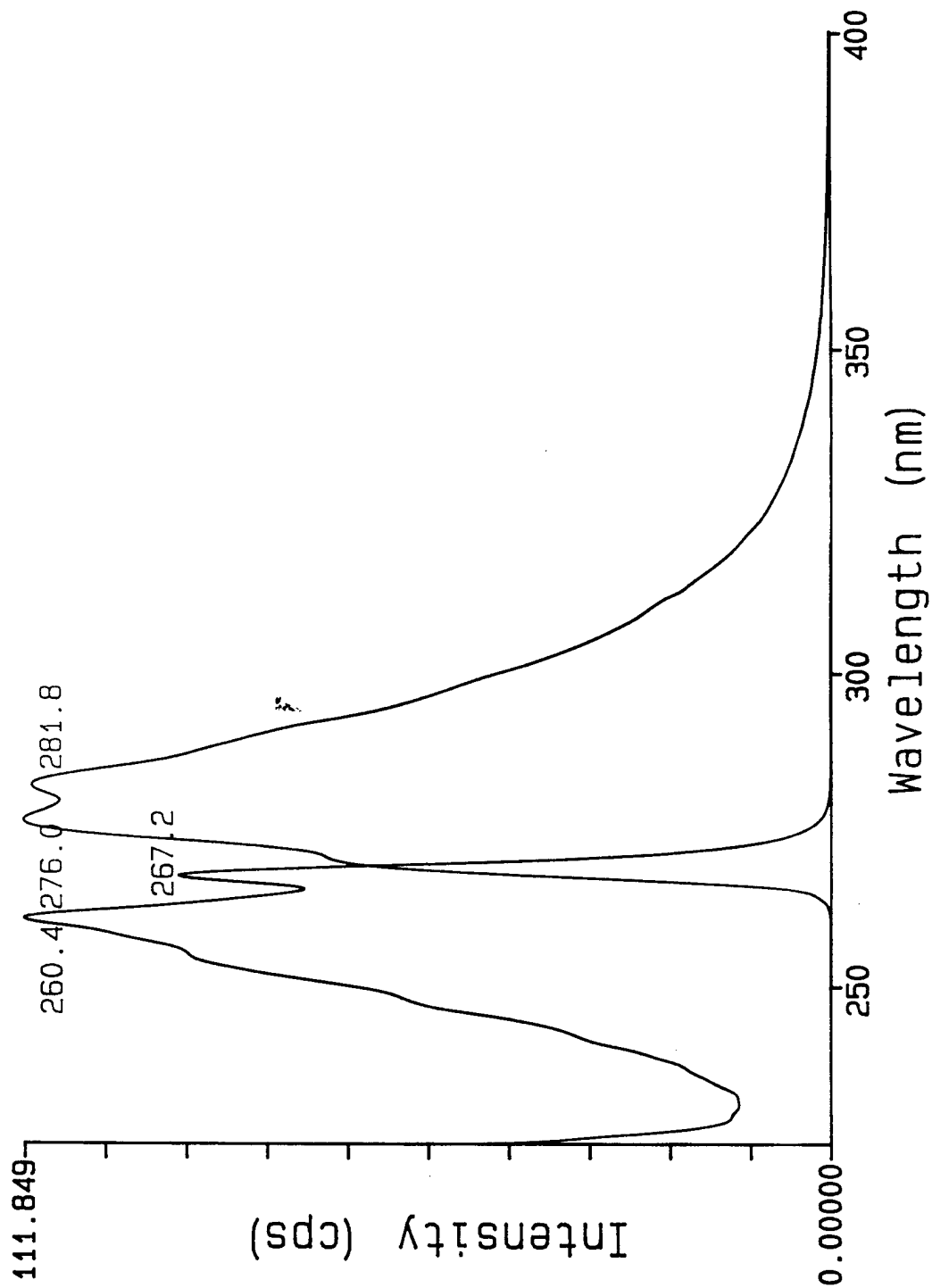
PROBENZX.SPT Propylbenzene .8\4 m305
PROBENZM.SPT Propylbenzene 4\.8 x268
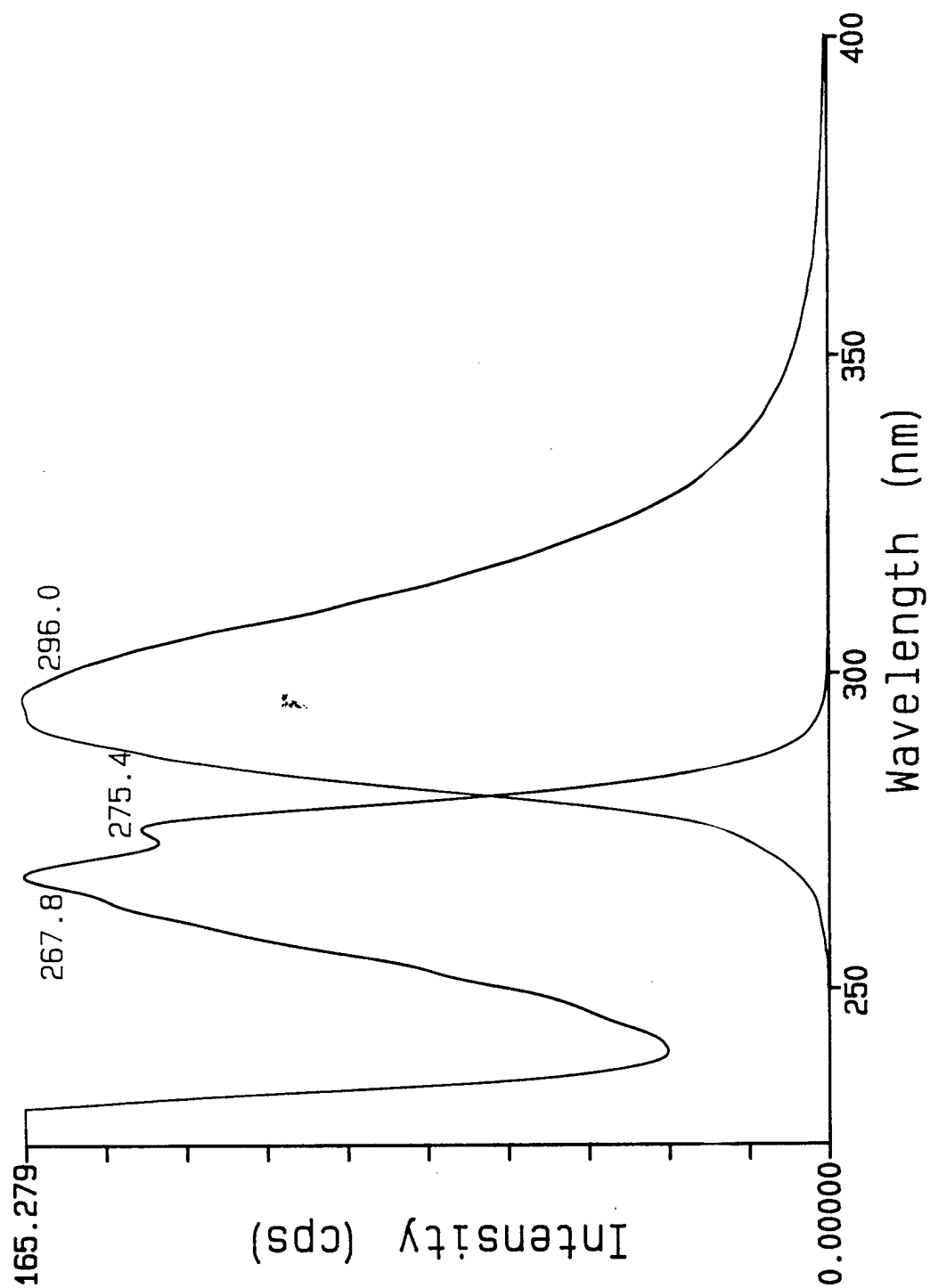
Wavelength (nm)

Intensity (cps)

165.279

0.00000

296.0

275.4

267.8

94
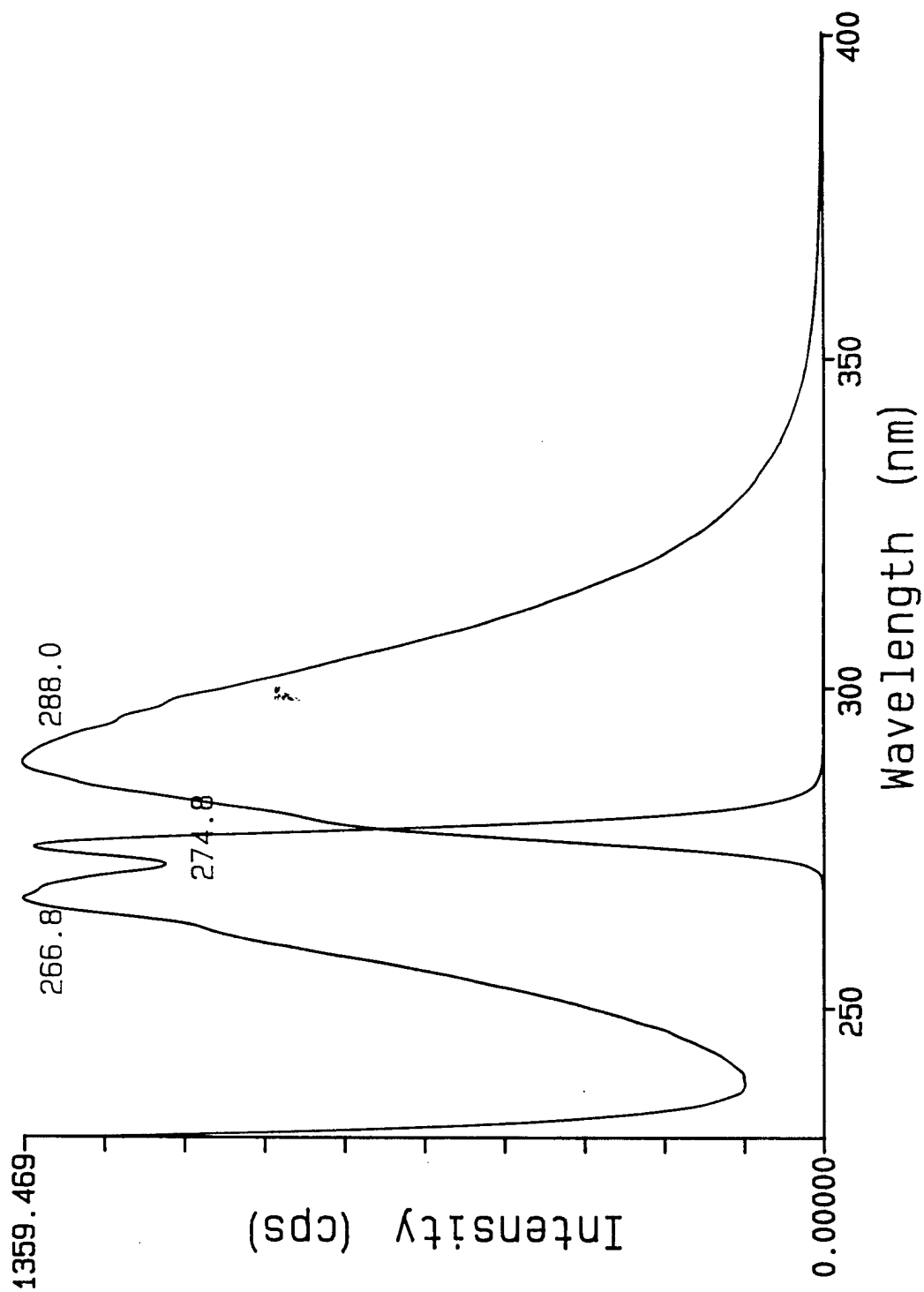
PHENOLX.SPT Phenol .5\4 m295
PHENOLM.SPT Phenol 4\.7 x265

294.8

269.8

1313.723

0.00000

Intensity (cps)

Wavelength (nm)
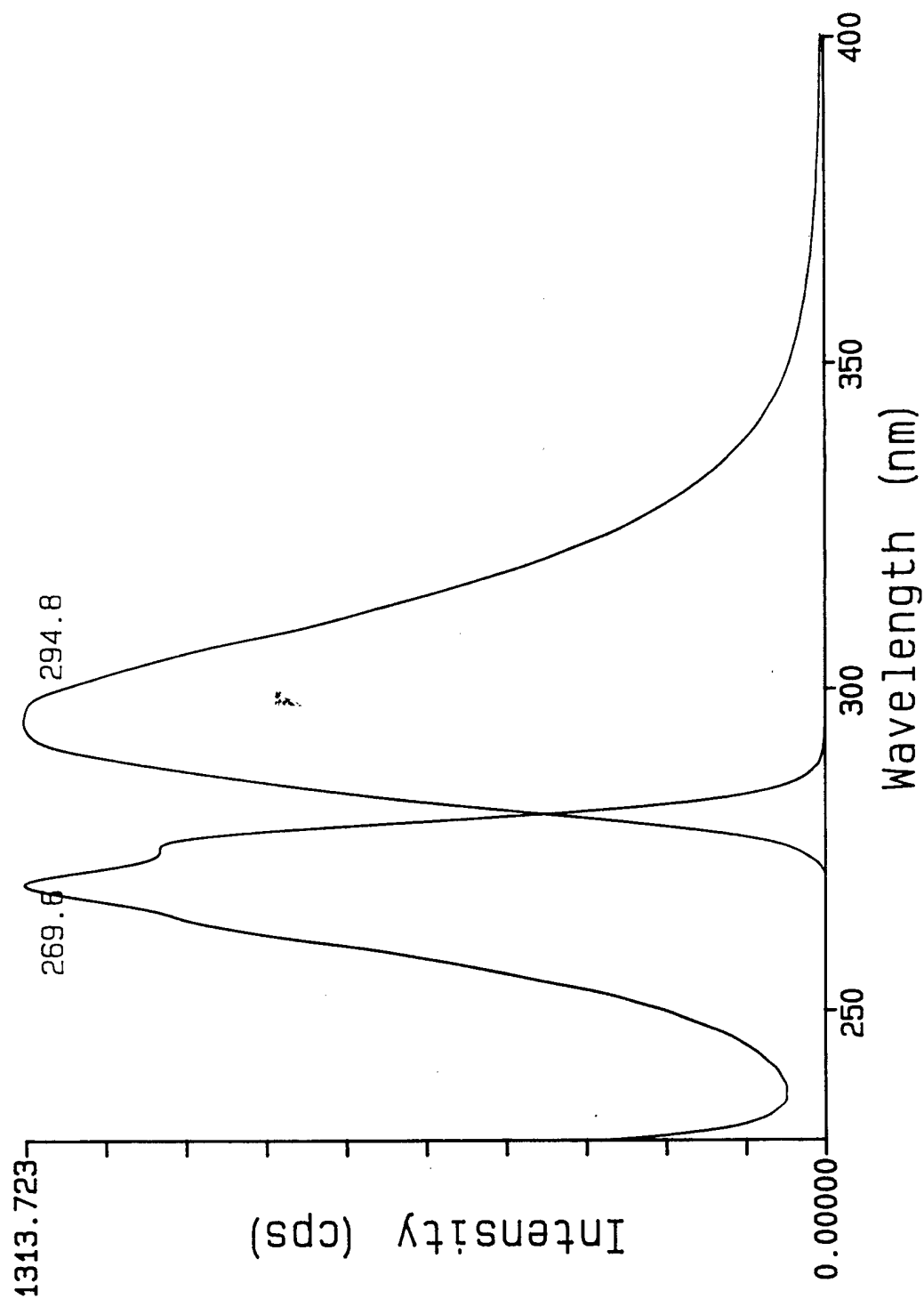
OCRESOLX.SPT o-Cresol .5\4 m305
OCRESOLM.SPT o-Cresol 3\.7 x271

298.4

270.6

Wavelength (nm)

Intensity (cps)

1019.472

0.00000

96
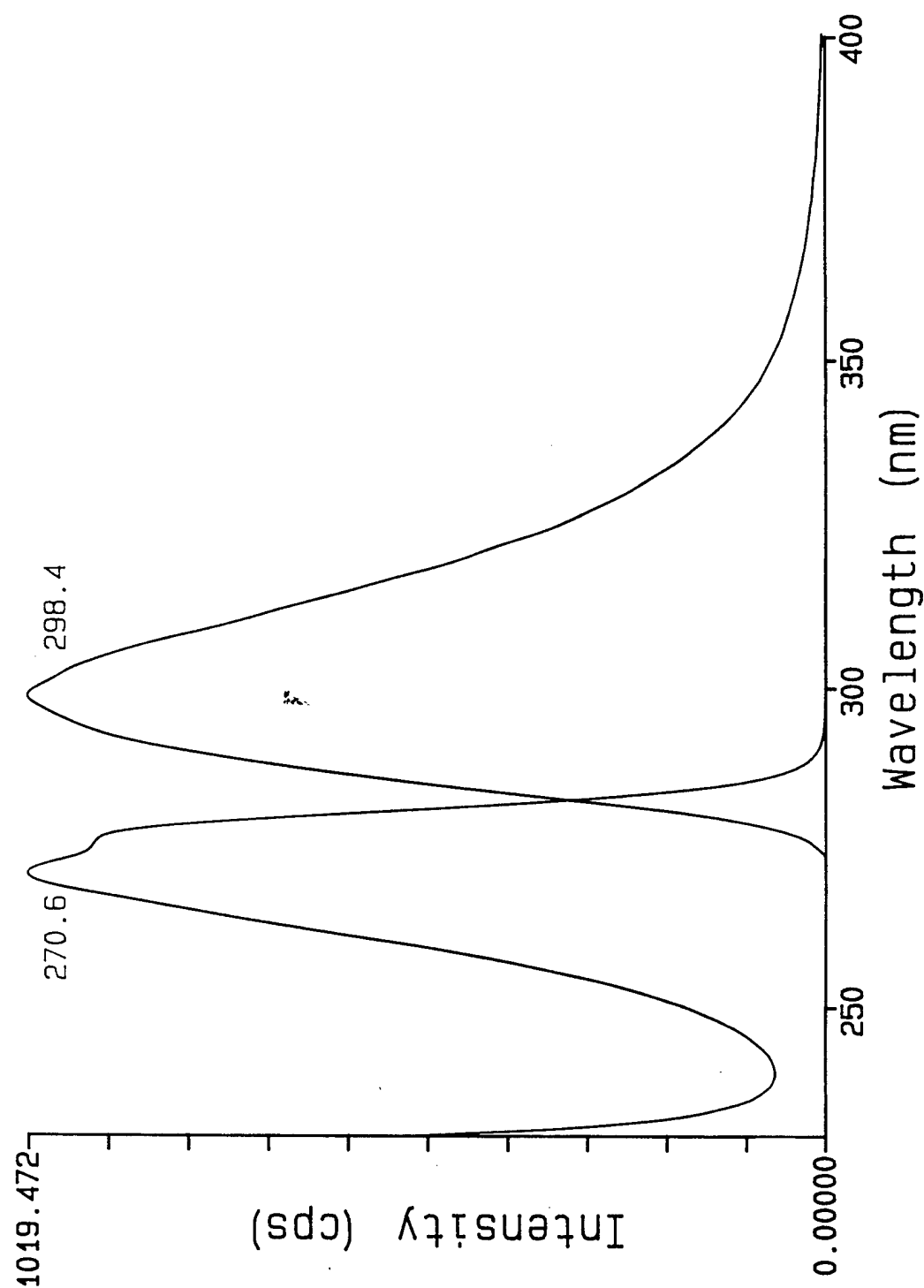
MCRESOLX.SPT m-Cresol .5\4 m305
MCRESOLM.SPT m-Cresol 4\.7 x272

297.8

277.8

272.4

Wavelength (nm)

Intensity (cps)

1301.786

0.00000

400

350

300

250
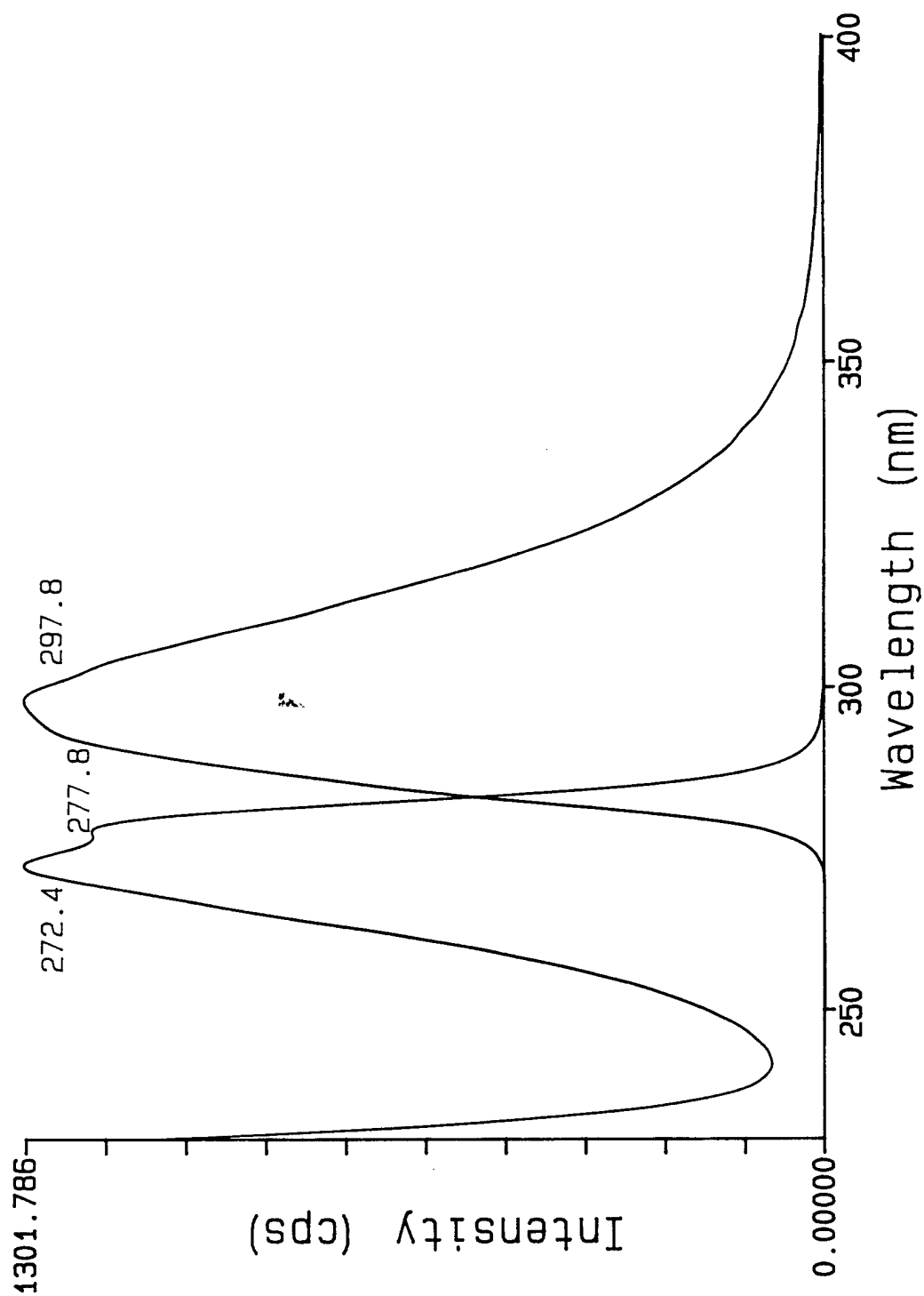
97
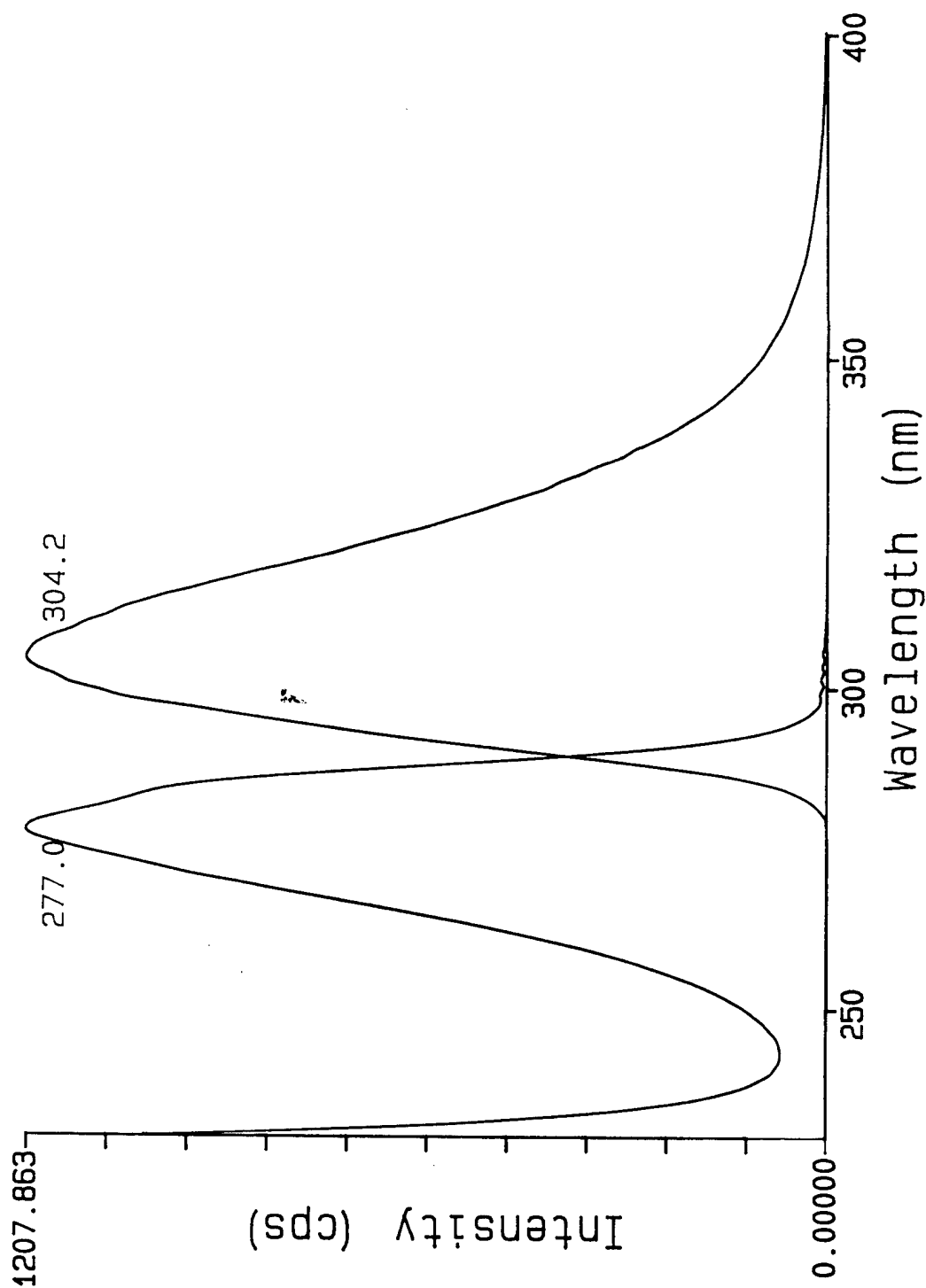
NAPHTHX.SPT Naphthalene .6\4 m335

1-Methylnaphthalene
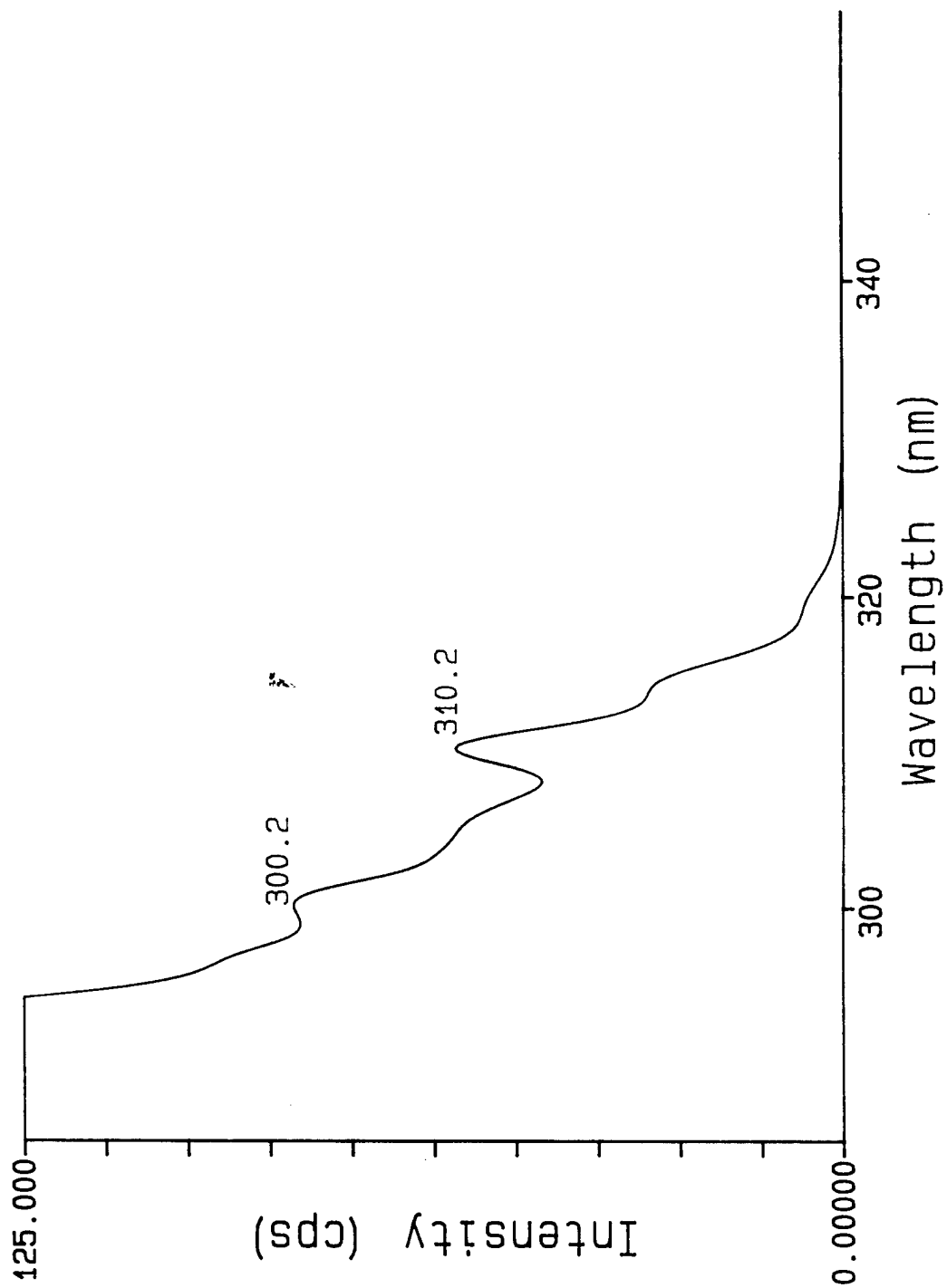
—— 1MNAPHX.SPT	1-Methylnaphthalene	.7\4 m333
—— 1MNAPHM.SPT	1-Methylnaphthalene	4\.6 x282
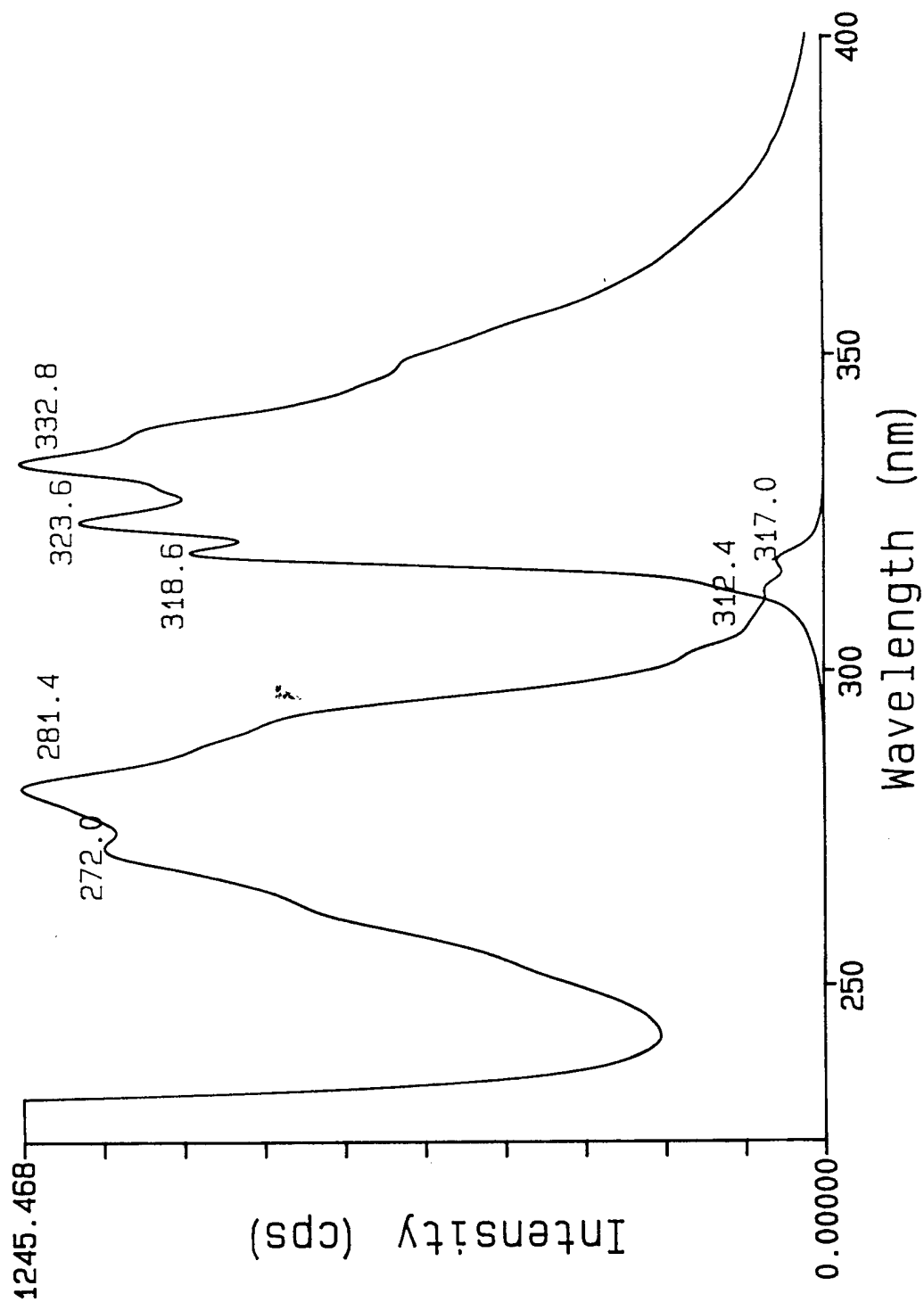
2MNAPHX.SPT 2-Methylnaphthalene .7\4 m334
2MNAPHM.SPT 2-Methylnaphthalene 4\.6 x276
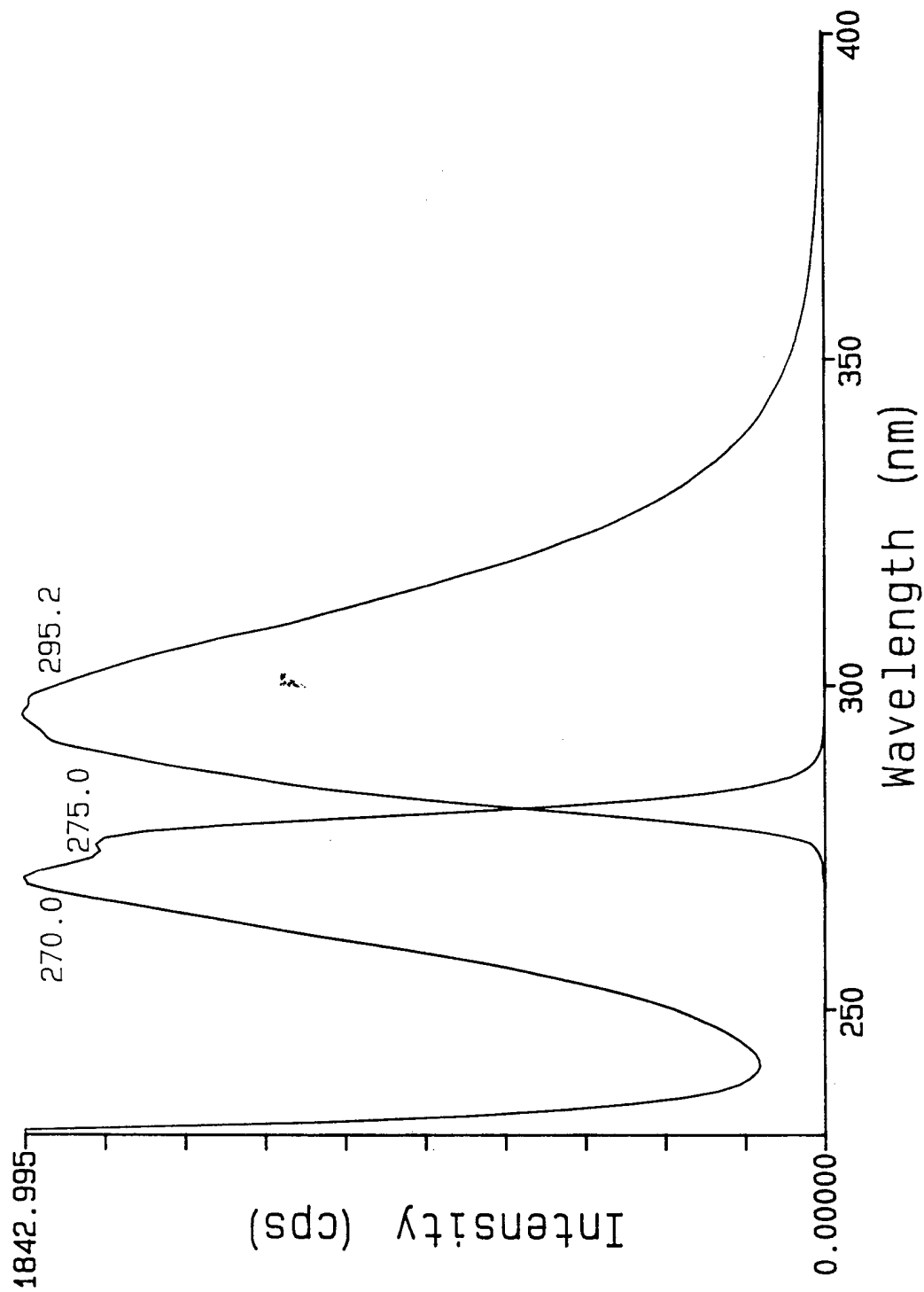
102
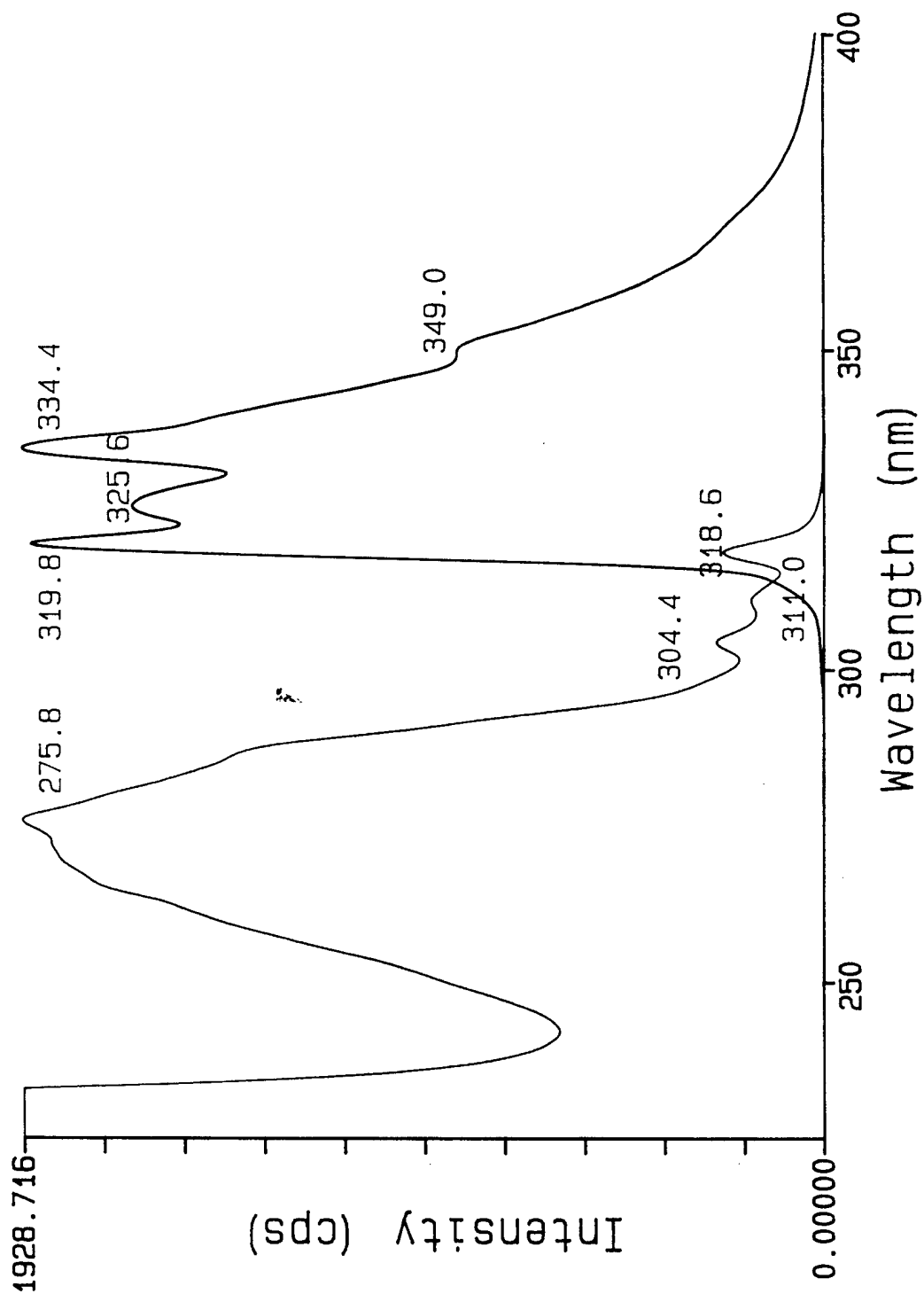
1NAPHTX.SPT   1-Naphthol .5\4 m474
1NAPHTM.SPT   1-Naphthol 3\.7 x296

Wavelength (nm)

Intensity (cps)

304.756

0.00000

473.6

294.2

307.2

321.8
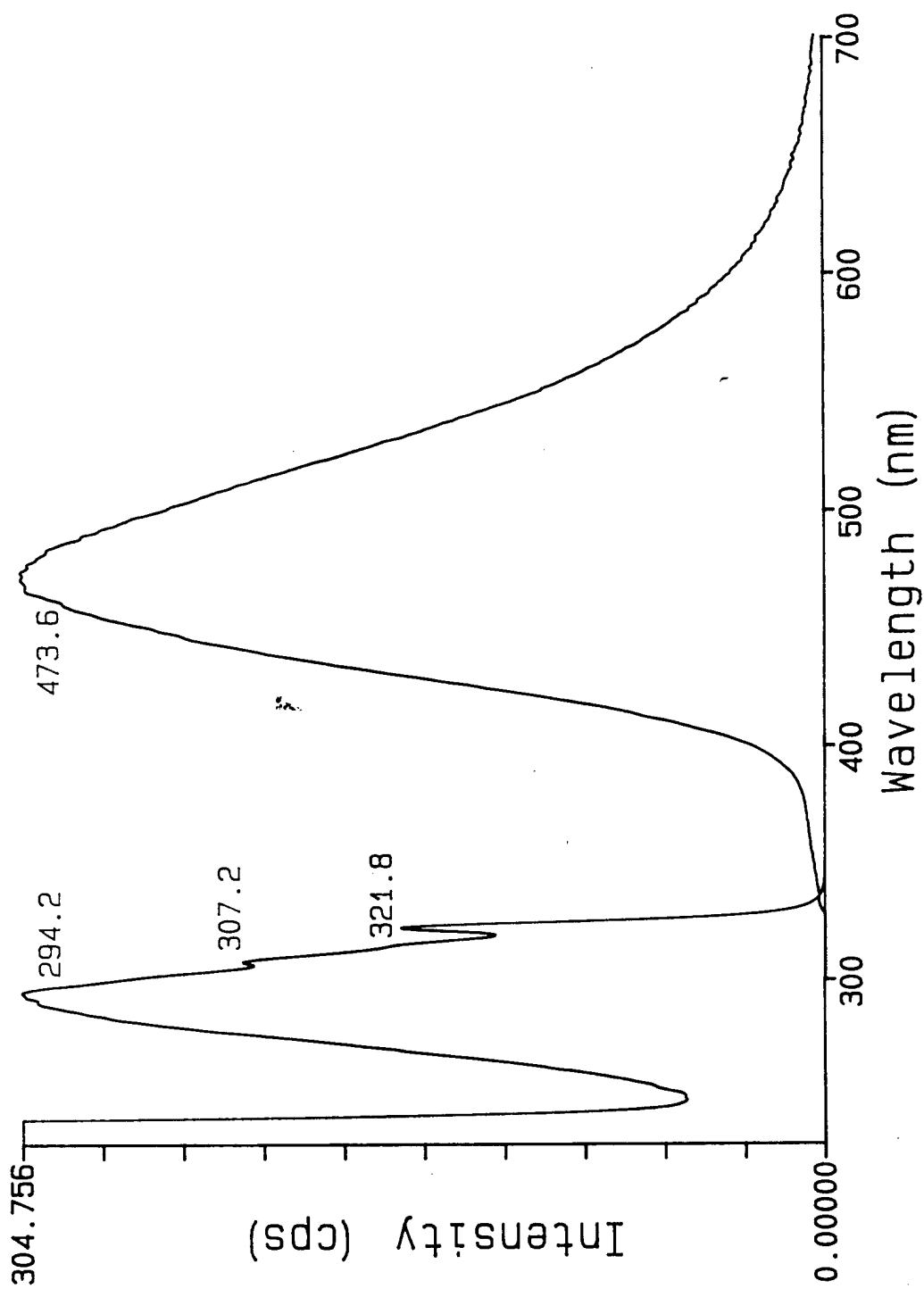
2-Naphthol .6\4 m355
2-Naphthol 4\.8 x274

2NAPHTX.SPT
2NAPHTM.SPT

353.6
273.8
284.8
264.0
327.8
315.6
409.2

Wavelength (nm)

Intensity (cps)

1252.423

0.00000

104
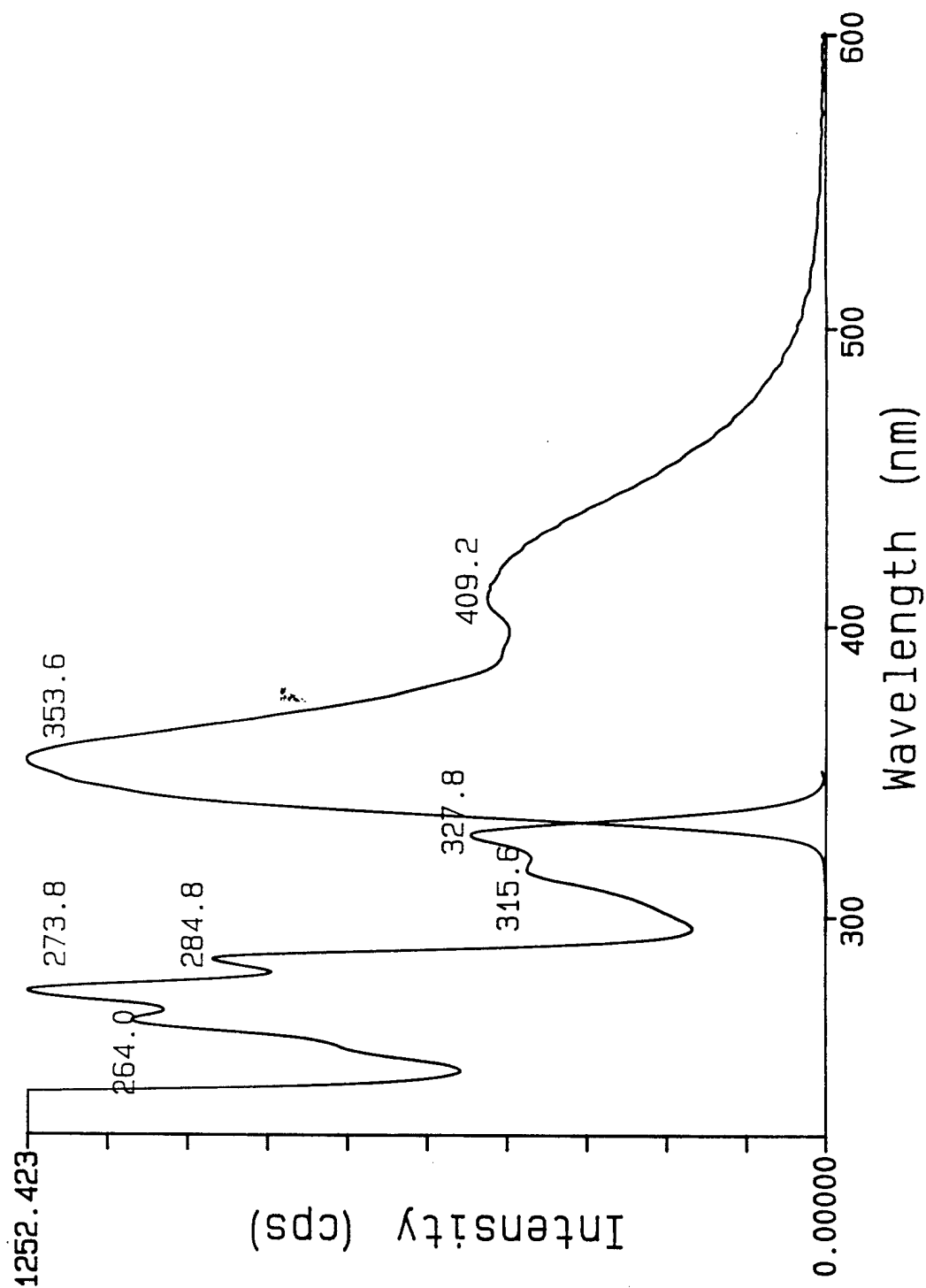
ANISOLEX.SPT Anisole .5\4 m292
ANISOLEM.SPT Anisole 4\.7 x268

Wavelength (nm)

Intensity (cps)
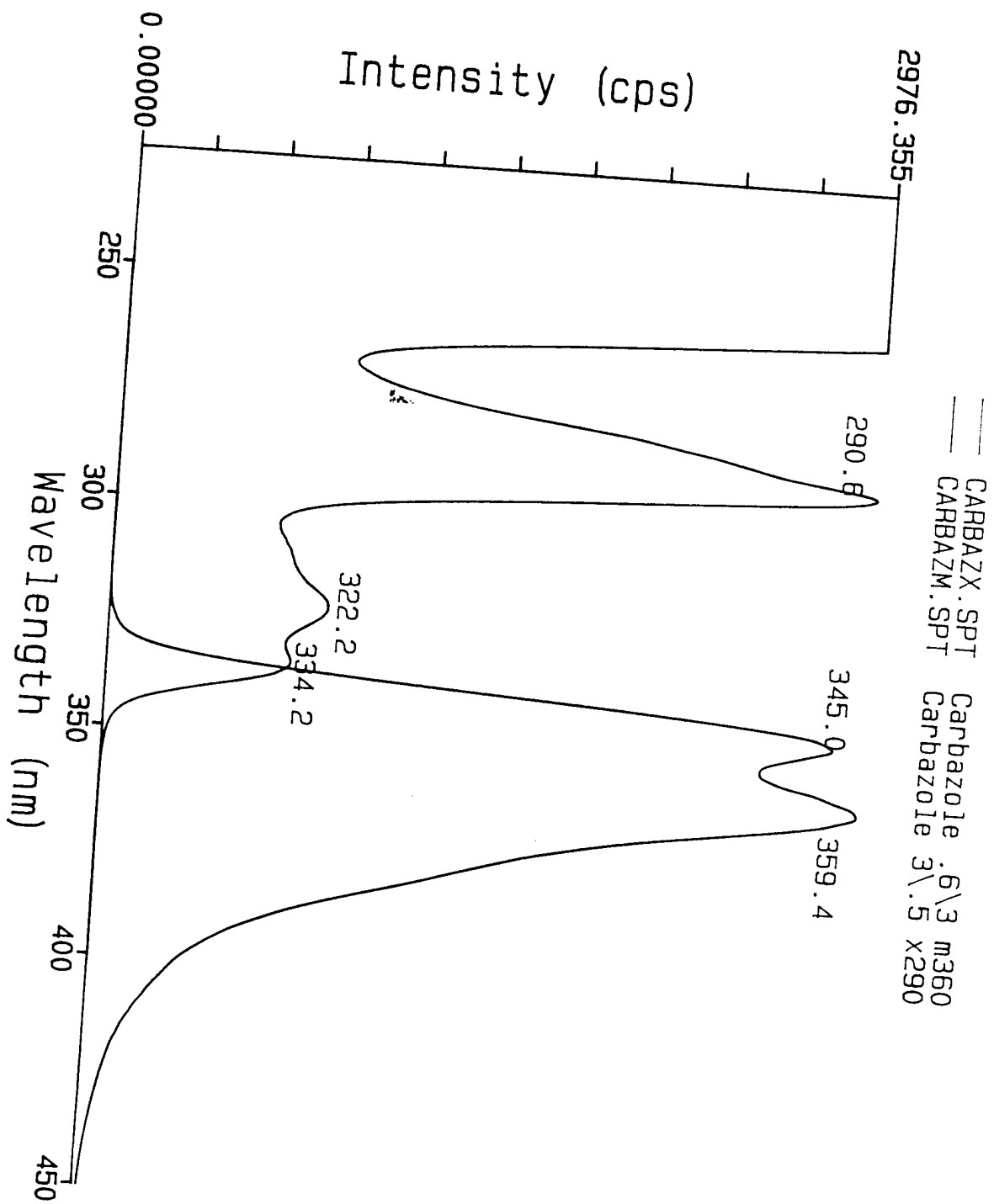
1804.340

0.00000

291.4
275.0
268.8

105
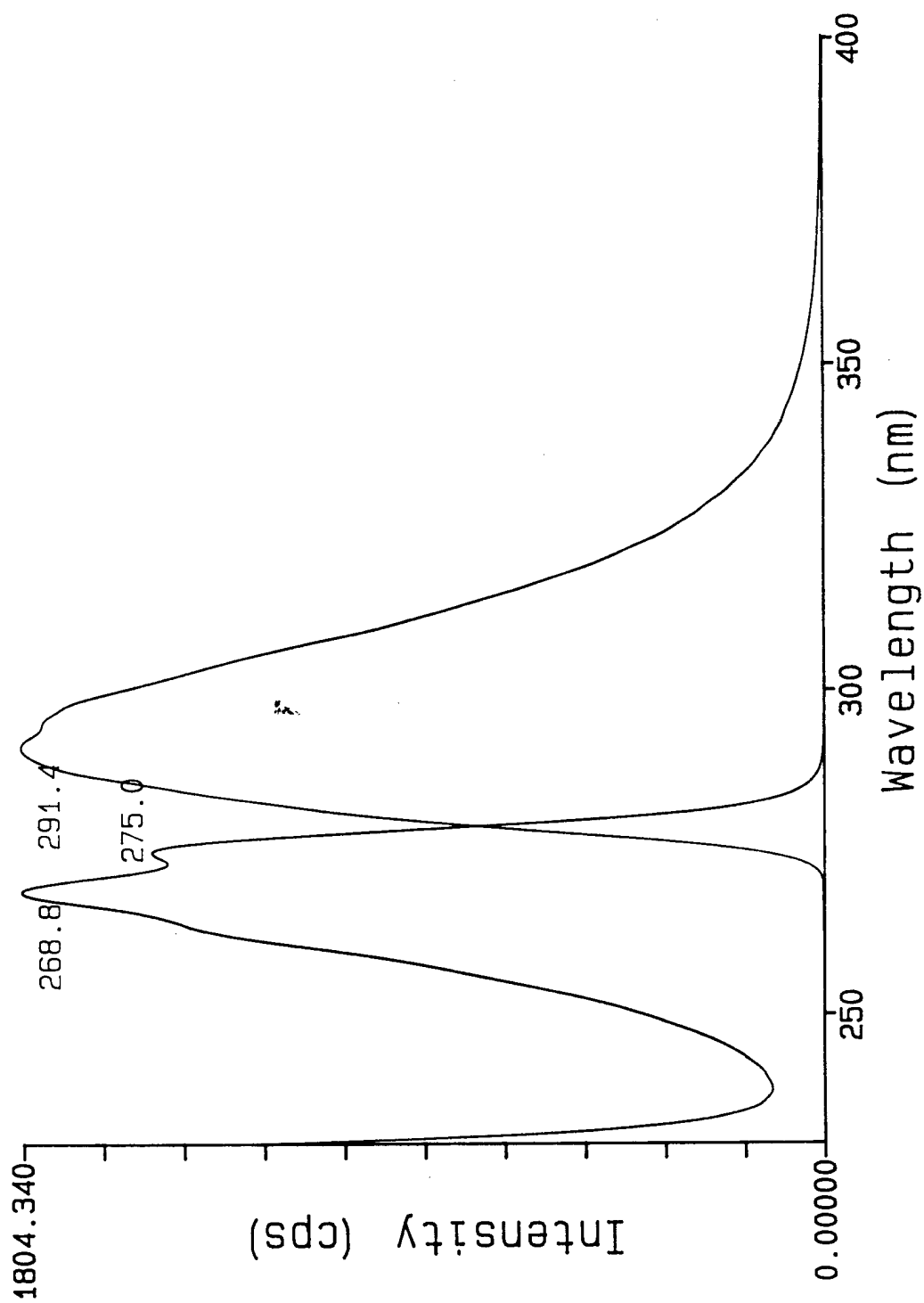
4MANISX.SPT 4-Methylanisole .5\4 m305
4MANISM.SPT 4-Methylanisole 4\.5 x276

302.0

276.4
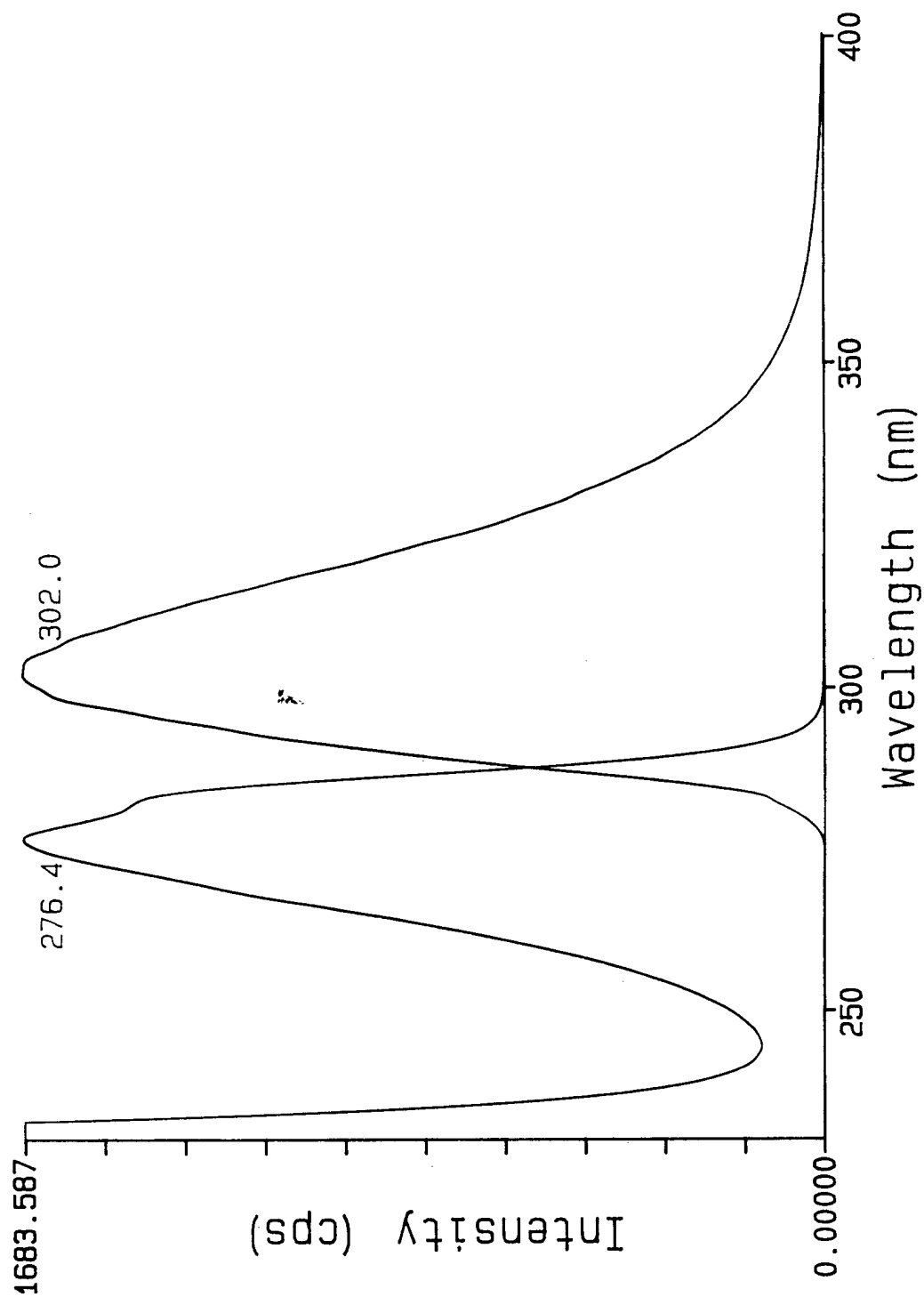
BIPHENX.SPT Biphenyl .8\3 m313
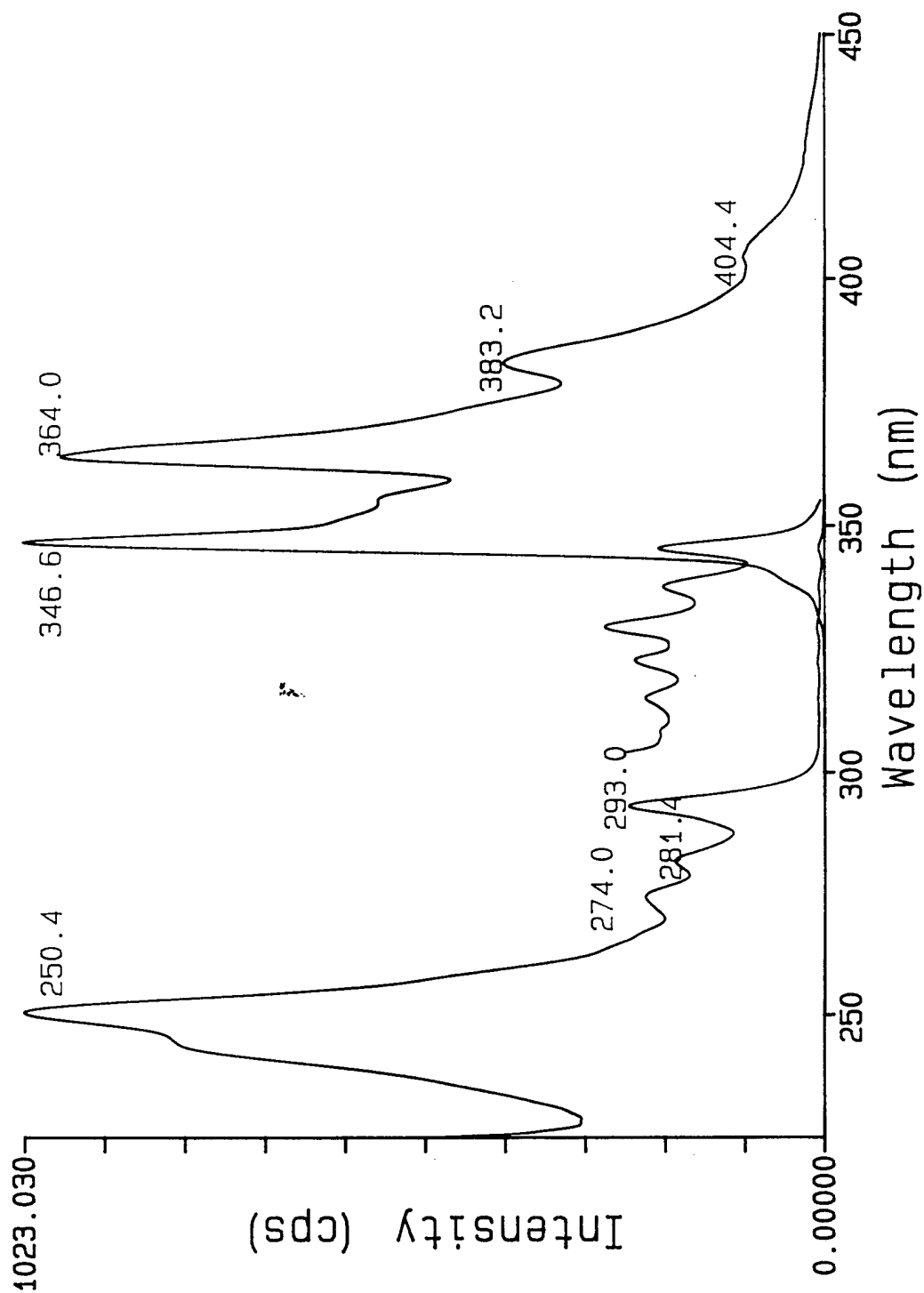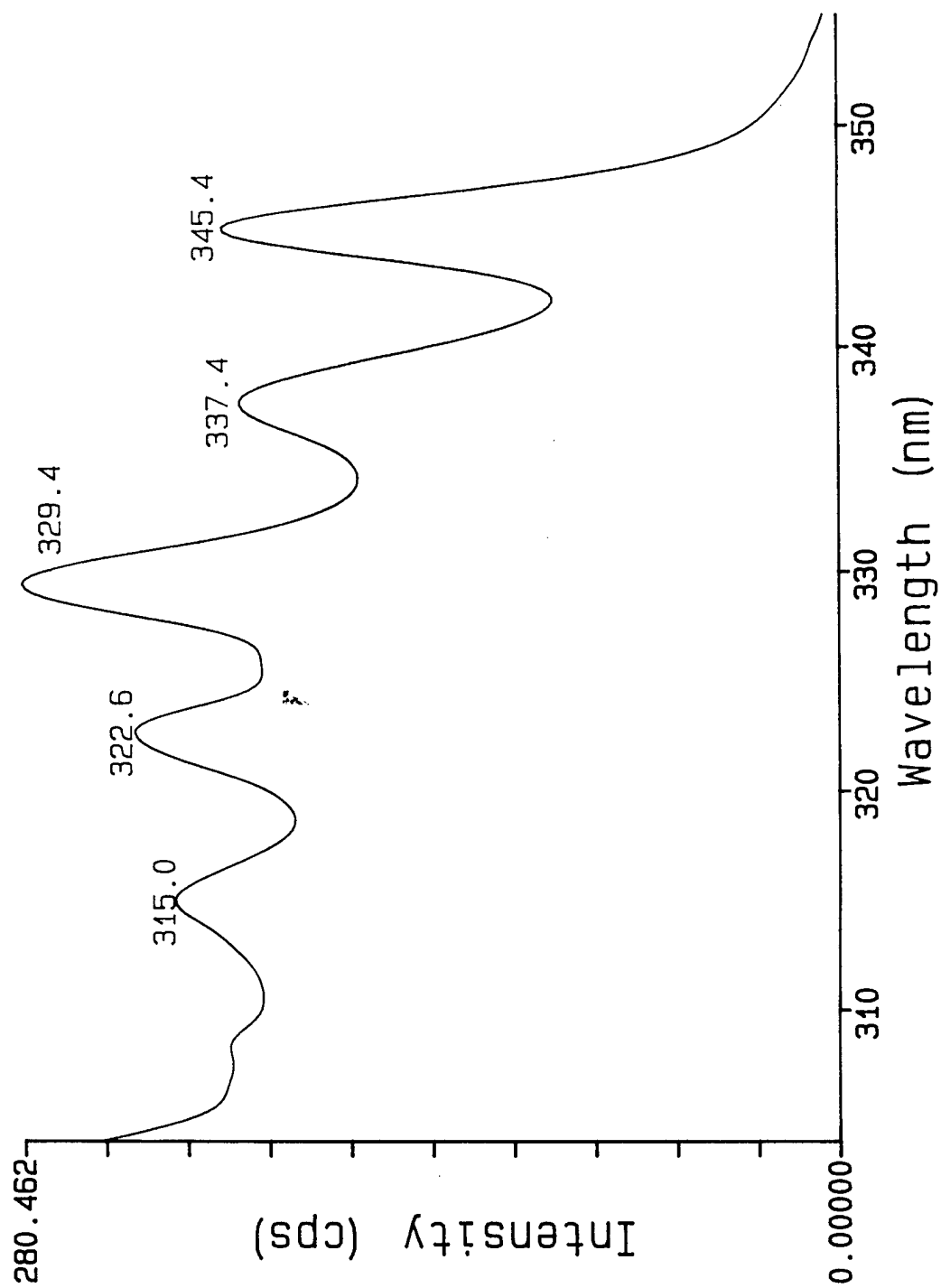BIPHENM.SPT Biphenyl 3\.8 x247

Carbazole fluorescence spectrum showing Intensity (cps) versus Wavelength (nm). Peaks labeled: 290.8, 322.2, 334.2, 345.0, 359.4. Legend: CARBAZX.SPT Carbazole .6\3 m360; CARBAZM.SPT Carbazole 3\.5 x290. Intensity axis range 0.00000 to 2976.355.

109
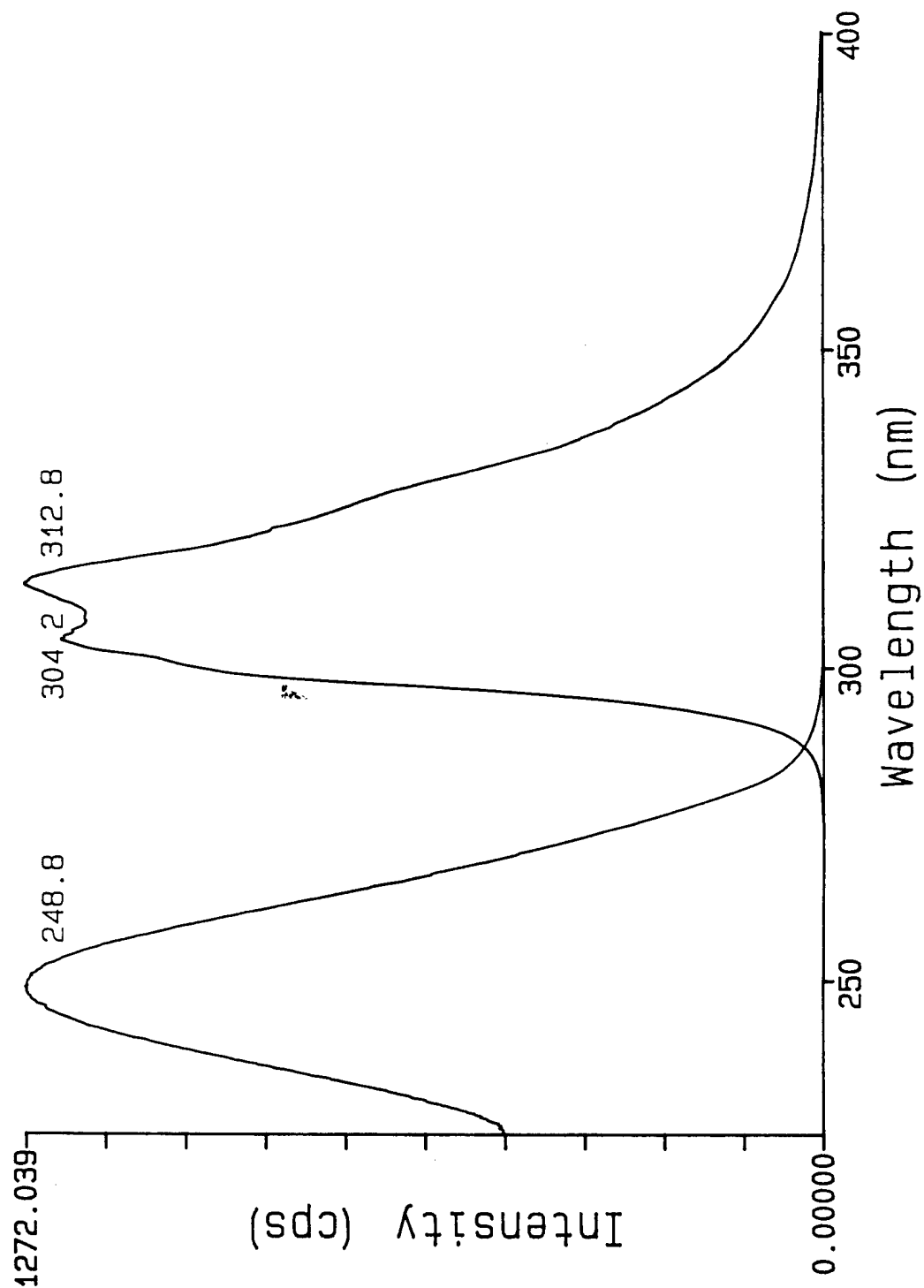
DIPHMEX.SPT Diphenylmethane .5\4 m292
DIPHMEM.SPT Diphenylmethane 4\.5 x269

248.8   304.2   312.8

Intensity (cps)

385.847   0.00000

Wavelength (nm)
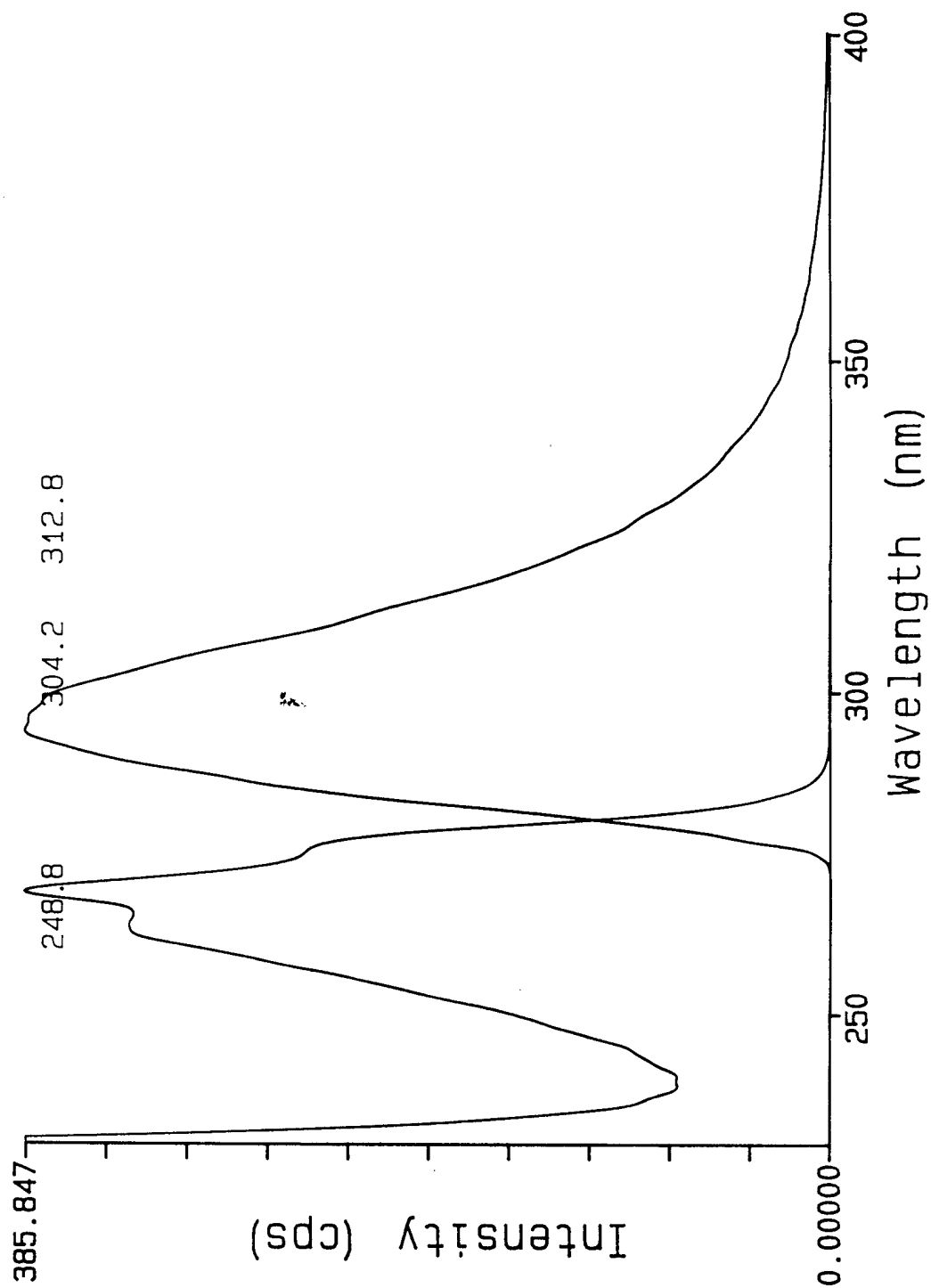
250   300   350   400

EXPAND1.SPT   PHENANX*30

Fluorene .6\3 m315
Fluorene 4\.6 x263

FLUOREX.SPT
FLUOREM.SPT

301.8
298.6
287.8
263.0

Wavelength (nm)

Intensity (cps)

6314.740

0.00000